

**Structural Phase Transitions and Formation of Novel
Phases involving Intra-Group IV elements at High P-T
Conditions**

by

SORB Y A

(Enrollment No: PHYS02200704022)

Indira Gandhi Center for Atomic Research, Kalpakkam

*A thesis submitted to the
Board of Studies in Physical Sciences
In partial fulfillment of requirements
For the degree of*

DOCTOR OF PHILOSOPHY

of

HOMI BHABHA NATIONAL INSTITUTE



FEBRUARY, 2013

Homi Bhabha National Institute

Recommendations of the Viva Voce Board

As members of the Viva Voce Board, we certify that we have read the dissertation prepared by **Sorb Y A** entitled “**Structural Phase Transitions and Formation of Novel Phases involving Intra-Group IV Elements at High P-T Conditions**” and recommend that it may be accepted as fulfilling the dissertation requirement for the Degree of Doctor of Philosophy.

_____ **Date:**
Chairman –

_____ **Date:**
Convener/Guide –

_____ **Date:**
Co-Guide –

_____ **Date:**
Member –

_____ **Date:**
Member –

_____ **Date:**
Member –

Final approval and acceptance of this dissertation is contingent upon the candidate's submission of the final copies of the dissertation to HBNI.

Date:
Place:

CERTIFICATE

I hereby certify that I have read this dissertation prepared under my direction and recommend that it may be accepted as fulfilling the dissertation requirement.

Date:

Place:

(N. Subramanian)

STATEMENT BY AUTHOR

This dissertation has been submitted in partial fulfillment of requirements for an advanced degree at Homi Bhabha National Institute (HBNI) and is deposited in the library to be made available to borrowers under rules of the HBNI.

Brief quotations from this dissertation are allowable without special permission, provided that accurate acknowledgement of source is made. Requests for permission for extended quotation from or reproduction of this manuscript in whole or in part may be granted by the Competent Authority of HBNI when in his or her judgment the proposed use of the material is in the interests of scholarship. In all other instances, however, permission must be obtained from the author.

Sorb Y A

DECLARATION

I, hereby declare that the investigation presented in the thesis has been carried out by me. The work is original and has not been submitted earlier as a whole or in part for a degree / diploma at this or any other Institution / University.

(Sorb Y A)

Dedicated to

My mother

ACKNOWLEDGEMENTS

I express my sincere gratitude to my research supervisor Dr. N Subramanian for his valuable guidance, scholarly inputs, and consistent encouragement and also for giving proper direction to carry out research. I am grateful to Dr. P. Ch. Sahu who taught me handling the diamond anvil cell for high pressure research and also his support and guidance throughout my research career.

I would like to extend my heartfelt thanks to Dr. T. R. Ravindran for helping me using the micro-Raman facility which is a major part of this work. Whenever I asked time schedule for Raman measurement, he never said no. I am thankful to Dr. D. Sornadurai for valuable suggestions in X-ray analysis of high pressure data. I express my gratitude to Mr. N. R. Sanjay Kumar who taught me handling Laser Heated Diamond Anvil Cell technique. I also thank Dr. N. V. Chandra Shekar for his valuable suggestions and help throughout this work. I sincerely thank Mr. M. Sekar, Dr. Anthony Arul Raj and Mr. B. M. Shukla for their help at various stages of my thesis work. I record my sincere thanks to Shri L. M. Sundaram for his technical help.

I express my heartfelt gratitude to doctoral committee chairman, Dr. C. S. Sundar for his suggestions and help throughout my research career. I also thank doctoral committee members Dr. A. K. Arora and Shri. V. Sankara sastry for periodic evaluation of the research work and also giving valuable suggestions. I would like to express my heartfelt thanks to Dr. Baldev Raj for allowing me to pursue my doctorate in High Pressure Physics Section. I thank Dr. M. Sai Baba for his constant support and taking care of our needs in various aspects. I am thankful to Shri. S. C. Chetal (former Director, IGCAR) and Dr. P. R. Vasudev Rao, Director, IGCAR for their

encouragement. I also thank Shri. M. P. Janawadkar, Head, CMPD, IGCAR for his support.

I thank all research scholars at IGCAR, Kalpakkam for having unforgettable days with them. I thank DAE for granting me SRF. Finally, but not the least, I am ever grateful to my loving mother, who sacrificed immensely to lift me up to this level.

CONTENTS

TITLE NO	TITLE	PAGE NO
	CHAPTER I	
	INTRODUCTION and MOTIVATION	1
1.1	Effect of Pressure and Temperature on Materials	2
1.2	High Pressure Behavior of Group IV Elements	3
1.2.1	Silicon & Germanium	3
1.2.2	Carbon	6
1.2.3	Tin	8
1.2.4	Lead	9
1.3	Pressure Dependence of Phonon Modes of Group IV Elements	9
1.4	IV-IV Systems	11
1.4.1	Si-Ge System	12
1.4.2	Si-C System	13
1.4.3	Ge-Sn System	13
1.4.4	Ge-C System	14
1.5	Relevance of LHDAC Technique for the High Pressure- High Temperature Synthesis of IV-IV Systems	15
1.6	Matlockite Compounds	16
1.7	Structural Stability of Matlockite Compounds under High Pressure	18
1.7.1	HPXRD Studies	18
1.7.2	Raman Spectroscopy of Matlockites	19
1.8	Scope of the Thesis	20
1.9	References	22

CHAPTER II

Experimental Details and Characterization Techniques

2.1	Introduction	34
2.2	Generation of High Pressures	34
2.2.1	Piston-Cylinder Apparatus	35
2.2.2	Opposed Anvil Device	35
2.2.3	Bridgman Opposed Anvil Device	35
2.2.4	Diamond Anvil Cell (DAC)	37
2.2.5	Mao-Bell type Diamond Anvil Cell	39
2.3	Pressure Calibration	41
2.3.1	Equation of State Method	41
2.3.2	Ruby Fluorescence Method	43
2.4	Heating of Samples in a Diamond Anvil Cell	45
2.4.1	Resistive Heating	45
2.4.2	Laser Heating	46
2.4.2.1	IR Optics	47
2.4.2.2	Nano Motion System	47
2.4.2.3	Imaging System	48
2.4.2.4	Temperature Measurement	49
2.5	High Pressure X-ray Diffraction Studies	50
2.5.1	X-ray Diffraction	50
2.5.2	Rotating Anode X-ray Diffractometer	51
2.5.3	Synchrotron Facility at INDUS-2	53
2.6	Raman Spectroscopy	54
	References	55
	CHAPTER III	62
	Exploration of Formation of Novel Intra-Group Phases involving Group IV Elements using LHDAC Technique	
3.1	Introduction	62
3.2	Experimental Details	65

3.3	Investigation of Ge-Sn Formation using Bridgman Opposed Anvil Apparatus	67
3.4	Formation of Ge-Sn Bonds at High P-T Conditions in Laser Heated Diamond Anvil Cell	68
3.5	HPXRD study of Ge-Sn Synthesized using LHDAC and Characterized at INDUS-2	75
3.6	Evidence for Ge-C Bond Formation at High P-T Conditions using <i>in-situ</i> Raman Spectroscopy	77
3.7	Investigation of Pb-C at HP-HT Conditions using LHDAC	80
3.8	Conclusion	82
	References	83
	CHAPTER IV	90
	Pressure Induced Structural Phase Transition Studies of PbFX (X=Cl, Br) Systems	
4.1	Introduction	90
4.2	Experimental Details	91
4.3	High Pressure Structural Stability Studies of PbFCl using X-ray Diffraction	93
4.4	Pressure Induced Tetragonal to Orthorhombic Structural Transition in PbFBr	102
4.5	Summary	107
	References	107
	CHAPTER V	111
	High Pressure Raman Spectroscopy of PbFCl	
5.1	Introduction	111
5.2	Experimental Details	112
5.3	Results and Discussion	113
5.4	Conclusion	122
	References	123

CHAPTER VI

126

Summary

List of Publications

132

LIST OF FIGURES

FIGURE NO	TITLE	PAGE NO
Fig.1.1	Crystal structure of β -Sn. The lattice information is taken from crystallography open data base. The space group and the atomic positions of Sn atoms are <i>I41/amd</i> and Sn (0 0 0) respectively	4
Fig.1.2	The crystal structure of <i>Cmca</i> phase of Ge. Orange red and dark green colors indicate the positions of the of Ge1 and Ge2 atoms respectively. The atomic sites of Ge1 and Ge2 are 8(f):(0.221 0.000 0.000) and 8(d):(0 0.1721 0.3138) respectively	5
Fig.1.3	Unit cell of PbFCl compound. The spheres with the labels F^- , Pb^{2+} and Cl^- represent the type of ions. The lattice information is taken from crystallography open data base. Ionic positions are Pb (0 0.5 0.2); F (0 0 0) and Cl (0 0.5 0.65).	17
Fig.2.1	Photograph of the 500 T hydraulic press. The main components are hydraulic pump, digital pressure indicator, and high current transformer	36
Fig.2.2	A schematic diagram of the opposed diamond anvil assembly	38
Fig.2.3	Home built Mao-Bell type diamond anvil cell used for high pressure experiments for this thesis	39
Fig.2.4	Ruby spectra at ambient and 6 GPa pressures. R_1 and R_2 represent two well defined ruby peaks at the wavelengths	44

694.2 nm and 692.6 nm respectively

- Fig.2.5** Schematic of the LHDAC set-up at IGCAR. M_1 - M_4 mirrors; 48
BS, beam steerer; BX, beam expander; FL_1 and FL_2 , Focusing
lenses; CL, Collecting lens
- Fig.2.6** Photograph of the LHDAC set-up at the author's laboratory. 49
The set up is mounted on a granite table. A special foundation
is made to isolate the whole set up from the rest of the
building to minimize vibrations
- Fig.2.7** Temperature measurement of Ge-Sn sample laser heated at ~ 9 50
GPa. Inset is the calibration curve generated using a standard
light source
- Fig.2.8** High Pressure Angle Dispersive X-ray Diffraction system used 52
for the high pressure experiments at our laboratory
- Fig.2.9** Lay out of Indus-2 Beam lines 53
- Fig.2.10** Renishaw *in-via* Raman spectrometer used for the Raman 55
measurements
- Fig.3.1** XRD study of Ge-Sn sample at ambient using synchrotron 67
beam at INDUS-2
- Fig.3.2** Raman Spectra of Ge-Sn before and after laser heating at 7.6 69
GPa and at other reduced pressures. The dotted line indicates
the pressure dependence of Raman modes after laser heating
- Fig.3.3** Pressure dependence of phonon modes of Ge, Sn, $GeSn_1$ and 70
 $GeSn_2$

- Fig.3.4** Raman spectra of Ge-Sn sample. The stick pattern shows the 72
frequencies (in cm^{-1}) of the phonon modes of SnO_2 , GeCl_4 , SnCl_2
and GeO_2
- Fig.3.5** HPXRD patterns of Ge+Sn system heated at ~ 9 GPa and 76
 ~ 2000 K. The stick patterns from JCPDS are matched with
the ambient pattern of Ge, Sn and the NaCl
- Fig.3.6** Raman spectra of Ge+C system at 300 K, depicting softening of 79
the Ge vibrational mode post laser heating at 9.3 GPa
- Fig.3.7** Raman spectra of Ge+C system at 300 K 80
- Fig.3.8** HPXRD pattern of Pb+C mixture pressurized up to 5.2 GPa 81
and then laser heated using CO_2 laser
- Fig.3.9** Raman spectra of Pb-C at ambient and 5.2 GPa in the graphite 82
range
- Fig.4.1** Unit cell of PbFCl compound. The spheres with the labels F^- , 91
 Pb^{2+} and Cl^- represent the type of ions. Ionic positions of
 PbFCl are Pb (0 0.5 0.2); F (0 0 0) and Cl (0 0.5 0.65)
- Fig.4.2** The angle dispersive X-ray diffraction spectra of PbFCl at 93
various pressures. The slanted arrow indicates the emergence
of new peaks. 'Au' is the pressure marker. The intensity of
 $(301)_o$ peak for the high pressure orthorhombic phase also
increases upward arrow indicates the intensity enhancement of
the new peaks. 'g' is the gasket peak. The dotted line indicates
the intensity enhancement of the new peak at around 18 GPa
- Fig.4.3** Splitting of $(101)_T$ peak of the tetragonal phase at around 38 94

GPa. The dotted line indicates the intensity enhancement of the new peak. Inset is the intensity ratio of the new peak $(200)_M$ for the monoclinic phase to the $(101)_T$ peak of the tetragonal phase

Fig.4.4 The X-ray diffraction pattern of PbFCl at ambient, 21 GPa and 95 at 38 GPa. The suffixes ‘T’, ‘O’, and ‘M’ to the (h k l) indices represent the tetragonal, orthorhombic and monoclinic phases respectively

Fig.4.5 Pressure dependence of lattice parameters and c/a ratio of 96 tetragonal phase. The pressure dependence of a and c up to 10 GPa is shown as inset

Fig.4.6 Pressure dependence derivative of lattice parameters a 98 and c of tetragonal phase

Fig. 4.7 P Vs $d_{(hkl)}$ spacings of PbFCl before and after the phase 99 transitions

Fig.4.8 P-V data of the tetragonal phase of PbFCl. The solid line is 100 the best fit to the Murnaghan equation of state

Fig.4.9 X-ray diffraction pattern of PbFBr at various pressures. The 102 stick patterns from JCPDS are matched with the ambient pattern of PbFBr. Pt (111), Pt (200) and Pt (220) are the peaks obtained from “Pt” which is used as pressure calibrant. The stick patterns of “Pt” from JCPDS are also matching well with the ambient pattern of “Pt”

Fig.4.10 The HPXRD patterns of PbFBr at ~13 GPa and ~15 GPa. The 103

dotted line indicates the increase in intensity of the new peak. The slanted arrow with the index $(120)_O$ is the new peak. Inset is to show appearance of the new peak and the new peaks are fitted to Lorentzian

- Fig.4.11** The indexing of XRD pattern at ambient and at around 15 104
GPa. The indices with subscripts “T” indicate the starting tetragonal phase and the indices with subscripts “T” and “O” indicate the mixture of tetragonal and orthorhombic phase. The Pt (111), Pt (200) and Pt (220) indicate the Pt peaks which are used as pressure calibrant
- Fig.4.13** The pressure dependence of lattice parameters and c/a ratio of 105
PbFBr
- Fig.4.14** The pressure dependence of lattice spacings $d_{(hkl)}$ of PbFBr at 105
different pressures
- Fig.4.15** P-V data of the tetragonal phase of PbFCl. The solid line is 106
the best fit to the Murnaghan equation of state
- Fig.5.1** The atomic displacements of phonon modes $A_{1g}(1)$, $A_{1g}(2)$, 114
 $E_g(1)$, $E_g(2)$ and $E_g(3)$ of PbFCl compound. This figure is drawn based on the theoretical calculations carried out by Mohammadou M’erawa *et al* to study the atomic displacements of BaFCl compound
- Fig.5.2** Raman spectra of PbFCl at various pressures. The modes are 115
designated below the ambient pattern (10^{-4} GPa). The mode named 1 belongs to the orthorhombic phase and 2 and 3 modes belonging to the monoclinic phase

- Fig.5.3** Pressure dependence of Raman modes of PbFCl. The numbers 116
1,2 and 3 indicate the pressure dependence of new modes
corresponding to the orthorhombic (mode1) and monoclinic
phases (modes 2 and 3)
- Fig.5.4** Pressure dependence of Grüneisen parameters of PbFCl. Inset 117
is the pressure vs intensity ratio between $A_{1g}(1)$ and $E_g(2)$
modes. Pressure dependence of Grüneisen parameters of
PbFCl. Inset is the pressure Vs intensity ratio between $A_{1g}(1)$
and $E_g(2)$ Raman modes
- Fig.5.5** Pressure dependence of FWHM of Raman modes of PbFCl. 119
The dotted vertical lines represent the transition pressures at ~
18 GPa and ~ 32 GPa respectively. T represents the tetragonal
phase. T and O represent the mixture of tetragonal and the
orthorhombic phases respectively. T, O and M represent the
Tetragonal, orthorhombic and the monoclinic phases
respectively.

LIST OF TABLES

TABLE	TITLE	PAGE NO
Table.3.1	Comparison of the equation of state of Ge with that reported in Ref. 24 assuming a general second order polynomial equation: $\omega \text{ (cm}^{-1}\text{)} = a_0 + a_1 p + a_2 p^2$, a_0 , a_1 and a_2 in cm^{-1} , $(\text{cm}^{-1}/\text{GPa})$ and $(\text{cm}^{-1}/\text{GPa}^2)$ respectively; P in GPa.	69
Table.3.2	Mode Grüneisen parameters of various phonon Modes at $(d\omega/dp)_{p=0}$	73
Table.4.1	Experimental and computed bulk moduli of different matlockite compounds	101
Table.4.2	Phase transition pressures of BaFCl and PbFCl compounds	101
Table 5.1	Grüneisen parameters (γ) of phonon modes $A_{1g}(1)$, $A_{1g}(2)$, $E_{1g}(1)$, $E_{1g}(2)$, $E_{1g}(3)$ and mode 3 at $P=0$	120

Chapter I

Introduction and Motivation

Pressure and temperature are the two commonly employed thermodynamic variables to vary the interatomic distances in matter. In respect of the solid state these offer the cleanest means to manipulate the bond length, bond angle and even the nature of the bonding compared to chemical means. Application of pressure and temperature separately or simultaneously can induce a variety of phase transitions (structural, electronic, magnetic-nonmagnetic, metal-insulator, normal-superconductor) and enable novel chemistry. This thesis provides example of both aspects. The first part illustrates the fascinating role that simultaneous application of pressure and temperature can play in inducing chemical bond formation between seemingly unreactive elements belonging to Group IV of the periodic table. The second part describes observation of interesting structural and dynamical behavior induced by high pressure in a class of layered mixed halides of lead, known as “Matlockites”. This introductory chapter starts with a section discussing in general terms the effect of pressure and temperature on materials (Sec.1.1). High pressure structural phase transitions of group IV elements and their structural stability studies reported in the literature are discussed next in the context of the present thesis problems with focus on X-ray diffraction and Raman spectroscopy (Sec.1.2&1.3). Motivation for studying binary systems constituted of pairs of Group-IV elements is discussed in detail in the section on IV-IV compounds (Sec.1.4). The relevance of using Laser Heated Diamond Anvil Cell technique (LHDAC) for attempting synthesis of novel

materials such as the IV-IV systems is discussed in Sec.1.5. Introduction to the second part of the thesis is precluded by a brief review of the pressure induced structural phase transitions of layered matlockite compounds in Sec.1.6&1.7. The chapter concludes with the scope of the thesis (Sec.1.8).

1.1 Effect of Pressure and Temperature on Materials

Pressure, temperature and chemical composition are the three important thermodynamic variables which determine the stability and reactions of molecules and solids [1]. By manipulating temperature and composition, a rich number of structures and compounds can be obtained. Compared to the other two variables “high pressure” has an important place in condensed matter physics. Pressure is a special case of generalized stress, by which one can change the volume of a system or the average particle density [2]. The unit of pressure used in this thesis is Pascal (Pa), $1 \text{ Pa} = 1 \text{ N/m}^2$ and $1 \text{ bar} = 10^6 \text{ dynes/cm}^2 = 10^5 \text{ Pa}$, $1 \text{ GPa} = 10^6 \text{ Pa} = 10 \text{ kbar}$. The pressure of the order of tens to hundreds of atmosphere shows significant effects on organic and inorganic chemistry. But these pressures are very low to cause any substantial changes in chemical bonding or crystal packing in condensed matter system [1]. Pressurizing materials to ~kbars and above offers a route to "breaking down" the electronic structure of the atoms and to the possibility of having entirely different bulk properties, as was first demonstrated extensively by Percy Bridgman [3]. At pressure of ~100 GPa, the energy density achieved on compression is comparable to the chemical bond energies (few electron volts) [4]. Using pressure, much more extreme states of condensed matter can be achieved as compared to the effect of temperature. As pressure causes increase the coordination number-which is related to the changes in electron hybridization-it can

induce chemical reactions that do not occur at normal conditions and also it can speed up or slow down a chemical reaction (change in chemical reactivity) [2]. The heating of the sample which is squeezed inside a high pressure apparatus can provide kinetics required for the reacting species to overcome the activation barriers and thereby react to form novel compounds [5]. In this way we can synthesize materials with exotic mechanical, optical or electronic properties.

1.2 High Pressure Behavior of Group IV Elements

The first part of the thesis describes exploration of formation of inter-group alloys or compounds involving the Group-IV elements employing the HP-HT synthesis route. According to the Hume-Rothery conditions of alloy formation, one of the conditions is the similarity of structure of the elements involved in the alloy formation. So for the HP-HT synthesis of binary alloys, it is very essential to know the high pressure behavior of the elements of interest in the required pressure range. High-pressure behavior of the elements involving the group-IV; C, Si, Ge, Sn and Pb has been the subject of many experimental and theoretical investigations [6]. These elements undergo a series of pressure induced structural phase transitions and high pressure behavior of these systems is interesting from the view point of basic research. The rest of this section gives a brief overview of the pressure induced behavior of the group-IV elements.

1.2.1 Silicon & Germanium

The properties of both Ge and Si under high pressures are almost similar. Si and Ge are indirect band-gap semiconductors and crystallize in cubic diamond structure [7]. Around

10 GPa, both Ge and Si undergo a pressure induced structural phase transition from the cubic diamond structure to the β -Sn structure. High pressure β -Sn phase of Ge has a tetragonal structure. The crystal structure of β -Sn is shown in Fig.1.1. On further applying pressure, the β -Sn phase transforms into a simple hexagonal (sh) phase via an intermediate body centered orthorhombic structure at $\sim 13.2(3)$ GPa with space group *Imma* [8-10]. Like Si, the stability range of the *Imma* phase of Ge is observed in the pressure range ~ 75 to ~ 85 GPa [10-12]. High pressure studies on Ge using nanocrystalline material reveal that the transition from β -Sn to *Imma* phase is second order phase transition whereas that of *Imma* to sh phase is of first order with the corresponding transition pressures at ~ 66 GPa and ~ 90 GPa respectively [12].

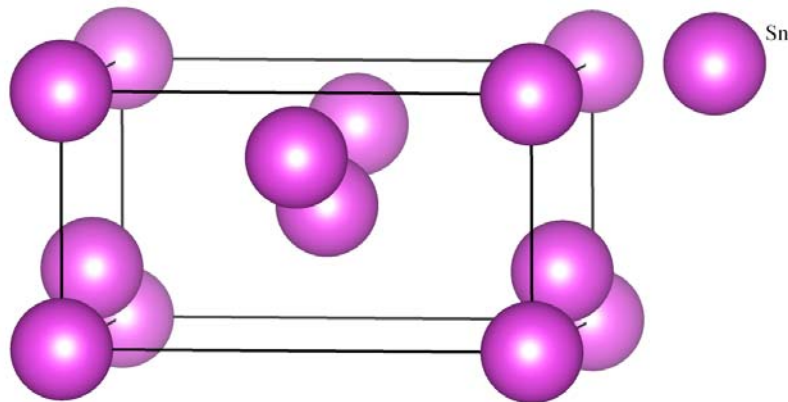


Fig.1.1. Crystal structure of β -Sn. The lattice information is taken from crystallography open data base. The space group and the atomic positions of Sn atoms are *I41/amd* and Sn (0 0 0) respectively.

For Ge at ~ 135 GPa, another high pressure phase with space group *Cmca* with 16 atoms in the unit cell are observed [13-16]. This structure does not occur in any elemental solid at ambient conditions. The *Cmca* phase of Ge is stable in the pressure

range of 91-155 GPa [17]. Angle-dispersive x-ray diffraction studies of Ge by Takemura *et al* confirms that the orthorhombic phase exists at pressures between about 100 and 170 GPa [18]. Full profile Rietveld refinement shows that this phase is an orthorhombic phase with space group *Cmca* ($Z=16$) and atom position parameters very similar to those of Si-VI stable near 42 GPa [18]. The structure of *Cmca* phase of Ge is shown in Fig.1.2. On further applying pressure to the Si and Ge systems, the *Cmca* structure undergoes a phase transition to the hexagonal-close-packed (hcp) structure. This transition is seen in Si around 41 GPa whereas that of Ge seen at much higher pressure of 160-180 GPa [18-19]. The evidence for the existence of *Cmca* phase of Si was observed for the first time by Olijnyk *et al* [16, 19-20]. The hcp structure of Si undergoes another phase transition to the face centered cubic (fcc) structure at about 87 GPa and this structure remains stable

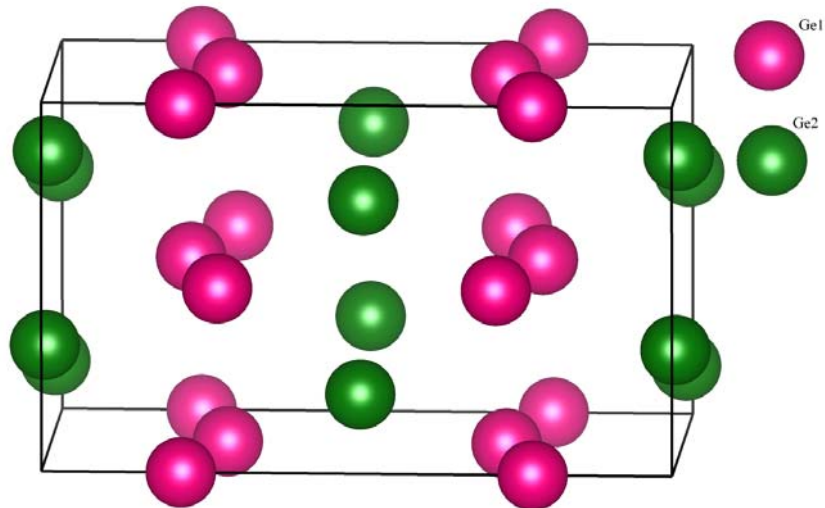


Fig.1.2 The crystal structure of *Cmca* phase of Ge. Orange red and dark green colors indicate the positions of the of Ge1 and Ge2 atoms respectively. The atomic sites of Ge1 and Ge2 are 8(f):(0.221 0.000 0.000) and 8(d):(0 0.1721 0.3138) respectively.

up to 248 GPa [21]. But the hcp structure of Ge does not undergo further phase transition up to 190 GPa [18].

In summary, the sequence of pressure induced structural phase transitions observed in Si and Ge systems are: cubic diamond (cd) \rightarrow β -Sn \rightarrow Imma \rightarrow simple hexagonal (sh) \rightarrow Cmca \rightarrow hcp. In addition to this, a further phase transition observed in Si is from hcp \rightarrow fcc at \sim 87 GPa [7]. This sequence of phase transitions indicates a monotonic increase in coordination number of the high pressure phases on increasing pressure.

When pressure is released from high pressure phase of Si and Ge systems, at room temperature, they do not directly recover to the ambient cd phase; instead they form several other high denser tetrahedral phases. If the β -Sn phase of Si is decompressed slowly, at about 10 GPa it forms rhombohedra r8 phase and also form bc8 phase at about 2 GPa [22]. This transition is found to be perfectly reversible. At normal conditions, the bc8 phase remains as a metastable phase [23]. The slow decompression of Ge β -Sn phase leads to the tetragonal st12 phase and this phase persists as metastable phase at ambient pressure [24-26]. If the pressure of the Ge sample is released rapidly, then another new phase, bc8 is formed. This phase is similar to the phase observed in Si and unlike Si this phase does not persist for a long period of time [27-28]. So when a synthesis experiment is performed with these elements, depending on the P-T conditions these phases also have to be considered. The knowledge of these phases is essential to confirm whether the phase formed is a new compound or high pressure phases of constituent elements.

1.2.2 Carbon

Antoine Lavoisier in 1792 and Smithson Tenet in 1797 demonstrated that

diamond and graphite are allotropic forms of carbon. Since then man has been interested in converting abundant graphite on the earth into the much rarer diamond [29]. Graphite is one of the pure forms of carbon and stable under normal conditions. It is built from hexagonal planes of carbon atoms stacked in an ABAB manner. The arrangement of atoms in crystals of graphite consists of parallel stacking of layers containing carbon atoms in the hexagonal rings. In graphite lattice, the carbon atoms are bonded by strong covalent bonds whereas the adjacent planes are bonded by much weaker bonds. Hence the interlayer distance (3.35 Å) of graphite is higher than that of the in-plane nearest-neighbor distance (1.42 Å). This strong anisotropy of the bonding is reflected in the elastic and vibrational properties of graphite [30]. The nearest neighbors within a layer in the graphite has stiff sp^2 covalent bonding whereas the adjacent layers are bonded by weak Van der Waals bonding which makes the graphite more compressible than diamond and also functions as a very good solid lubricant [7]. The first diamond synthesis was carried out at the General Electric Company based on the idea that diamonds can be crystallized from troilite, a rare iron sulfide mineral with the formula of FeS [29]. In this experiment, “Belt” apparatus was used to achieve high pressure. At 1650°C and 95,000 atmospheres, carbon atoms obtained from graphite or metallic carbides in the reaction mixture migrate through FeS solvent and precipitate as diamond [29]. The refractive index of the man made diamond was in the range 2.4-2.5 [31]. Yusa *et al* were successful in synthesizing diamond by converting graphite to diamond by heating the sample in a diamond anvil cell at ~13.9 GPa and around 3000 K [32]. Due to very large activation energy, the graphite to diamond transition need high pressure and high temperature of the order of (~ 5-9 GPa and 1200-2800 K) in the presence of transition-

metal catalysts. The diamond phase of carbon is insulator with indirect band gap whereas graphite is a zero gap semimetal. The high hardness of diamond is due to its sp^3 bonding. Graphene is an allotrope of carbon. It is a carbon sheet having a single or few atomic layer thicknesses which has unusual physical properties and is the fundamental building block of carbon materials including graphite. The graphite is made up of stacks of sp^2 bonded planar graphene sheets [33]. Raman spectra of all carbons have common features in the range $800\text{-}2000\text{ cm}^{-1}$ [34, 35, 36]. Carbon has a doubly degenerate, E_{2g} phonon mode at $\sim 1580\text{ cm}^{-1}$ (G peak) at the centre of the Brillouin zone. Another mode called breathing mode of sp^2 ring (D peak) is at $\sim 1350\text{ cm}^{-1}$, which requires a defect for its activation. In addition to this, graphite has a rigid layer shear mode at $\sim 42\text{ cm}^{-1}$. High pressure study of graphite shows the rigid-layer shear mode $E_{2g}(1)$ at $\sim 44\text{ cm}^{-1}$ and the in-plane mode $E_{2g}(2)$ at $\sim 1579\text{ cm}^{-1}$ increase sublinearly with pressure. High pressure study of graphene shows that the properties of graphene under compression are intrinsically similar to graphite [37].

1.2.3 Tin

Below 286 K and at normal pressure, tin transforms from the cubic diamond structure (α -Sn) into the metallic β -tin structure. The $\alpha \rightarrow \beta$ transition is accompanied by a volume collapse of $\sim 20\%$. When the sample is pressurized, around 9.5 GPa, the β -tin structure is transformed to the body-centered tetragonal structure [38]. On further pressurizing the sample, at around 40 GPa, the body centered tetragonal structure is transformed into body-centered cubic structure [39]. High pressure study of Sn has been studied up to a maximum pressure of ~ 120 GPa and do not observe any new phase at

higher pressure [40].

1.2.4 Lead

At room temperature lead crystallizes in the face-centered-cubic structure and at ~ 13 GPa, it transforms to the hexagonal-close-packed structure [41]. On further increasing the pressure, at ~ 110 GPa, a further transition from the hcp structure to bcc structure is observed [42]. In both of the above phase transitions, the change in volume is very small and there is a large region of co-existence of phases.

1.3 Pressure Dependence of Phonon Modes of Group IV Elements

Since Si and Ge are semiconductors and also these adopt different crystal structures at high pressure, it is very interesting to study the pressure dependence of phonon modes of these elements. Most of the studies on these materials have been aimed at finding the mode Grüneisen parameter which gives the information about the lattice-dynamical properties (anharmonicity) of the materials. The first-order Raman spectra of these materials are obtained by the scattering of long-wavelength optical phonons. In polar semiconductors with different atoms in the unit cell, a study of the splitting of longitudinal optical (LO) and the transverse optical (TO) phonon modes give information of the dependence of their ionicity on volume [19]. The first order optical vibrational modes of lattices of diamond structure are Raman active, but not infrared active [43]. The first order Raman spectra of Si and Ge are reported at $\sim 520.2 \pm 0.5 \text{ cm}^{-1}$ and $\sim 300.7 \pm 0.5 \text{ cm}^{-1}$ respectively [44]. Both Ge and Si undergo phase transformations at ~ 10 GPa and ~ 12 GPa respectively [43, 19]. A group-theoretical analysis of lattice vibrations in the β -tin lattice shows that at the Γ point of the Brillouin zone the optical modes have

one LO phonon mode and a doubly degenerate TO mode. Both of the above modes are Raman active. The Raman spectra of Si in its high pressure β -Sn phase shows the frequency of the TO mode increases with pressure whereas that of LO mode decreases and broadens with pressure. In Ge, the frequency of TO mode increases with pressure similar to Si whereas LO mode initially increases with pressure and reaches a maximum value at ~ 50 GPa [45].

Graphite is built from hexagonal planes of carbon atoms and it contains four atoms in the unit cell with space group $P63/mmc$ (D_4^{6h}) [46]. The irreducible representations of the zone-center optic modes can be decomposed into the following [47-48]

$$\Gamma = A_{2u} + 2B_{2g} + E_{1u} + 2E_{2g}$$

where the A_{2u} and E_{1u} modes are IR active modes, observed at ~ 867 and ~ 1588 cm^{-1} respectively. The E_{2g} modes are Raman active, which are observed at ~ 42 and ~ 1581 cm^{-1} . The B_{2g} modes are optically inactive. One of these modes has been reported at ~ 127 cm^{-1} and the other nearer to A_{2u} using neutron scattering experiments. The Ramp-Wave Compression (RWC) techniques show that the diamond phase of carbon is stable and strong up to 800 GPa [50]. In the case of Ge, the TO mode shifts to higher frequencies with increasing pressure, whereas the LO mode frequency initially increases slightly with pressure and reach a maximum at around 50 GPa [45].

The Raman study of tin shows that at ambient pressure two phonon modes at ~ 42.5 cm^{-1} and ~ 126.6 cm^{-1} [49]. Both of the above modes are blue shifted with pressure and the initial slope of TO phonon mode is five times that of LO phonon mode [49]. At

room temperature tin has tetragonal (β -tin) structure with 2 atoms in the unit cell and has three acoustical and three optical branches [49]. Group theoretical analysis carried out by Chen shows that at the Γ point of the Brillouin zone, the optical modes consist of one LO branch and a doubly degenerate TO branch at higher frequencies [51]. The phonon dispersion relations for acoustical and the optical branches for β -Sn at 110 K was studied by Rowe using inelastic neutron scattering experiments [52]. In this study, he reported the phonon dispersion relation of symmetry and some nonsymmetry branches with wave vectors along the $[0, 0, \zeta]$, $[1,0,\zeta]$, $[\zeta,0,0]$ and $[\zeta, \zeta, 0]$ (Λ , V , Σ and Δ) directions. The effect of pressure on Γ (TO) phonon mode is affected much more than that of Γ (LO). In the case of lead, it doesn't have any Raman active modes.

1.4 IV-IV Systems

The intra group-IV semiconductor alloys formed from Carbon, Silicon, Germanium and Tin have immense potential for applications in the next generation of electronic and photonic devices [53-54]. The alloys and compounds of Si-Ge, Si-Sn and Ge-Sn are expected to be having unique optoelectronic properties for usage in quantum-well inter-subband technology [55]. The band gap and strain engineering of Si/SiGe heterostructures can be possible using silicon technology to improve the microelectronic device performance. The $\text{Ge}_{1-x}\text{Sn}_x$ alloys with diamond cubic structures are very important in the optoelectronic industry due to the theoretical prediction and the experimental evidence for the existence of tunable direct band gap [56]. The band structure calculations of germanium carbide (Ge-C) predict its properties are similar to Si-C, and can be used in electronic and optoelectronic applications. Also it has a wide

band gap, high bulk modulus and its percentage of covalency is comparable to Si-C [57]. The high pressure study on Si-C using ab initio pseudopotential calculation predicts the zinc-blende structure of Si-C transforms into the rocksalt phase at hydrostatic pressure of 66 ± 5 GPa [58]. This section describes some of the important IV-IV systems and highlights the novel techniques adopted to form them.

1.4.1 Si-Ge System

Si-Ge is a technologically important alloy due to its range of applications in Optoelectronic devices including mobile phones. Since the development of Si-Ge has improved the performance of silicon transistors using the developments of the Si-Ge heterostructure bipolar transistor (HBT) and strained-Si complementary metal oxide semiconductor (CMOS) technologies [53]. It is expected that in future all silicon based transistors, electronic and optoelectronic devices might be having some Si-Ge material [53]. At ambient pressure, the Si-Ge system forms a complete solid solution and is used in heterojunction bipolar devices [59]. Using Si technology, the band-gap and strain of Si/SiGe heterostructures can be engineered [53]. The $\text{Si}_{1-x}\text{Ge}_x$ alloy crystallizes in cubic diamond structure with the Si and Ge atoms distributed randomly [60]. Both Ge and Sn systems are indirect band gap semiconductors. The atomic radii ratio of Ge and Si is below 15 %, both of them have same crystal structures at ambient pressure. Hence they easily form a complete Ge-Si solid solution [61]. McGaff *et al* reported the high pressure synthesis of Ge-Si solid solution in β -Sn structure [60]. In this study they recovered Ge-Si alloy from the HP-HT conditions of ~ 15 GPa and ~ 1500 K. The atomic and electronic properties of the recovered Ge-Si phase were different from those of cubic Ge-

Si alloy.

1.4.2 Si-C System

Silicon carbide (Si-C) is a wide band-gap semiconductor and it has electronic, optoelectronic, optical, thermal and mechanical applications in high-power and high temperature devices. Due to its unique mechanical, chemical, electrical and thermal properties, it is used in various technological applications. Under normal conditions, it adopts many stable and long-range ordered modifications (polytypes) [62]. Due to its outstanding mechanical properties, Si-C is used as an abrasive. The bulk modulus of Si-C is quite high (321.9 GPa) [63].

A considerable number of research work has been reported to find the suitable experimental conditions to achieve high quality c-SiC films to grow pseudomorphically on silicon surfaces [64]. For that, several carbon sources have been reported to grow silicon carbide films on Si. For the synthesis of c-SiC films, the substrate temperature plays a crucial role to incorporate carbon atoms in the silicon matrix. The c-SiC films can be synthesized by the exposure of a hot silicon substrate at the temperature range between 600 and 900°C to acetylene, ethylene, graphite and C₆₀ [65].

1.4.3 Ge-Sn System

Ge-Sn alloy is expected to have more potential applications than Si-Ge due to the prediction of direct band gap formation and lattice matching with Si [66-67]. The thermodynamic solubility of Sn in Ge is less than 0.5 at %, while that of Ge in Sn is zero [68]. Thin films of Ge_{1-x}Sn_x alloy have been synthesized using chemical vapor

deposition (CVD) methods [69], pulsed UV laser annealing using excimer lasers etc [70]. The electronic theory based on pseudo potentials and the virtual crystal approximation predicts the formation of a bulk Ge-Sn solid solution under high pressure [71]. A first principle calculation based on density functional theory predicts the stability of Ge-Sn alloy in the zinc-blende phase up to 9 GPa [72]. However, the bulk synthesis of Ge-Sn has not been realized yet. The challenges involved in the bulk synthesis of Ge-Sn are large lattice mismatch, low solubility, different crystal structures and different electro negativities of Ge and Sn at ambient pressure. Recently, bulk synthesis of a $\text{Ge}_{0.9}\text{Sn}_{0.1}$ system has been reported using piston-cylinder apparatus or multi-anvil press at ~ 2000 K and in a narrow pressure range of 9-10 GPa. The structural phase transitions in both Ge (diamond-type to β -Sn-type) and Sn (β -Sn to bct-Sn) in this narrow pressure range are deemed important to bring about the reaction on account of optimal match of the atomic radii and electronic structures [73-74]. In the section 1.5, we discuss the requirement of fast quenching of the sample laser heated at predetermined pressure using the laser Heated Diamond Anvil Cell technique (LHDAC).

1.4.4 Ge-C System

The Ge-C and Sn-C alloy systems formed as thin films on Si substrate seem to be a wide range of tunable band gap energies extending from the infrared to the near ultraviolet region of the electromagnetic spectrum. Since the elemental constituents forming the Ge-C, Sn-C, Ge-Sn etc alloys are immiscible under normal P and T conditions, the epitaxial stabilization of these alloys were attempted by various workers. The structural, electronic and optical properties of Ge-C epitaxial films have been

investigated both experimentally and theoretically [75-76]. Total energy calculations at 0 K based on pseudo potential approximation done by Sankey *et al* shows that Ge-C is unstable towards bond formation up to ~15 GPa [77]. But in this calculation, the energy released during the phase transition from cubic diamond to β -Sn structure at around 9 GPa was not taken into account. In addition, if the above energy released during phase transition was included in the total energy of the system, then it would change the transition pressure value. Also, the calculations based on the density functional theory shows that there is a propensity towards stable Ge-C alloy formation only above ~25 GPa and in this calculation also, the energy released during the phase transition from cubic diamond to β -Sn at around 9 GPa is not taken into account [75]. The bulk synthesis of these completely immiscible systems is not successful using conventional methods.

1.5 Relevance of LHDAC Technique for the High Pressure-High Temperature Synthesis of IV-IV Systems

Laser-heated diamond anvil cell technique (LHDAC) is a unique method to attain ultrahigh static pressure and temperature conditions of $P > 200$ GPa and $T \sim 12000$ K [78-80]. After the invention of LHDAC in late 1960s, it has been coupled with various experimental techniques such as *in situ* Synchrotron x-ray diffraction [80], X-ray spectroscopy [81], optical spectroscopy [78] and visual observations [82-83]. Using this technique, a variety of materials such as silicates, oxides, metals and metal alloys have been subjected to extreme pressures and temperatures. The equations of state, crystal structures and structural dynamics of these materials have been examined by *in situ* x-ray diffraction and Raman spectroscopy. This technique is also used to synthesize novel and

super-hard materials under high pressure and temperature conditions. The laser heating of the sample squeezed between the diamond anvils in a DAC is used to provide the kinetics necessary for the reactant species to overcome the activation barriers and react to form novel materials which may have exotic properties [5].

Except “Si-C”, the formation of other compounds from group IV elements is not successful by the conventional equilibrium methods. Non-equilibrium techniques like pulsed laser ablation, chemical vapor deposition, molecular beam epitaxy and sputtering were employed to synthesize thin films of binary alloys from group IV elements. The difficulty in the bulk synthesizing of IV-IV compounds are due to their small electro negativity difference, low and positive formation enthalpy, large difference between the melting points of the elements (For example, Ge (1211 K) and Sn (505.1 K)), surface segregation of one of the elemental components due to low surface energy and difference in their structures at ambient P and T [63, 84-85]. Fast heating and quenching of samples at high pressure, mimicking nearly non-equilibrium conditions, can be achieved by employing a high power infra red laser focused on to the sample in a DAC [86]. The LHDAC technique has not yet been exploited to explore formation of the IV-IV systems. Apart from easily arriving at the required P-T conditions, the technique also paves way for *in situ* characterization vide XRD or optical spectroscopy. For instance Raman spectroscopy of laser heated mixtures of IV-IV elements at high pressure can instantaneously reveal signatures of new bond formations, if any.

1.6 Matlockite Compounds

The second part of the thesis describes the role of pressure in the structural behavior of layered matlockite compounds. The experimental study of the effect of

pressure on the structural properties of layered ionic compounds has been extensively investigated due to their importance in geophysics, and also to understand how the high pressure affects weak and strong bonds in condensed matter [87]. Ionic layered compounds of the form MF₂X, where M is a divalent metallic cation (Ca²⁺, Sr²⁺, Ba²⁺, Pb²⁺ or Eu²⁺) and X = Cl⁻, Br⁻ or I⁻, crystallize in tetragonal structure with space group *P4/nmm* [88]. A typical unit cell of MF₂X has two formula units in which the arrangement of atomic layers perpendicular to the c-axis is in the following sequence

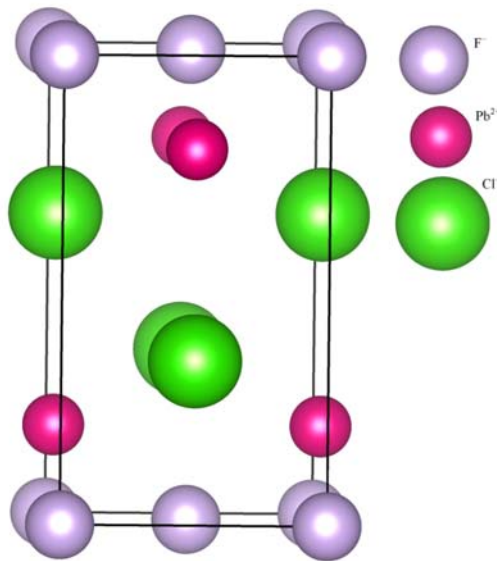
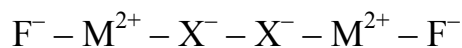


Fig.1.3. Unit cell of PbFCl compound. The spheres with the labels F⁻, Pb²⁺ and Cl⁻ represent the type of ions. The lattice information is taken from crystallography open data base. Ionic positions are Pb (0 0.5 0.2); F (0 0 0) and Cl (0 0.5 0.65).



The unit cell of PbFCl compound (matlockite) is shown in Fig.1.6. These materials have interesting properties such as photoconductivity [89], photoluminescence [90] and aniso-

tropic ionic conductivity [91] and find application in various fields. For example, BaFBr doped with Eu^{2+} ($\text{BaFBr}:\text{Eu}^{2+}$) has been successfully applied for detecting X-rays as Imaging phosphors due to the photo stimulated luminescence property [92]. Similarly $\text{BaFCl}:\text{Sm}^{2+}$ is used as a pressure sensor in the high pressure experiments [93]. Though the bonding in the solid is primarily ionic, the binding is weak between the two Cl^- layers. The apparent binding between the Cl^- layers stems from the large polarizability of Cl^- ions and Coulombic attraction exerted on the Cl^- ions in one layer by the M^{2+} ions in the second nearest neighbor layer. These therefore have anisotropic bonding scheme which manifests in their physical properties such as compressibility, conductivity and optical properties.

1.7 Structural Stability of Matlockite Compounds under High Pressure

1.7.1 HPXRD Studies

High pressure structural stability of the layered matlockite compounds BaFCl and BaFBr have been reported up to a maximum pressure of ~ 35 and ~ 60 GPa respectively [94-95]. These systems undergo a series of symmetry lowering structural transitions: tetragonal \rightarrow orthorhombic \rightarrow monoclinic and have been attributed to a gradual anisotropic distortion of the charge distribution in the planes perpendicular to the stacking direction [94-96]. In BaFCl system at around 10.8 GPa, the starting tetragonal phase is transformed to the orthorhombic phase and on further applying pressure, at around 21 GPa, the orthorhombic phase is transformed into monoclinic phase with space group $P2_1/m$. Similarly, the BaFBr compound undergoes a pressure induced structural transition from starting tetragonal phase to monoclinic phase via an intermediate

orthorhombic phase at around 12 and 27 GPa respectively. The phase transition reported is sluggish in nature probably due to the small Gibb's free energy differences between the parent and daughter phases [97]. Observation of co-existence of parent and high pressure phases are reported in these compounds [95, 97]. High pressure study of BaFI compound has been reported up to a maximum pressure of ~102 GPa [95]. The study shows that like other matlockite compounds, this compound also undergoes a similar structural phase transitions at around 2.4 and 55 GPa respectively [95]. The reason for this sequence of phase transitions in these compounds is explained below. In MFX (M=Ba and X=Cl, Br or I) compounds, the adjacent X^- ion layers are bonded by weak ionic bonding. There exists an attraction of the M^{2+} ions with both X^- and F^- ions. Similarly there exists repulsion between the adjacent layers containing halide ions (Fig.1.3). Since the pressure affects primarily on weak bonding, as the pressure is increased, there will be large compression of weakly bonded X^- ions along the c-axis. Due to this anisotropic compression of electron charge density of X^- ions along the c-axis, the redistribution of electron charge density along a-b plane causes the distortion of the lattice [94]. The structural stability of these compounds is due to the combined effect of anisotropic coordination of the halogen X^- ions and the large polarizability of M^{2+} and X^- ions [94].

1.7.2 Raman Spectroscopy of Matlockites

In-situ Raman spectroscopy is a powerful tool to study the structural stability and lattice dynamics of matlockite compounds and is being used as a short-range order probe. The BaFX (X = Cl, Br and I) crystallizes in PbFCl type tetragonal symmetry D_{4h}^7 or $P4/nmm$ with two formula units per unit cell. The site symmetries of barium and halogen

(Cl, Br and I) atoms are C_{4v} and at D_{2d} . Factor group analysis of the $PbFCl$ compound with space group $P4/nmm$ and having two formula units in the unit cell, shows that the following vibrational modes can be expected at the centre of the Brillouin zone [95, 98-101]

$$\Gamma_{18} = 2A_{1g} + B_{1g} + 3E_g + 3E_u + 3A_{2u}$$

There are six Raman active modes namely $2A_{1g}$, B_{1g} and $3E_g$, four IR active modes; $2A_{2u}$ and $2E_u$ and two acoustic modes; A_{2u} and E_u . The modes $E_g(1,2,3)$ correspond to the atomic motion of M (Pb or Ba), Cl and F along b-axis. The modes $A_{1g}(1,2)$ belong to the anti symmetric vibration of M (Pb or Ba) and Cl atoms along c-axis. The mode B_{1g} corresponds to the anti symmetric vibration of F-atoms along c-axis [99].

The pressure dependence of the phonon modes of BaFI compound is studied by Decremps *et al* up to the phase transition near 55 GPa [95]. They observed a large variation of Grüneisen parameter of the A_{1g} phonon mode between 0 and 10 GPa and the variation is attributed to a gradual layer-nonlayer transformation of the compound under pressure.

1.8 Scope of the Thesis

This thesis focuses on two major themes. The first part discusses exploratory experiments to attempt synthesis of binary compounds like Ge-Sn, Ge-C and Pb-C formed from the elements involving group IV of the periodic table. These compounds cannot be synthesized by using conventional equilibrium techniques. But the synthesis can be possible by non-equilibrium techniques. For this thesis work, HP-HT route using Laser heated diamond anvil cell technique has been adopted. The second part of the thesis

reveals high pressure study of matlockite compounds in the form MFX where M= Pb and X=Cl or Br. This work is aimed at understanding the structural phase transitions in matlockite compounds.

This thesis consists of six chapters. Chapter II of this thesis presents the details of the various experimental tools and the characterization techniques used. Also it gives a brief description of pressure generating devices like Bridgman HP-HT cell and diamond anvil cell. The characterization tools used for this work viz high-pressure diffractometer that employs a RIGAKU rotating anode X-ray generator (UltraX 18) as the source and imaging plate detector, Raman spectroscopy and the angle dispersive X-ray diffraction facility at INDUS-2 are described briefly. Chapter III explains the synthesis of intra-group alloys/compounds involving group IV elements of the periodic table. The successful synthesis of Ge-Sn system by LHDAC technique as indicated by *in situ* Raman spectroscopy is discussed. Also attempts to synthesize Ge-C and Pb-C systems are presented in this chapter. Chapter IV describes high pressure structural behavior of matlockite compounds. The layered matlockite compounds such as PbFCl and PbFBr were synthesized using solid state reaction method and high pressure studies on these compounds was studied up to ~47 GPa and ~17 GPa respectively using X-ray diffraction technique. Similar to BaFX (X=Cl, Br or I) systems, PbFCl also undergoes pressure induced structural phase transitions in the sequence: tetragonal \rightarrow orthorhombic at ~18 GPa and orthorhombic \rightarrow monoclinic at ~38 GPa. In PbFBr, tetragonal to orthorhombic transition was observed at around 13 GPa. The bulk moduli of these compounds were obtained from their P-V variation and compared to similar matlockite compounds. Chapter V of this work presents high pressure Raman spectroscopy of PbFCl compound

up to ~41 GPa. The pressure dependence of phonon modes of PbFCl at ambient pressure and also new modes formed at high pressures are also discussed. The variation of $A_{1g}(2)$, $E_g(2)$ and $E_g(3)$ modes with pressure are almost similar. But the behavior of $A_{1g}(1)$ mode with pressure is totally different. This mode shows an anomalous behavior. The anomalous behavior of this mode can be due to the weakly bonded adjacent chloride ion layers along the c-axis. The instability of $A_{1g}(1)$ mode above ~24 GPa is due to the change of nature of bonding from layer to non-layer type. The Grüneisen parameters of all the modes are calculated. Finally in chapter VI a summary of the thesis and potential future research relevant to the present work are discussed.

References

- [1] Paul F. McMillan, “Chemistry of materials under extreme high pressure-high temperature conditions” *Chem. Commun.* 919-923 (2003)
- [2] Russell J. Hemley and Neil W. Ashcroft, “The Revealing Role of Pressure in the Condensed Matter Sciences” *Physics Today* **51** 26-32 (1998)
- [3] P. W. Bridgman, “Physics of High Pressure”, (Dover, New York, 1976)
- [4] Raymond Jeanloz, “Physical Chemistry at Ultrahigh Pressures and Temperatures” *Annu. Rev. Phys. Chem.* **40** 237-259 (1989)
- [5] N. Subramanian, N. V. Chandra Shekar, N. R. Sanjay Kumar and P. Ch. Sahu, “Development of laser-heated diamond anvil cell facility for synthesis of novel materials” *Current Science* **91** 175-182 (2006)
- [6] Steven P. Lewis and Marvin L. Cohen, “Theoretical Study of Raman modes in

- high-pressure phases of Si, Ge, and Sn” *Physical Review B* **48** 3646-3653 (1993)
- [7] M. Mujica, Angel Rubio, A. Munoz and R. J. Needs, “High-pressure phases of group-IV,III-V and II-VI compounds” *Review of Modern Physics* **75** 863-912 (2003)
- [8] M. I. McMahon and R. J. Nelmes, “New high-pressure phase of Si” *Physical Review B* **47** R8337- R8340 (1993)
- [9] Steven P. Lewis and Marvin L. Cohen, “Theoretical study of high-pressure orthorhombic silicon” *Physical Review B* **48** R16144-R16147 (1993)
- [10] Steven P. Lewis and Marvin L. Cohen, “Prediction of an Orthorhombic phase of Germanium” *Solid State Communications* **89** 483-486 (1994)
- [11] R. J. Nelmes, H. Liu, S. A. Belmonte, J. S. Loveday, and M. I. McMahon, “Imma phase of germanium at ~80 GPa” *Physical Review B* **53** R2907-R2909 (1996)
- [12] Xiao-Jia Chen, Chao Zhang, Yue Meng, Rui-Qin Zhang, Hai-Qing Lin, Viktor V. Struzhkin, and Ho-kwang Mao, “ β -tin \rightarrow Imma \rightarrow sh phase transitions of Germanium” *Physical Review Letters* **106** 135502-135504 (2011)
- [13] U. Schwarz, K. Takemura, M. Hanfland, and K. Syassen, “Crystal Structure of Cesium-V” *Physical Review Letters* **81** 2711-2714 (1998)
- [14] M. I. McMahon, R.J. Nelmes, N. G. Wright and D. R. Allan, “Pressure dependence of the Imma phase of silicon” *Physical Review B* **50** 739-743 (1994)
- [15] M. Hanfland, U. Schwarz, K. Syassen and K. Takemura, “Crystal Structure of the High-Pressure Phase Silicon VI” *Physical Review Letters* **82** 1197-1200 (1999)

- [16] Filipe J. Ribeiro and Marvin L. Cohen, “Theoretical prediction of the high-pressure phase Ge-Cmca” *Physical Review B* **62** 11388- 11391 (2000)
- [17] Mujica, S. Radescu¹, A. Munoz and R J Needs, “High-pressure phases of germanium” *J. Phys.: Condens. Matter* **13** 35-42 (2001)
- [18] K. Takemura, U. Schwarz, K. Syassen, M. Hanfland, N. E. Christensen, D. L. Novikov and I. Loa, “High-pressure Cmca and hcp phases of germanium” *Physical Review B* **62** R10603- R10606 (2000)
- [19] H. Olijnyk, S. K. Sikka and W. B. Holzapfel, “Structural Phase Transitions in Si and Ge under pressures up to 50 GPa” *Physics Letters* **103A** 137-140 (1984)
- [20] Yogesh K. Vohra, Keith E. Brister, Serge Desgreniers, Arthur L. Ruoff, K. J. Chang and Marvin L. Cohen, “Phase-Transition Studies of Germanium to 1.25 Mbar” *Physical Review Letters* **56** 1944-1947 (1986)
- [21] Steven J. Duclos, Yogesh K. Vohra, and Arthur L. Ruoff, “Experimental study of the crystal stability and equation of state of Si to 248 Gpa” *Physical Review B* **41** 12021-12028 (1990)
- [22] J. Crain, G. J. Ackland, J. R. Maclean, R. O. Piltz, P. D. Hatton, and G. S. Pawley, “Reversible pressure-induced structural transitions between metastable phases of silicon” *Physical Review B* **50** R13043-R13046 (1994)
- [23] J. Crain, S. J. Clark, G. J. Ackland, M. C. Payne, V. Milman, P. D. Hatton, “Theoretical study of high-density phases of covalent semiconductors. I. Ab initio treatment” *Physical Review B* **49** 5329- 5340 (1994)

- [24] J. S. kasper and S. M. Richards, “The Crystal Structures of New Forms of Silicon and Germanium” *Acta Crystallogra.* **17** 752-755 (1964)
- [25] F. P. Bundy and J. S. Kasper, “A New Dense Form of Solid Germanium” *Science* **139** 340-341 (1963)
- [26] R. J. Nelmes, M. I. McMahon, N. G. Wright, D. R. Allan and J. S. Loveday, “stability and crystal structure of BCS germanium” *Physical Review B* **48** R9883-R 9886 (1993)
- [27] S. B. Qadri, E. F. Skelton and A. W. Webb, “High pressure studies of Ge using synchrotron radiation” *J. Appl. Phys.* **54** 3609 (1983)
- [28] Carmen S. Menoni, Jing Zhu Hu and Ian L. Spain, “Germanium at high pressures” *Physical Review B* **34** 362- 368 (1986)
- [29] H. Tracy Hall, “The Synthesis of Diamond” *Journal of Chemical Education* **38** 484-489 (1961)
- [30] M. Hanfland, H. Beister and K. Syassen, “Graphite under pressure: Equation of state and first-order Raman modes” *Physical Review B* **39** 12598- 12603 (1989)
- [31] F. P. Bundy, H. T. Hall, H. M. Strong and R. H. Wentorf, “Man made diamonds” *Nature* **176** 51-55(1955)
- [32] H. Yusa, K. Takemura, Y. Matsui, H. Morishima, and K. Watanabe, H. Yamawaki and K. Aoki, “Direct transformation of graphite to cubic diamond observed in a laser-heated diamond anvil cell” *Appl. Phys. Lett.* **72** 1843-1845 (1998)
- [33] Joe Hodkiewicz, “Characterizing Carbon Materials with Raman Spectroscopy”

Thermo Fisher Scientific, Madison, WI, USA

- [34] T. M. G. Mohiuddin, A. Lombardo, R. R. Nair, A. Bonetti, G. Savini, R. Jalil, N. Bonini, D. M. Basko, C. Galiotis, N. Marzari, K. S. Novoselov, A. K. Geim and A. C. Ferrari, “Uniaxial strain in graphene by Raman spectroscopy: *G* peak splitting, Grüneisen parameters, and sample orientation” *Physical Review B* **79** 2 05433 (1-8) (2009)
- [35] C. Ferrari and J. Robertson, “Interpretation of Raman spectra of disordered and amorphous carbon” *Physical Review B* **61** 14095-14107 (2000)
- [36] F. Tuinstra and J. L. Koenig, “Raman Spectrum of Graphite” *J. Chem. Phys.* **53** 1126-1130 (1970)
- [37] John E. Proctor, Eugene Gregoryanz, Konstantin S. Novoselov, Mustafa Lotya, Jonathan N. Coleman and Matthew P. Halsall, “High-pressure Raman spectroscopy of graphene” *Physical Review B* **80** 073408(1-4) 2009
- [38] J. D. Barnett, V. E. Bean, and H. T. Hall, “X-Ray Diffraction Studies on Tin to 100 kilobars” *J. Appl. Phys.* **37** 875-877 (1966)
- [39] H. Olijnyk and W. B. Holzapfel, *J. Phys. (Paris) Colloq.* **45** Suppl. 11, C8-153 (1984)
- [40] Serge Desgreniers, Yogesh K. Vohra and Arthur L. Ruoff, “Tin at high pressure: An energy-dispersive x-ray-diffraction study to 120 GPa” *Physical Review B* **39** 0359-10361 (1989)
- [41] T. Takahashi, H. K. Mao and W. A. Bassett, “X-ray diffraction study of a high-pressure polymorph” *Science* **165** 1352-1353 (1969)

- [42] H. K. Mao, Y. Wu, J. F. Shu, J. Z. Hu, R. J. Hemley and D. E. Cox, ‘High pressure phase transition and equation of state of lead to 238 GPa’ *Solid State Communications* **74** 1027-1029 (1990)
- [43] Diego Olego and Manuel Cardona, ‘Pressure dependence of Raman phonons of Ge and 3C-SiC’ *Physical Review B* **25** 1151- 1160 (1982)
- [44] J. H. Parker, D. W. Feldman and M. Ashkin, ‘Raman Scattering by Silicon and Germanium’ *Physical Review B* **155** 712-714 (1967)
- [45] Helmut Olijnyk, ‘Raman Scattering in Metallic Si and Ge up to 50 GPa’ *Physical Review Letters* **68** 2232- 2234 (1992)
- [46] Stephanie Reich and Christian Thomsen, ‘Raman spectroscopy of graphite’ *Phil. Trans. R. Soc. Lond. A* **362**, 2271-2288 (2004)
- [47] K. K. Mani, R. Ramani, ‘Lattice Dynamics of Graphite’ *physica status solidi (b)* **61** 659-668 (1974)
- [48] R. J. Nemanich and S. A. Solin, ‘First- and second-order Raman scattering from finite-size crystals of graphite’ *Physical Review B* **20** 392-401 (1979)
- [49] Helmut Olijnyk, ‘Pressure dependence of Raman phonons of metallic β -Sn’ *Physical Review B* **46** 6589- 6591 (1992)
- [50] D. K. Bradley, J. H. Eggert, R. F. Smith, S. T. Prishrey, D. G. Hicks, D. G. Braun, J. Biener, V. Hamza, R. E. Rudd and G. W. Collins, ‘Diamond at 800 GPa’ *Physical Review Letters* **102** (075503-1)-(075503-4) (2009)
- [51] S. H. Chen, ‘Group-Theoretical Analysis of Lattice Vibrations in Metallic β -Sn’ *Physical Review* **163** 532-546 (1967)

- [52] J. M. Rowe, "Crystal Dynamics of Metallic β -Sn at 110° K" *Physical Review* **163** 547-551 (1967)
- [53] Douglas J Paul, "Si/SiGe heterostructures: from material and physics to devices and circuits" *Semicond. Sci. Technol.* **19** R75-R108 (2004)
- [54] Ravindra Pandey, Michel Rerat and Mauro Causa, "First-principles study of stability, band structure, and optical properties of the ordered Ge_{0.50} Sn_{0.50} alloy" *Applied Physics Letters* **75** 4127-4129 (1999)
- [55] Richard A. Soref, "Silicon-based group IV heterostructures for optoelectronic Applications" *J. Vac. Sci. Technol. A* **14** 913-918 (1996)
- [56] Gang He and Harry A. Atwater, "Interband Transitions in Sn_xGe_{1-x} Alloys" *Physical Review Letters* **79** 1937-1940 (1997)
- [57] A. Mahmood, L. Enrique Sansores, "Band structure and bulk modulus calculations of germanium carbide" *J. Mater. Res.* **20** 1101-1106 (2005)
- [58] K. J. Chang and Marvin L. Cohen, "Ab initio pseudo potential study of structural and high-pressure properties of Si-C" *Physical Review B* 358196-8201 (1987)
- [59] J. Schilz and V. N. Romanenko, "Bulk growth of silicon-germanium solid-solutions-Review, *J. Mater. Sci. Mater Electron.* **6** 265-279 (1995)
- [60] J. McGaff, G. Serghiou and D. J. Frost, "Metal nitride and alloy synthesis using high pressures and temperatures" *High Pressure Research* **28** 491-495 (2008)
- [61] J. F. Shackelford, Introduction to Materials Science for Engineers, *Prentice Hall*, NewYork, 1999
- [62] P. Kackell, B. Wenzien, and F. Bechstedt, "Influence of atomic relaxations on the structural properties of SiC polytypes from ab initio calculations" *Physical Review*

B **50** 17037- 17046 (1994)

- [63] Charles Kittel, “Introduction to Solid State Physics”, Eighth Edition, John Wiley & Sons, P.51
- [64] M. De Crescenzi, R. Bernardini, R. Gunnella, P. Castrucci, “Structure and morphology of c-SiC films obtained by acetylene reaction with Si(111) surface” *Solid State Communications* **123** 27-32 (2002)
- [65] G. Dufour, F. Rochet, F.C. Stedile, Ch. Ponchey, M. De Crescenzi, R. Gunnella and M. Froment, “SiC formation by reaction of Si(001) with acetylene: Electronic structure and growth mode” *Phys. Rev. B* **56** 4266-4282 (1997)
- [66] P. Ball, “Let there be light” *Nature* **409** 974-976 (2001)
- [67] P. Zhang, V. H. Crespi, E. Chang, S. G. Louie and M. L. Cohen, “Computational design of direct-band gap semiconductors that lattice-match silicon” *Nature* **409** 69-71 (2001)
- [68] R. W. Olesinski and G. J. Abbaschian, *J. Phase Equilibria* **5** 2659(1984)
- [69] J. Taraci, S. Zollner, M. R. McCartney, J. Menendez, M. A. Santana-Aranada, D. J. Smith, A. Haaland, A. V. Tutukin, G. Gunderson, G. Wolf and J. Kouvetakis, “Synthesis of Silicon-Based Infrared Semiconductors in the Ge-Sn System Using Molecular Chemistry Methods” *J. Am. Chem. Soc.* **123** 10980-10987 (2001)
- [70] S. Oguz, W. Paul, T. F. Deutsch, B-Y. Tsaur and D. V. Murphy, “Synthesis of metastable, semiconducting Ge-Sn alloys by pulsed UV laser crystallization” *Appl. Phys. Lett.* **43** 848-850 (1983)

- [71] T. Soma, K-I. Kamada and H-M. Kagaya, "Prediction of α -phase Ge-Sn solid" *Solid State Communications* **67** 155-158 (1988)
- [72] R. Pandey, M. Rerat, M. Causa, "First-principles study of stability, band structure, and optical properties of the ordered Ge_{0.50}Sn_{0.50} alloy" *Appl. Phys. Lett.* **75** 4127-4129 (1999)
- [73] Christophe Guillaume, George Serghiou, Andrew Thomson, Jean-Paul Morniroli, Dan J. Frost, Nicholas Odling and Mohamed Mezouar, "Tuning between Mixing and Reactivity in the Ge-Sn System Using Pressure and Temperature" *J. Am. Chem. Soc.* **131** 7550-7551 (2009)
- [74] G. Serghiou, C. L. Guillaume, C. E. Jeffree, A. Thomson, D. J. Frost, J. P. Morniroli and N. Odling, "Imaging of mixing and reaction in group IV systems recovered from high pressures and temperatures" *High Pressure Research* **30** 44-50 (2010)
- [75] Ravindra Pandey, Michel Rerat, Clovis Darrigan and Mauro Causa, "A theoretical study of stability, electronic, and optical properties of GeC and SnC" *Applied Physics Letters* **88** 6462- 6466 (2000)
- [76] Jason T. Herrold, Vikram L. Dal, "Growth and properties of microcrystalline germanium-carbide alloys grown using electron cyclotron resonance plasma processing" *Journal of Non-Crystalline Solids* **270** 255-259 (2000)
- [77] Otto F Sankey, Alexander A Demkov, William T Petuskey and Paul F McMillan, "Energetics and electronic structure of the hypothetical cubic zinc blende form of GeC" *Modelling Simul. Mater. Sci. Eng.* **1** 741-754 (1993)

- [78] Jung-Fu Lin, Mario Santoro, Viktor V. Struzhkin, Ho-kwang Mao and Russell J. Hemley, “In situ high pressure-temperature Raman spectroscopy technique with laser-heated diamond anvil cells” *Rev. of Sci. Instrum.* **75** 3302-3306 (2004)
- [79] F. Goncharov, J. A. Montoya, N. Subramanian, V. V. Struzhkin, A. Kolesnikov, M. Somayazulu and R. J. Hemley, “laser heating in diamond anvil cells: developments in pulsed and continuous techniques” *J. Synchrotron Rad.* **16** 1-4 (2009)
- [80] L. Dubrovinsky, N. Dubrovinskaia, O. Narygina, I. Kantor, A. Kuznetsov, V. B. Prakapenka, L. Vitos, B. Johansson, A. S. Mikhaylushkin, S. I. Simak and I. A. Abrikosov, “Body-Centered Cubic Iron-Nickel Alloy in Earth’s Core” *Science* **316** 1880-1883 (2007)
- [81] Jung-Fu Lin, Eugene Gregoryanz, Viktor V. Struzhkin, Maddury Somayazulu, Ho-kwang Mao and Russell J. Hemley, “Melting behavior of H₂O at high pressures and temperatures” **32** L11306-L11410 (2005)
- [82] Alexander F. Goncharov, Jonathan C. Crowhurst, “Raman Spectroscopy under Extreme Conditions” *J. of Low Temp. Phys.* **139** 727-737 (2005)
- [83] R. Boehler, “High-pressure experiments and the phase diagram of lower mantle and core materials” *Rev. Geophysics* **38** 221-245 (2000)
- [84] C. I. Ventura, J. D. Fuhr and R. A. Barrio, “Nonsubstitutional single-atom defects in the Ge_{1-x}Sn_x alloy” *Physical Review B* **79** 155202 (1-12)
- [85] Ming-Hsien Lee, Po-Liang Liu, Yung-An Hong, Yen-Ting Chou, Jia-Yang Hong and Yu-Jin Siao, “Electronic band structures of Ge_{1-x}Sn_x semiconductors: A first-

- principles density functional theory study” *J. Appl. Phys.* **113** 063517 (1-4) (2013)
- [86] R. Bindu, N. Subramanian, “Novel luminescence of pristine BaFBr prepared by non-equilibrium laser-heating technique” *Materials Chemistry and Physics* **115** 52-55 (2009)
- [87] F. Decremps, M. Fischer, A. Polian, J. P. Itie and M. Sieskind, “Prediction of cell variations with pressure of ionic layered crystal Application to the matlockite family” *Eur. Phys. J. B* **9** 49-57 (1999)
- [88] W. Nieuwenkamp and J. M. Bijvoet *Z. Kristallogr.* **81** 469 (1932)
- [89] F. Halff and J. Schoonman, “The Ionic Conductivity of PbFCl” *J. Solid State Chem.* **27** 397-405 (1979)
- [90] J. H. Eijkelenkamp, “Some Observations on the Photoluminescence of PbFCl and PbFBr Single Crystals” *J. Solid State Chem.* **19** 313-323 (1976)
- [91] J. Schoonman, A. F. Halff and G. Blasse, “Mixed anionic conduction in PbFCl” *Solid State Commun.* **13** 677-679 (1973)
- [92] Kenji Takahashi, Katsuhiko Kohda, Junji Miyahara, Yoshihiko Kanemitsu, Koji Amitani, Shigeo Shionoya, “Mechanism of Photostimulated Luminescence in BaFX:Eu²⁺ (X=Cl, Br) phosphors” *Journal of Luminescence* **31/32** 266-268 (1984)
- [93] P. Comodi and P. F. Zanazzi, “Improved calibration curve for the Sm²⁺:BaFCl pressure sensor” *J. Appl. Crystall.* **26** 843-845 (1993)
- [94] N. Subramanian, N. V. Chandra Shekar, P. Ch. Sahu, M. Yousuf and K. Govinda Rajan, “Crystal structure of the high-pressure phase of BaFCl” *Physical Review B* **58** R555-R558 (1998)

- [95] N. Subramanian, N. V. Chandra Shekar, P. Ch. Sahu, K. Govinda Rajan and A. L. Ruoff, "Evidence of an intermediate high-pressure phase in BaFBr and BaFI" *Physica B* **351** 5-10 (2004)
- [96] F. Decremps, M. Gauthier, J-C. Chervin, M. Fischer and A. Polian, "Unexpected value of transition pressure in the ionic layered BaFI compound observed by Raman scattering" *Physical Review B* **66** 024115(1-5) (2002)
- [97] B. Sundarakannan, T. R. Ravindran, R. Kesavamoorthy and S. V. M. Satyanarayana, "High pressure Raman spectroscopic study of BaFCl" *Solid State Communications* **124** 385-389 (2002)
- [98] R. Mittal, S. L. Chaplot, A. Sen, S. N. Achary and A. K. Tyagi, "Lattice dynamics and inelastic neutron scattering studies of MFX (M=Ba, Sr, Pb; X=Cl, Br,I)" *Physical Review B* **67** 134303(1-12) (2003)
- [99] N. Yedukondalu and G. Vaitheeswaran, "Vibrational properties of BaClF, BaBrF and BaIF under high pressure" *Journal of Physics: Conference Series* **377** 012070(1-5) (2012)
- [100] F. James Scott, "Raman Spectra of BaClF, BaBrF and SrClF" *J. Chem. Phys.* **49** 2766-2769 (1968)
- [101] Rulmont, "Spectres infrarouges et Raman des fluorohalogenures de plomb PbFX (X = Cl, Br, I) *Spectrochimica Acta* **30A** 161 (1974)

Chapter II

Experimental Details and Characterization Techniques

2.1 Introduction

This chapter deals with the experimental tools and the characterization techniques used for both the high pressure X-ray Diffraction and the Laser Heated Diamond Anvil Cell (LHDAC) experiments. The chapter is divided into two parts. The first part describes the various experimental tools used for generating high pressures and high temperatures. The second part describes high pressure X-ray diffraction and *in-situ* Raman spectroscopy which were used as characterization techniques. The synthesis experiments were carried out by the state-of-the-art LHDAC facility at our laboratory.

2.2 Generation of High Pressures

The use of pressure as a parameter in the study of materials was pioneered by Professor P. W. Bridgman who investigated most of the elements and many other materials using diverse techniques and he was awarded the Nobel Prize in physics for his achievements in high pressure research [1-2]. Here we discuss some important pressure generating devices which are relevant to our work.

The static pressures on materials can be generated by

- (i) Piston-Cylinder Apparatus and
- (ii) (ii) Opposed Anvil Devices.

2.2.1 Piston-Cylinder Apparatus

It consists of two opposed pistons made of cemented tungsten carbide which compress the sample in a single walled cylinder made of high strength steel [3]. The hydrostaticity can be achieved by using pressure transmitting fluid like silicon oil and methanol-ethanol mixture. Using this device, a pressure of ~ 3 GPa can be achieved. Pressure capability of this device can be further increased by giving additional supports to both the piston and cylinder.

2.2.2 Opposed Anvil Devices

Opposed anvil devices are widely used for attaining high pressures. In this work, we used opposed anvil devices to generate high pressures. The opposed anvil devices function on the “Principle of Massive Support” [4]. A large pressure is generated at the smaller area known as working area by applying sufficiently large load on the larger area called loading face. Opposed anvil devices are further classified into (i) Bridgman Opposed Anvil Device and (ii) Diamond Anvil Cell. The diamond anvil cell is now being widely used for in-situ high pressure and high temperature studies.

2.2.3 Bridgman Opposed Anvil Device

This is a high pressure-high temperature cell in an opposed anvil configuration and has two symmetrical assemblies placed one above the other. In this apparatus, an electrically powered hydraulic pump is used to apply load to the sample and heating of the sample achieved by high power transformer [5]. The pressure of the sample is estimated by loading pressure calibrants like bismuth, tin and lead inside the sample

assembly along with the sample. The sample can be heated in sealed atmosphere by enclosing the sample in a pyrophyllite gasket with graphite ring and the temperature of the sample is measured by placing a thermocouple close to the sample assembly. The electrical leads are made of gold coated tungsten leads having diameter of 0.2 mm. Temperature is measured by using Pt/Pt-10% Rh or a chromel-alumel thermocouple of diameter 0.2 mm. The maximum size of the sample can be accommodated in this device



Fig.2.1. Photograph of the 500 T hydraulic press. The main components are hydraulic pump, digital pressure indicator, and high current transformer [6].

is ~ 4 mm. Steatite or boron nitride is used as the pressure transmitting medium. Using this device, a maximum pressure of ~ 10 GPa and a temperature of $\sim 700^\circ\text{C}$ can be achieved. The disadvantages with this method are the frequent failure of anvils at higher pressures and difficulties in performing *in-situ* measurements. However, using multi-

anvil apparatus in conjunction with synchrotron X-radiation, many innovative *in situ* experiments have been reported to understand the physical properties of materials at high pressure and temperature conditions. Using this device, pressure close to 100 GPa can be achieved at high temperatures [7]. A six-axis cubic anvil press with wide open window to access the neutron radiation is reported and by using this device neutron diffraction experiments can be performed [8]. Optical window design for the large volume press (LVP) is reported for the bulk synthesis of materials [9]. In this apparatus, the *in situ* measurements like ruby fluorescence, Raman spectroscopy etc can be studied by using a small cylindrical aperture through the Bridgman anvil ending at the back of diamond anvil. This permits the optical access to the sample. Using this device, large sample size of the order of several millimeters can be studied with maximum pressure of 14 GPa.

2.2.4 Diamond Anvil Cell (DAC)

Synthetic diamond was successfully synthesized in 1954 by Hall which paved a way for the development of new apparatus and techniques [10]. It also showed the potential of high- pressure applications for industrial purposes and stimulated a new era in the field of high pressure research for the investigations of properties of materials. Since diamond is the hardest substance, diamond anvils are used to generate very high pressures. The Diamond Anvil Cell (DAC) is a versatile ultra-high-pressure device, and using this device new states of matter and understanding of the basic physics behind high pressure phenomena are being discovered [11-12]. This device is capable of generating megabar pressures and its size can fit into the palm of the hand and a variety of sophisticated measurements can be performed on materials of microscopic dimensions.

A DAC consists of a piston-cylinder assembly in which the piston can move freely inside the cylinder. The diamond anvils are fastened on the rockers and then fixed on the piston. Belleville spring-loaded lever-arm mechanism is mainly used for generating thrust in a diamond anvil cell.

In a typical Diamond Anvil Cell, sample is held between two flat-polished gem-quality diamonds using a gasket and the pressure is generated on the sample by applying

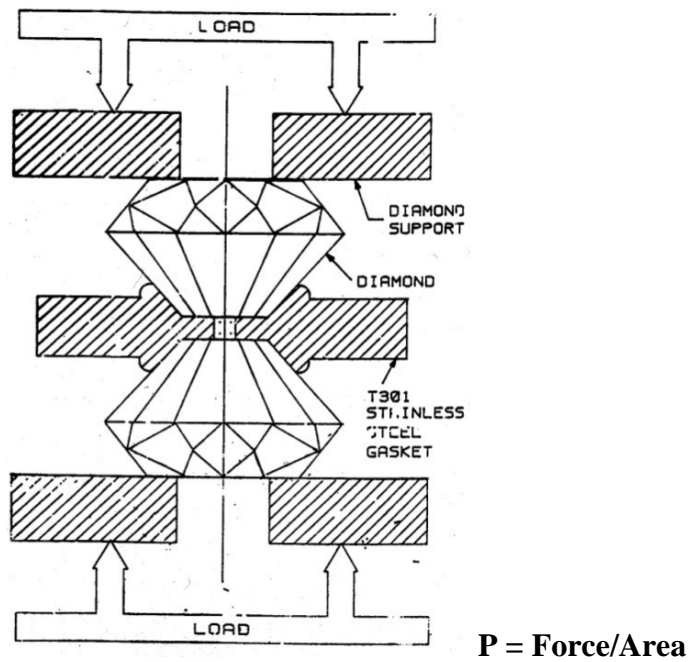


Fig.2.2. A schematic diagram of the opposed diamond anvil assembly.

load. Depending on the mechanism of force generation and the anvil alignment, the diamond anvil cell is classified into (i) NBS cell (ii) Bassett cell (iii) Mao-Bell cell (iv) Syassen-Holzapfel cell and (v) Merrill-Bassett cell. Gas membrane cell and symmetric cell are also widely used for high pressure research in recent years. Figure 2.2 shows working principle of a diamond anvil cell. Using anvils with culet diameter $\sim 300 \mu\text{m}$ pressures up to $\approx 80 \text{ GPa}$ can easily be achieved. The pressure range can be increased by

introducing bevels and by which Ruoff *et al* have reached 560 GPa using a DAC with their own design [13]. In this thesis work we have used Mao-Bell type diamond anvil cell for generating high pressures. The DAC is described in the next section.

2.2.5 Mao-Bell type Diamond Anvil Cell

Mao-Bell type diamond anvil cell was designed in 1978 by Mao and Bell at the Geophysical laboratory in Washington DC [14]. In our laboratory, we use a home built

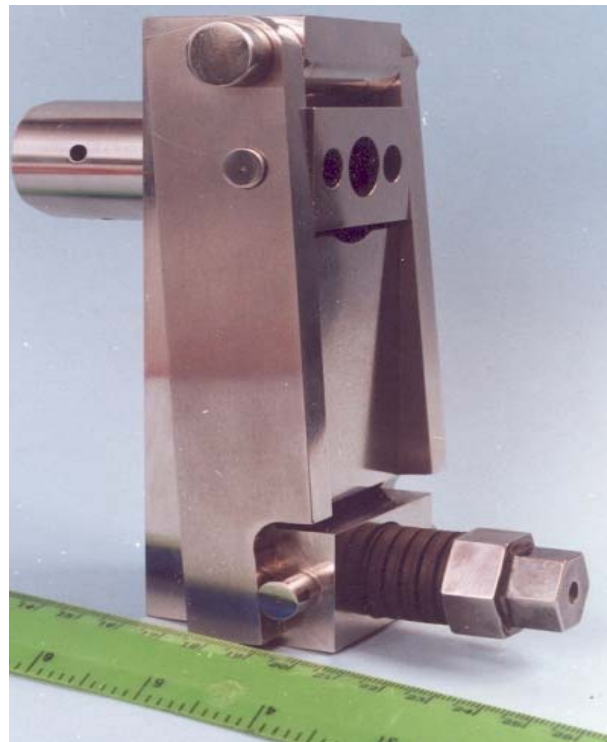


Fig.2.3. Home built Mao-Bell type diamond anvil cell used for high-pressure experiments for this thesis.

Mao-Bell type DAC [15]. A Mao-Bell type diamond anvil cell has (i) Piston Cylinder assembly (ii) Pressure Cell holder (iii) Rockers (iv) Diamond Anvils (v) X-ray Collimator and (vi) Belleville Springs. (The components of piston-cylinder assembly and

pressure cell holder are made of maraging steel with hardness RC 60. The heart of a diamond anvil cell is a pair of brilliant cut gem quality diamonds ($\sim 1/3$ - $1/5$ carats; 1carat =0.2 g). Since diamond has very high compressive strength than maraging steel, a tungsten carbide rocker is used as an intermediate material between them.

Diamonds are classified into type I and type II depending on their physical properties like IR absorption, UV absorption, X-ray diffraction, photo-conductivity and birefringence. Type I diamonds are slightly yellow due to the presence of nitrogen impurity. Type IIa diamonds are white, and do not absorb strongly in the infrared absorption region. The criterion for the diamonds for the usage in spectroscopic studies is that the intensity of the second order Raman spectra of diamond should be about three times that of fluorescence background. Since Type II diamonds satisfy these criteria, they are preferred for the light scattering studies [16]. The diamonds surface should be free from scratches, inclusions, micro cracks and should have low birefringence. The diamonds are cut with culet and table parallel to the (100) plane. Diamond is an ideal choice for X-ray diffraction studies because of its low absorption of X-rays due to its low atomic number. The diamond anvils are fastened to the centre of the tungsten carbide rockers using suitable stycast. The centering of diamonds with respect to the rockers is done by an appropriate diamond alignment jig [17]. The cylindrical and the hemispherical rockers are mounted in troughs at the piston and the cylinder assembly of the diamond anvil cell. The translational and the angular motion of the cylindrical and the hemispherical rockers are adjusted to make the anvil faces exactly matched and parallel to each other [18]. If the diamond anvils are not exactly aligned, then at high pressures there will be a risk of breaking the diamond anvils.

2.3 Pressure Calibration

Pressure is a fundamental parameter to be estimated in high pressure research. There are two standards used for the pressure determination of the sample. They are (i) Primary standards and (ii) Secondary standards. For high pressures, the only practicable primary pressure standard is the pressure-volume equation of state which can be derived from independent determination of a pair of equation of state parameters P and V. Similarly, in shock wave experiments, the pair of variables is particle velocity and shock velocity from which the pressure-density relations are obtained. The direct determinations of pressure in these ways are called primary standards. Once calibrated against a primary standard, any other pressure-dependent variable is known as secondary standard. In primary standards pressure is directly determined from the P-V equation of state of the calibrant whereas in the secondary standards the pressure dependent variable is calibrated against the primary standards [19]. There are two principal methods based on the primary and the secondary standards used for the pressure determination of sample in a diamond anvil cell. They are (i) Equation of state method and (ii) Ruby fluorescence method.

2.3.1 Equation of state method

In this method, a small quantity of pressure calibrant is loaded along with the sample. The pressure is determined by studying the variation of lattice parameter of the calibrant by X-ray diffraction technique. The calibrant should have the following properties [5]

- (i) Should be cubic [Due to high symmetry of cubic structure, it produces minimum

number of diffraction peaks. So the overlapping of sample peaks with the calibrant peaks will be minimum]

- (ii) Should not react with the sample
- (iii) Large volume change with pressure
- (iv) The high intense peaks of the calibrant should not merge with the sample peaks
- (v) Should not undergo phase transition in the required pressure range

Some commonly used calibrants are gold, silver and platinum. More recently materials like cubic Boron Nitride (c BN) and cubic SiC have been shown to be excellent pressure standards [20]. Other substances used as pressure calibrants are NaCl, CsCl, KCl, Cu, Mo, W, Pd, Al and Pb. In this work, NaCl, Au and Pt were used as pressure calibrants.

The pressure is determined by the P-V compression data of the calibrant. Since the sample is under hydrostatic pressure, the pressure felt by the calibrant is approximately same as that of the sample. If V_0 is the volume at ambient P and V is the volume at a pressure P, then pressure of the sample can be calculated by the following equations of state:

- (1) Murnaghan Equation of State

$$P(V) = \left(\frac{B_0}{B_0'} \right) \left[\left(\frac{V}{V_0} \right)^{-B_0'} - 1 \right] \text{ GPa}$$

where B_0 is the bulk modulus at zero pressure, B_0' is its first derivative and V_0 is the volume at ambient P [21]

- (2) Birch-Murnaghan Equation of State [22].

$$P(V) = \left(\frac{3B_0}{B'_0} \right) \left[\left(\frac{V}{V_0} \right)^{-7/3} - \left(\frac{V}{V_0} \right)^{-5/3} \right] \left\{ 1 + \frac{3}{4} (B'_0 - 4) \left[\left(\frac{V}{V_0} \right)^{-3/2} - 1 \right] \right\} \text{ GPa}$$

(3) Vinet Equation of State [23]

$$P(V) = 3B_0 \left[\left(1 - \left(\frac{V}{V_0} \right)^{1/3} \right) \left(\frac{V}{V_0} \right)^{-2/3} \exp \left[\frac{3}{2} (B'_0 - 1) \left(1 - \left(\frac{V}{V_0} \right)^{1/3} \right) \right] \right] \text{ GPa}$$

2.3.2 Ruby Fluorescence Method

Ruby is chromium doped aluminium oxide [$\text{Al}_2\text{O}_3:\text{Cr}^{3+}$ (0.005%)] and used as a secondary standard. It is calibrated against primary standards like Ag, Cu, Mo, Pd, Ag and Cu using shock wave measurements. This simple, rapid and continuous secondary pressure calibration scale was developed at NBS in 1972 by R. A. Forman *et al* [24-26]. In this method, a small chip of ruby ($\sim 5\text{-}10 \mu\text{m}$) is placed inside the sample chamber along with the sample. The crystal structure of ruby consists of corundum (Al_2O_3) in which some of the Al^{3+} ions are replaced by Cr^{3+} ions. The structure of corundum is made of hexagonal-close packed oxygen lattice in which the aluminium is occupying two-thirds of octahedral sites. The site symmetry of these octahedral sites are distorted by the repulsive interactions between the aluminium ions [trigonal distortion]. The electronic energy levels of ruby are described by ligand-field theory [27-28]. The crystal structure of ruby consists of corundum (Al_2O_3) in which some of the Al^{3+} ions are replaced by Al^{3+} ions. Al_2O_3 has a hexagonal-close-packed oxygen lattice in which aluminum occupying two-thirds of the octahedral sites. The octahedral crystal field strength increases with pressure causes large positive frequency shifts of some of the Cr^{3+} levels. If there is no distortion in the lattice then the site symmetry of the octahedral sites

will be cubic. The cubic field on d electrons split the single-electron wave function into the states having their symmetry labels t_{2g} and e_g . For d^3 electrons the O_h site symmetry has the energy terms ${}^4A_2(t_2^3)$, ${}^2E(t_2^3)$, ${}^2T_1(t_2^3)$, ${}^4T_2(t_2^2e)$, ${}^2T_2(t_2^3)$ and ${}^4T_1(t_2^2e)$. The energies of the 2E states depend on the difference in crystal field splitting of free-ion

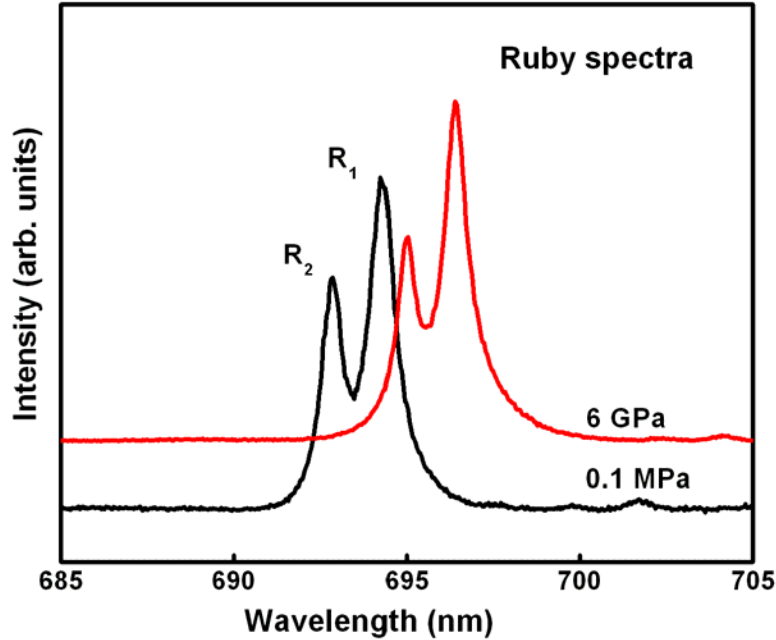


Fig.2.4. Ruby spectra at ambient and 6 GPa pressures. R_1 and R_2 represent two well defined ruby peaks at the wavelengths 694.2 nm and 692.6 nm respectively.

levels 4F and 2G. The electronic transitions are taking place between the 2E and 4A_2 states. When ruby is excited by a suitable laser, the two distinct doublets R_1 and R_2 at the wavelengths 694.2 nm and 692.6 nm respectively are emitted at atmospheric pressure. The R_2 line shift is the same for compression along a or c-axis and also the same as the shift of line obtained by hydrostatic conditions, whereas for the R_1 line the compression more along a-axis than c-axis. Hence R_2 line shift should be used as the pressure marker

instead of R_1 line shift [29-31]. The shift of ruby lines is calibrated against standard substances to construct ruby pressure scale. Up to ~ 30 GPa, the shift is almost linear at the rate of $0.365 \text{ nm GPa}^{-1}$ [11]. The equation of state for the non-linear region is [32]

$$P(\text{GPa}) = 1904/B \left[\left(1 + (\Delta\lambda/694.24) \right)^B - 1 \right]$$

where $\Delta\lambda$ is the ruby R_1 line shift in 'nm' and the parameter $B=5$ for non-hydrostatic conditions and $B=7$ for quasi hydro-static conditions. The estimate of error in the above equation at 1 Mbar is less than 3%.

2.4 Heating of Samples in a Diamond Anvil Cell

Pressure induces large changes in the behavior of electronic orbitals and hence enhances the chemical reactivity of the materials. When a material is heated under high pressure, the heat energy provides sufficient kinetics required for the material to overcome the activation barriers which are necessary for the materials to react to form new compounds with novel properties. The widely used methods for heating the samples at high pressure are

- (i) Resistive heating and (iii) Laser heating.

2.4.1 Resistive Heating

The resistive heating of samples in DAC can be done either by internal heating or external heating. In internal heating, the heating of sample can be achieved by passing the electric current through the miniature sample assembly [33]. In external heating, the

heating is achieved by placing the whole DAC assembly in a furnace [34]. Another way of external resistive heating is by assembling electrical heater coils surrounding the diamond anvils. The temperature can be measured by the thermocouple attached to the DAC. The disadvantage with this method is the heating of the stress bearing components like gasket, diamonds, rockers and body of DAC. The peak sample temperature is limited up to 1500 K due to the softening of components at elevated temperatures. The oxidation of the diamonds and the gasket while heating can be avoided by loading inert and reducing gases like argon with 5% H₂ [35]. The disadvantages with this method are (i) graphitization of diamond around 1200 °C [33] (ii) the failure of gasket material (iii) deformation of DAC at high temperatures. If the sample is conducting electricity, the sample itself can be used as heater [36]. Using the above method, a temperature of few thousand degrees Celsius inside the sample chamber can be achieved while maintaining the DAC body at much lower temperatures. The heating elements used in this method should be miniature, inert and well insulated from the diamond anvils [36].

2.4.2 Laser Heating

Laser heated diamond anvil cell (LHDAC) technique is a fast growing tool to understand the behavior of materials under extreme high pressure and high temperature conditions [40]. Using this technique, ground-breaking results in material synthesis, earth science, planetary interiors etc have been achieved. The idea that laser heating of materials to few thousands of Kelvin can be achieved by focusing an IR laser beam on to the sample squeezed between diamond anvils was first introduced by Ming and Bassett in 1974 [37-38]. Since diamond is transparent to IR radiation, the sample can be heated to

very high temperatures at megabar pressures. Using pulsed IR laser heating temperature in excess of 10^4 K has been achieved recently [39]. The advantages of this technique over resistive heating methods are, localized heating of the sample, contamination free environment of the sample by using inert gases as pressure transmitting media, studies using *in-situ* characterization techniques such as X-ray diffraction, Raman spectroscopy and fast quenching of the sample. Since the heating zone using LHDAC is very small, this results in steep temperature gradients in the sample region. The laser heated diamond anvil cell set up in our laboratory, and used for the experiments described in this thesis, makes use of a CO₂ laser (wavelength 10.6 μm ; Max power 125 W; CW; TEM₀₀ mode) focused to ~ 30 μm sized spot on the sample in the DAC and heat it [40]. This set up has the following key components (i) IR optics (ii) Nano motion system and (iii) Imaging system

2.4.2.1 IR Optics

The initial alignment of the optical components such as beam expander, beam steerer and focusing lenses are done with the help of He-Ne laser ($\lambda = 632.8$ μm). The He-Ne laser beam is allowed to traverse the same path length as the CO₂ laser ($\lambda = 10.6$ μm) for the alignment.

2.4.2.2 Nano Motion System

The essential requirement of the LHDAC set up is that the final CO₂ laser spot should fall on the sample squeezed inside the DAC. If it is not so, there is a possibility of damaging the DAC components. In order to achieve this, a nanomotion system is used. The diamond anvil cell is placed on a XYZ mounting stage and the stage can be moved

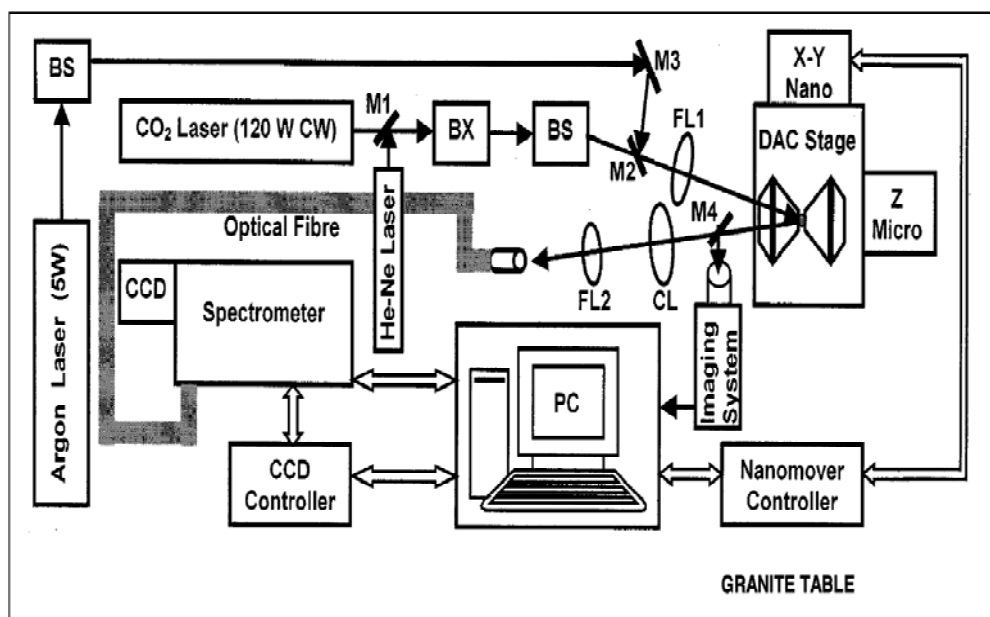


Fig.2.5. Schematic of the LHDAC set-up at IGCAR. M_1 - M_4 mirrors; BS, beam steerer; BX, beam expander; FL_1 and FL_2 , Focusing lenses; CL, Collecting lens [40].

along X-Y directions using two nanomovers. In addition, the stage can be moved along the beam direction for better focusing of the laser beam onto the sample. The DAC can be rastered with very small step size of the order of 10 nm to maximum of 2mm with respect to the laser spot so that uniform heating throughout the sample is achieved. In order to achieve this, a home built AMS-Nanomover software using LABVIEW (National Instruments Corporation, USA) has been used [41].

2.4.2.3 Imaging System

A CCD based imaging system is used for real-time imaging and to focus the CO_2 laser beam onto the sample. This also reduces any eye hazard to the personnel working with high power CO_2 laser.

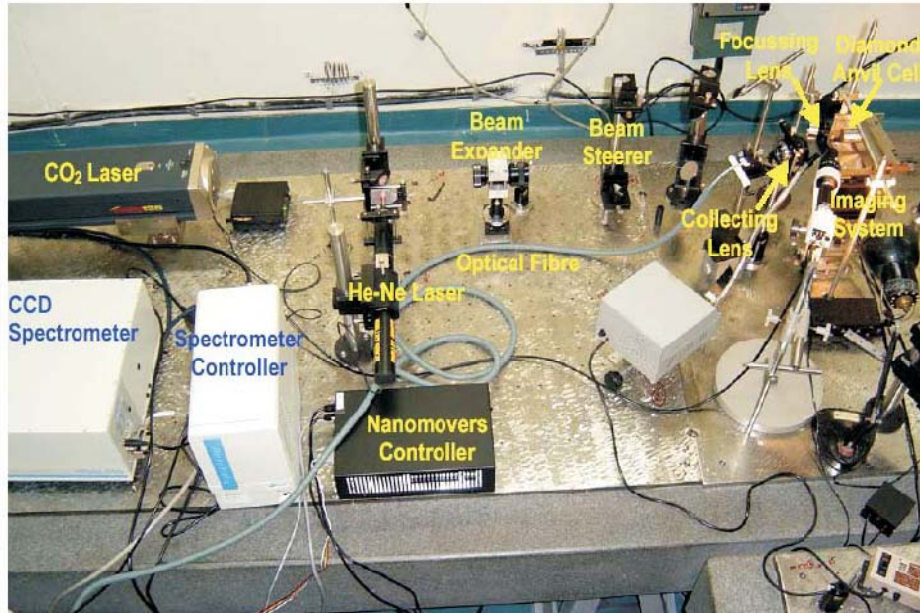


Fig.2.6. Photograph of the LHDAC set-up at the author’s laboratory. The set up is mounted on a granite table. A special foundation is made to isolate the whole set up from the rest of the building to minimize vibrations [40].

2.4.2.4 Temperature Measurement

Like pressure, temperature is another important thermodynamical parameter which has to be measured in the laser heating experiments. The pressure measurement has already been discussed in section [2.3]. Since the sample size and the final focused laser beam spot on the sample are very small, the measurement of temperature in high pressure laser heating experiments is very difficult. Various methods are adopted to measure the temperature of the hot samples squeezed inside the diamond anvil cell. Optical pyrometry [42], usage of small thermocouples [43], principle of detailed balance where the average temperature of the laser heated sample is measured by the temperature-dependent intensity asymmetry of the Raman spectra [44-45] and spectroradiometric technique [46-47]. For laser heating experiments, the spectroradiometric technique is the

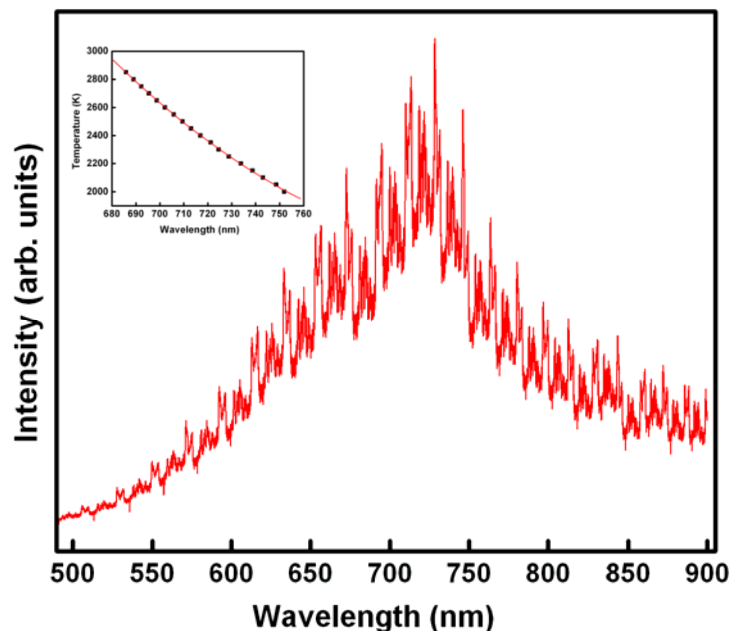


Fig.2.7. Temperature measurement of Ge-Sn sample laser heated at ~ 9 GPa. Inset is the calibration curve generated using a standard light source.

most elegant method for temperature measurement. We have used this to estimate the temperature of the hot samples in the LHDAC. Thermal radiation emitted from the hot sample is collected through an optical fiber and fed to a CCD based spectrometer. Temperature is estimated by fitting the thermal radiation collected from the hot in sample to the Planck's or Wien's distribution law [40]. The thermal radiations are collected in the temperature range of ~ 2000 - 2850 K with step size of ~ 50 K and calibration chart of temperature Vs peak wavelength (λ_{\max}) is generated as shown in Fig.2.7(inset) [40].

2.5 High Pressure X-ray Diffraction Studies

2.5.1 Xray Diffraction

X-ray diffraction is a well established technique for understanding the structural

behavior of pressure locked samples inside the diamond anvil cell. The fundamental equation governing the X-ray diffraction study is the Bragg's law and is given by

$$2 d \sin \theta = \lambda$$

where λ is the wavelength of X-rays, d is the inter planar spacings and θ is the diffraction angle. The d spacings of the different lattice planes of the sample can be determined by

(i) Angle Dispersive X-ray Diffraction (ADXRD) Method

$$2 d_{(hkl)} \sin \theta_{(hkl)} = \lambda$$

In this method, the wavelength (λ) of the incident X-ray beam is fixed by using monochromatic X-radiation and the diffraction patterns are recorded either using two dimensional, one dimensional or point detectors. The theta positions are measured from the diffraction patterns.

(ii) Energy Dispersive X-ray Diffraction (EDXRD) Method

$$2 d_{(hkl)} \sin \theta_{(hkl)} = h c / E_{(hkl)}$$

In this method, d spacings can be determined by using polychromatic (white) radiation at a fixed θ and the diffraction patterns at different energies are recorded by solid state or intrinsic Ge detectors.

In this thesis work, we have used *in-situ* high pressure X-ray diffraction techniques in ADXRD mode [48].

2.5.2 Rotating Anode X-ray Diffractometer

The X-ray diffraction studies have been carried out using a high-pressure diffractometer that employs a RIGAKU rotating anode X-ray generator (UltraX 18) as

the source. It is a high-stability, high frequency type 18 kW X-ray generator with Mo as target material. The X-ray beam generated from the Mo target is monochromatized with



Fig.2.8. High Pressure Angle Dispersive X-ray Diffraction system used for the high pressure experiments at our laboratory.

the help of graphite monochromator. The wavelength of the X-rays used for the experiments is 0.7107 \AA . The overall resolution of the diffractometer is $\delta d/d \sim 0.001$. An image plate based mar345dtb diffractometer is used to detect diffracted X-rays. The sample to detector distance was calibrated using LaB_6 . Generally, in high pressure studies using diamond anvil cell Mo is used as target. The linear absorption coefficient of diamond as a function of X-ray photon energy shows the transmission factor is more for Mo than Cr or Cu. So Mo is preferred for high pressure experiments using diamond anvil cell.

2.5.3 Synchrotron Facility at INDUS-2

The volume of sample used in high pressure experiment is relatively small and the absorption of radiation by the diamond anvils reduce the intensity of scattered radiation. The high X-ray flux of the synchrotron radiation dramatically enhances the counting statistics of the diffracted beam. The wavelength of the synchrotron beam can be tuned to shorter wavelengths. A shorter wavelength not only improves resolution ($\sin\theta/\lambda$) but it also increases the number of accessible families of reflecting planes from the sample. Hence for high pressure X-ray diffraction studies synchrotron radiation is preferred.

Synchrotron radiation is emitted by accelerating charged particles like electron and positron at velocity close to the speed of light and the direction of the particles are changed under the action of magnetic field. It is emitted as narrow cone

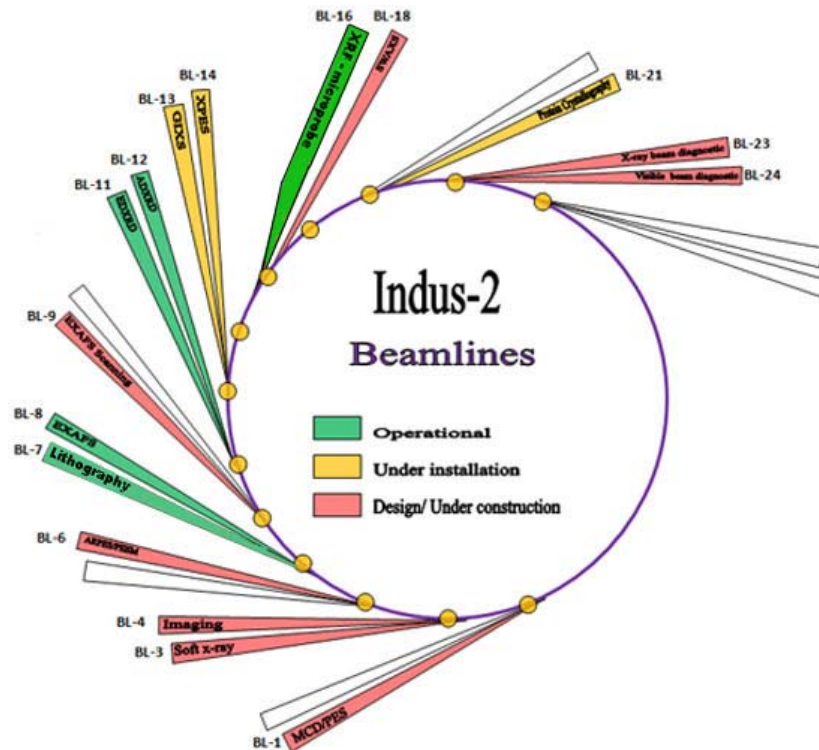


Fig.2.9. Lay out of Indus-2 Beam lines [49].

tangent to the particles orbit in the forward direction. The source of synchrotron radiation has components such as electron storage rings, bending magnets and the insertion devices. A high energy synchrotron source can produce highly intense, very small and well collimated X-ray beams. The combination of high brightness (intensity is hundreds of thousands of times more than that of conventional X-rays) and fine collimation of synchrotron X-radiation with the broad range of wavelength tunability makes it an ideal source for XRD characterization of materials as compared to conventional laboratory x- ray sources. Due to these unique properties, synchrotron radiation has made a revolution in the field of high pressure research. The high pressure XRD experiments on Ge-Sn sample described in this thesis has been carried out at INDUS-2 (BL-12) using angle dispersive X-ray diffraction (ADXRD) technique [50]. A beam current of about 100 mA at ~ 2.0 GeV is sufficient to get a reasonably good pattern in about 10 minutes. A plane bendable Si mirror coated with ~ 500 Å thick Pt layer is used to collimate the beam at the experimental station. Mar-345 image plate area detector is used as a detector in this facility.

2.6 Raman Spectroscopy

In situ Raman spectroscopy is an important characterization tool which is widely used for studying the structural, vibrational and electronic properties of materials under high pressure [50]. Micro Raman spectroscopy is the first technique for the *in-situ* characterization of the samples at high P-T conditions with μm spatial resolution. With this technique, valuable information about intermolecular interactions, phase transitions, structural changes of the materials are also obtained when matter is subjected to high pressure. For this thesis, the *in-situ* Raman spectroscopy of materials under high

pressure has been performed by using Renishaw(UK), *in-via* Raman spectrometer having 1-2 μm spatial resolution. An argon ion laser with wavelength 514.5 nm has been used



Fig.2.10. Renishaw *in-via* Raman spectrometer used for the Raman measurements.

as the excitation source for all the experiments. In this apparatus, an open space microscope is used to accommodate the DAC. Charge coupled device (CCD) is used to collect the Raman signals scattered from the sample. The Rayleigh line rejection filter used in the spectrometer allows ripple free measurement of the Raman spectra up to 50 cm^{-1} .

References

- [1] P. W. Bridgman, "Physics of High Pressure", (Dover, New York, 1976)
- [2] P. W. Bridgman, "Collected Experimental Papers", H. Brooks, F. Birch, G. Hatton and W. Paul (Eds) (Harvard University, Cambridge, 1964), Vol. 1-7

- [3] I. L. Spain and J. Paauwe (Eds.) “High Pressure Technology” (Marcell Dekker, New York, 1977), Vol.1, P.395
- [4] M. Yousuf and K. Govinda Rajan, “Principle of massive support in the opposed anvil high pressure apparatus” *Pramana* **18** 1-15 (1982)
- [5] P. Ch. Sahu, *PhD Dissertation* “Electrical Resistivity and X-ray Diffraction studies of Some Early Actinide Systems Under High Pressure and Temperature”, University of Madras 1994
- [6] M. Yousuf, P. Ch. Sahu and K. Govinda Rajan, “A high pressure-high temperature cell for electrical resistivity studies”, *Pramana* **24** 825-835(1985)
- [7] Robert C. Liebermann, “Multi-anvil, high pressure apparatus: a half-century of development and progress” *High Pressure Research* **31** 493-532 (2011)
- [8] Y. Zhao, D. He, J. Qian, C. Pantea, K. A. Lokshin, J. Zhang and L. L. Daemen, “Development of high P-T neutron diffraction at LANSCE - toroidal anvil press, TAO-98, in the HiPPO diffractometer”, *Advances in High-Pressure Technology for Geophysical Applications*
- [9] M. J. Lipp, W. J. Evans and C. S. Yoo, “Hybrid Bridgman anvil design: an optical window for in situ spectroscopy in large volume presses” *High Pressure Research* **25** 205 -210 (2005)
- [10] Hall, H. T, “The Synthesis of Diamond”, *J. Chem. Ed.*, **38** 484-489 (1961)
- [11] A. Jayaraman, “Diamond anvil cell and high-pressure physical investigations” *Reviews of Modern Physics* **55** 65-108 (1983)
- [12] William A. Bassett, “Diamond anvil cell, 50th birthday” *High Pressure Research* **29** 163-186 (2009)

- [13] L. Ruoff, H. Xia, "The effect of a tapered aperture on x-ray diffraction from a sample with a pressure gradient: Studies on three samples with a maximum pressure of 560 GPa" *Rev. Sci. Instrum* **63** 4342-4348 (1992)
- [14] H. K. Mao, and P. M. Bell, In Carnegie Institution of Washington Year Book (1978)
- [15] R. Deivasigamani, N. Gunasekaran, N. Easwaran, M. Yousuf, K. V Thomas Kutty, P. Ch. Sahu, N. V. Chandra Shekar, N. Subramanian and K. Govinda Rajan "Precision Fabrication of a Diamond Anvil Cell", *Advances in HighPressure Science and Technology* Edited by A. K. Singh, Tata McGraw-Hill, New Delhi (1995).
- [16] G. B. B. M. Sutherland, D. E. Blackwell and W. G. Simeral, "The Problem of the Two Types of Diamond" *Nature* **174** 901-903 (1954)
- [17] V. Kathirvel, Dayana Lonappan, N. V. Chandra Shekar and P. Ch. Sahu, "Novel and innovative jigs for mounting and alignment of diamond anvils in a Mao-Bell type diamond anvil cell" *J. Instrum. Soc. India* **40** 199 (2010)
- [18] D. J. Dunstan and I. L. Spain, "Technology of diamond anvil high-pressure cells: I. Principles, design and construction", *J. Phys. E: Sci. Instrum.* **22** 913-923 (1989)
- [19] H.-K. Mao, W. L. Mao, "Theory and practice - diamond-anvil cells and probes for high P-T mineral physics studies", Elsevier (2007)
- [20] Alexander F. Goncharov, Jonathan C. Crowhurst, John K. Dewhurst, Sangeeta Sharma, Chrystele Sanloup, Eugene Gregoryanz, Nicolas Guignot and Mohamed Mezouar, "Thermal equation of state of cubic boron nitride: Implications for a high-temperature pressure scale" *Physical Review B* **75** 224114(1-6) (2007)

- [21] F. D Murnaghan, “The compressibility of media under extreme pressures”, *Proc.Nat .Acad. Sci.* **30** 244-247 (1944)
- [22] F. Birch, “Finite Elastic Strain of Cubic Crystals” *Phys. Rev.* **71** 809-824 (1947)
- [23] S. K. Sikka, “Empirical equation of state theories at ultra-high pressures”” *Physics Letters A* **135** 129-131(1989)
- [24] R. A. Forman, G. J. Piermarini, J. D. Barnett, and S. Block, “Pressure measurement Made by the Utilization of Ruby Sharp-Line Luminescence”, *Science* **176** 284-285 (1972)
- [25] J. D. Barnett, S. Block, and G. J. Piermarini, “An optical fluorescence system for quantitative pressure measurement in the diamond-anvil cell”, *Rev. Sci. Instrum.* **44** 1-8 (1973).
- [26] G. J. Piermarini, and S. Block, “Ultrahigh pressure diamond-anvil cell and several semiconductor phase transition pressures in relation to the fixed point pressure scale”, *Rev. Sci. Instrum.* **46** 973-979 (1975).
- [27] J. H. Eggert, K. A. Goettel and I. F. Silvera, “Ruby at high pressure. I. Optical line shifts to 156 GPa” *Phys. Rev. B* **40** 5724-5732 (1989)
- [28] K. Syassen, “Ruby under pressure” *High Pressure Research* **28** 75-126 (2008)
- [29] Y. M. Gupta and X. A. Shen, “Potential use of the ruby R_2 line shift for static high-pressure calibration”, *Appl. Phys. Lett.* **58** 583-585 (1991)
- [30] S. M. Sharma and Y. M. Gupta, “Theoretical analysis of R-line shifts of ruby subjected to different deformation conditions”, *Phys. Rev. B* **43** 879-893 (1991)
- [31] P. D. Horn and Y. M. Gupta, “Luminescence R-line spectrum of ruby crystals shocked to 125 kbar along the crystal c axis” *Phys. Rev. B* **39** 973-979 (1989)

- [32] H. K. Mao, P. M. Bell, J. W. Shaner and D. J. Steinberg, "Specific volume measurements of Cu, Mo, Pd, and Ag and calibration of the ruby R_1 fluorescence pressure gauge from 0.06 to 1 Mbar" *J. Appl. Phys.* **49** 3276- 3283 (1978)
- [33] C. S. Zha and W. A. Bassett, "Internal resistive heating in diamond anvil cell for *in situ* x-ray diffraction and Raman scattering" *Rev. Sci. Instrum.* **74** 1255-1262 (2003)
- [34] M. I. Eremets, "High Pressure Experimental Methods" *Oxford University Press*, 1996 Yingwei Fei, Ho-kwang Mao, "In Situ Determination of the NiAs Phase of FeO at High Pressure and Temperature" *Science* **266** 1678-1680 (1994)
- [35] Yingwei Fei, Ho-kwang Mao, "In Situ Determination of the NiAs Phase of FeO at High Pressure and Temperature" *Science* **266** 1678-1680 (1994)
- [36] L. G. Liu and W. A. Bassett, "The melting of iron up to 200 kilobars" *Journal of Geophysical Research* **80** 3777-3782 (1975)
- [37] L. C. Ming and W. A. Bassett "Laser heating in the diamond anvil press up to 2000°C sustained and 3000°C pulsed pressures up to 260 kilobars" *Revi. Sci. Instrum* **45** 1115-1118 (1974)
- [38] W. A. Bassett, "The birth and development of laser heating in diamond anvil cells", *Rev.Sci. Instrum* **72** 1270-1272 (2001)
- [39] A. F. Goncharov, J. A. Montoya, N. Subramanian, V. V. Struzhkin, A.Kolesnikov, M. Somayazulu and R. J. Hemley, "Laser heating in diamond anvil cells: developments in pulsed and continuous techniques" *J. Synchrotron Rad.* **16** 1-4 (2009)
- [40] N. Subramanian, N. V. Chandra Shekar, N. R. Sanjay Kumar and P. Ch. Sahu,

- “Development of laser-heated diamond anvil cell facility for synthesis of novel materials” *Current Science* **91** 175-182 (2006)
- [41] N. Subramanian, M. Ummru, R. Bindu, N. R. Sanjay Kumar, M. Sekar, N. V. Chandra Shekar and P. Ch. Sahu, “An automated laboratory laser heating arrangement for materials synthesis is at high temperatures and high pressures’, e-print arXiv:0805.1251
- [42] W. A. Bassett and L. C. Ming, “Disproportionation of Fe_2SiO_4 to $2\text{FeO} + \text{SiO}_2$ at pressures up to 250 kbar and temperatures up to 3000°C ” *Phys. Earth Planet Int* **6** 154-160 (1972)
- [43] L. C. Ming, M. H. Manghnani, J. Balogh, S. B. Quadri, E. F. Skelton and J. C. Jamieson, “Gold as a reliable internal pressure calibrant at high temperatures” *J. Appl. Phys*, **54** 4390-4397 (1983)
- [44] J. F. Lin, M. Santoro, V. V. Struzhkin, H. K. Mao, and R. J. Hemley, “*In situ* high pressure-temperature Raman spectroscopy technique with laser-heated diamond anvil cells” *Rev. Sci. Instrum.*, **75** 3302-3306 (2004).
- [45] J. F. Lin, W. Sturhahn, J. Zhao, G. Shen, , H. K. Mao, and R. J. Hemley, “Absolute temperature measurement in a laser-heated diamond anvil cell” *Geophys. Res. Lett.* **31** L14611 (2004)
- [46] D. L. Heinz, and R. Jeanloz, Temperature measurements in the laser heated diamond cell. In *High-Pressure Research in Mineral Physics* (eds M. H Manghnani and Y Syono), Terra Scientific Publishing Co, Tokyo, and American Geophysical Union, DC, p. 113-127 (1987)
- [47] D. L. Heinz, J. S. Sweeney, and P. Miller, “A laser heating system that stabilizes

- and controls the temperature: Diamond anvil cell applications” *Rev. Sci. Instrum.* **62** 1568-1575 (1991).
- [48] S. K. Sikka, H. Sankaran, S. M. Sharma, Vijayakumar, B. K. Godwal and R., *Indian J. Pure Appl. Phys.* **27** 472 (1989)
- [49] Commissioning experiences of hard x-ray beam line (B-12) on Indus-2 for high-resolution powder diffraction. A. K. Sinha, G. M. Bhalerao, A. Jaiswal, R. K. Gupta, M. N. Singh, Adu Verma and R. V. Nandedkar, “*Proceedings of DAE Solid State Physics Symposium*” P-365 (2006).
- [50] John R. Ferraro, Kazuo Nakamoto and Chris W. Brown, *Introductory Raman Spectroscopy* second Edition p.147 (2003)

Chapter III

Exploration of Formation of Novel Intra-Group Phases involving Group IV Elements using LHDAC Technique

3.1 Introduction

The IV-IV semiconductors have attracted great attention in recent years for their various technological applications. Si-C is used in polishing and grinding applications [1]. Si-Ge is used in hetero junction bipolar devices [2]. Ge-Sn is predicted to be a semiconductor with tunable direct band gap [3-4], formed from Ge an indirect band gap semiconductor and Sn a semi-metal. Ge has an indirect band gap at the L point of the band structure and the direct band gap lies 0.13 eV higher in energy at the Γ point ($k=0$) of the Brillouin zone. Tight binding and the pseudopotential calculations based on virtual crystal approximation predicts the mixing of conduction band minimum of Sn and Ge causes formation of direct band gap in the composition range $0.55 > E_g > 0$ eV with $0.2 < x < 0.6$ for $\text{Sn}_x\text{Ge}_{1-x}$ alloy [4]. Optical measurement studies showed the optical energy gap undergoes an indirect to direct transition in the composition range $0.35 < E_g < 0.8$ eV with $0.15 > x > 0$ due to interband transitions in $\text{Sn}_x\text{Ge}_{1-x}$ alloy [4]. The thermodynamic solubility of Sn in Ge is less than 0.5 at%, while that of Ge in Sn is zero [5]. Due to wide range of interest, several experiments and theoretical works have been performed on these systems to explore the conditions for the compound formation. For example, the formation of trenches and wires oriented in $\langle 100 \rangle$ directions was observed during epitaxial growth of Ge-Sn alloys on Ge (100) due to the lateral migration of Sn islands on

its surface [6]. Heteroepitaxial Ge-Sn alloys on Si(100) were synthesized by using pulsed laser induced epitaxy and Molecular Beam Epitaxy (MBE) growth methods with virtual germanium buffer layer. Using Raman spectroscopy, the formation of homogenous Ge-Sn alloys with 1% substitutional Sn in the Ge matrix was observed [7]. Chemical vapor deposition (CVD) methods were used to grow thin layers/films of $\text{Ge}_{1-x}\text{Sn}_x$ semiconductors with the molecular precursor $(\text{Ph})\text{SnD}_3$ as the source for Sn atoms [8-9]. Metastable micro crystalline thin films of $\text{Ge}_{0.78}\text{Sn}_{0.22}$ alloys were synthesized by pulsed UV laser annealing using excimer lasers [10]. The effect of pressure on the phase diagrams of the Ge-Sn and Si-Sn disordered alloys were investigated by using the electronic theory based on pseudo potentials and the virtual crystal approximation [11-12]. In this calculation Soma *et al* observed that both Ge-Sn and Si-Sn alloys undergo pressure induced phase transition from the α -phase of substitutional diamond type to β -Sn of disordered white tin type structure. Also, they found that the heat of solution for $\text{Ge}_{1-x}\text{Sn}_x$ and $\text{Si}_{1-x}\text{Sn}_x$ alloys decreased with pressure and were large in Sn rich region. They predicted the formation of α -phase Ge-Sn solid solution under pressure [11]. The calculated phase boundary for the liquid, the solid solution and the phase mixture for $\text{Ge}_{1-x}\text{Sn}_x$ system up to 5 GPa is reported. A first principle calculation based on density functional theory predicts the stability of Ge-Sn alloy in the zinc-blende phase up to 9 GPa [13]. However, the bulk synthesis of Ge-Sn has proved to be very challenging. It is a challenging task to synthesize Ge-Sn in bulk due to the large lattice mismatch, low solubility, different crystal structures and different electro negativities of Ge and Sn at ambient pressure. At ~ 9 GPa, the atomic radii ratios of Ge and Sn will reduce below 13 % with same β -Sn structures in both elements [14-18]. The valency of these elements

reduces to the values between 2 and 0 which is +4 in their diamond structures at around 9 GPa. Also at this pressure range, both Ge and Sn are in metallic state and hence their electro negativities are similar. By heating Ge and Sn mixture at around this pressure range, it may be possible to react Ge and Sn to form a new phase. Based on these arguments, Guillaume *et al* have successfully synthesized Ge rich $\text{Ge}_{0.9}\text{Sn}_{0.1}$ solid solution using a multi anvil press [18-19]. The XRD of the recovered samples indicate the structure to be tetragonal with space group $P4_32_12$ [18].

The work done in compressing the system of interest to extremely high pressures (about 100 GPa) is of the order of few electron volts, which is comparable to the chemical bond energies. This will drastically change the electronic structure of the materials; and hence increase the reactivity of the materials. Laser heating of the sample under pressure provides kinetics required for the materials to overcome the activation barriers which is necessary for the materials to react to form novel materials with novel properties.

“Ge-C” is another possible candidate with wide-band gap similar to Si-C. Thin films of $\text{Ge}_x\text{C}_{1-x}$ have been reported to be formed by RF sputtering, magnetron sputtering etc [21-22]. However, Ge-C has not been yet synthesized in bulk. Total energy calculations at 0 K based on pseudo potential approximation done by Sankey *et al* shows that Ge-C is unstable to form Ge-C bond up to ~15 GPa [22]. Above this pressure, it is energetically favorable to form Ge-C. Other calculations based on the density functional theory show that a stable Ge-C alloy formation is possible only above ~25 GPa [23]. Both the theoretical approaches have assumed persistence of the cubic phase of Ge up to the maximum pressures studied [22-22]. However, it is well known that around 9 GPa

Ge undergoes a pressure induced structural phase transition from the ambient cubic diamond structure to β -Sn structure [24]. Hence, it may be interesting to subject both Ge and C to pressure close to the transition pressure of Ge and heated at this pressure to explore if there is any possible new bonds even at pressures below the predicted value of ~ 15 GPa. Pb-C is another IV-IV material. An observation of uniform PbC_2 layer between the interface of graphite and Lead Bismuth Eutectic (LBE) alloy (Pb: 55.5 wt%, Bi: 44.5 Wt %) annealed at 1073 K and for 100 hrs in He atmosphere is reported [25]. The synthesis of lead carbide by the reaction between calcium carbide and an aqueous lead(II) acetate $\text{Pb}(\text{CH}_3\text{COO})_2$ has been reported, but this result was not reproducible [26]. The crystal structure of this compound is unknown.

3.2 Experimental Details

A stainless steel gasket was preindented to a thickness of ~ 80 μm and a hole of diameter ~ 250 μm was drilled at the centre. The hole was completely filled with dry NaCl powder and was compressed using DAC so that NaCl layer becomes transparent. A small portion (60 μm depth and 100 μm radius) of the NaCl was scooped out from the centre of the hole where the sample of size ~ 100 μm was placed. A thin pellet of Ge+Sn was formed by squeezing the thoroughly mixed powders of Ge (99.999% pure) and Sn (99.95% pure) in 2:1 wt. ratio between two opposed anvils of the diamond anvil cell. Similarly, a thin Ge+C pellet was formed by placing thoroughly mixed Ge (99.999%) powder and C foils at 1:1 wt. ratio. After completing the sample assembly in the DAC, heating was carried out by focusing CO_2 laser (wavelength 10.6 μm ; power 125 W; CW; TEM_{00} mode) at all portions of the sample (spot size ~ 40 μm) and the heating of the

sample was achieved by the manipulation of beam as well as the diamond anvil cell (DAC) XYZ stage with the help of a nanomotion system controlled by a computer [27]. The sample was rastered across the laser beam for several minutes using nano movers. The thermal radiation emitted from the hot sample was collected by an optical fiber and was then fed to a CCD based spectrometer (Jobin Yvon, dual exit and entry ports; focal length 550 mm). The system was calibrated up to ~ 3000 K using a tungsten filament lamp. The thermal emission spectra from the sample were recorded and the temperature of the sample could be determined within $\sim \pm 100$ K from the calibration curve. Characterization of the sample before and after laser heating was carried out using *in-situ* Raman spectroscopy and the X-ray diffraction techniques. Both laboratory based rotating anode X-ray generator and synchrotron high intense X-ray beams at INDUS-2 were used. HPXRD experiments were performed on the sample in angle dispersive geometry using Mo $K_{\alpha 1}$ X-ray radiation obtained from an 18 kW rotating anode X-ray generator and monochromatized by a graphite monochromator. An image plate based mar345dtb diffractometer with overall resolution of $\delta d/d \sim 0.001$ was used for detecting the diffracted X-rays. The sample to detector distance was calibrated using LaB_6 . Each XRD pattern was recorded with an exposure time of ~ 2 hours. High pressure XRD experiments on Ge-Sn sample described in this thesis has also been carried out at INDUS-2 (BL-12) using angle dispersive X-ray diffraction (ADXRD) technique with wavelength, $\lambda = 0.729$ Å [28]. A beam current of about 100 mA at ~ 2.0 GeV is sufficient to get a reasonably good pattern in about 10 minutes. Mar-345 image plate area detector was used to detect the diffracted X-rays. The Raman-spectroscopy of the sample was studied using Renishaw in via Raman spectrometer, having $1 \mu\text{m}$ spatial resolution.

3.3 Investigation of Ge-Sn Formation using Bridgman Opposed Anvil Apparatus.

The synthesis of Ge-Sn system was tried first using Bridgman opposed anvil apparatus. A pellet of 4mm in diameter and 1.5 mm in thickness was prepared from the thoroughly mixed Ge and Sn samples at 2:1 wt. ratio. The sample was loaded in the high pressure cell and was pressurized up to ~5 GPa using hydraulic press. The difficulty with this device is due to the frequent failure of anvil material at high pressures. Hence the experiment was carried out up to 5 GPa. Then the pressurized sample was heated up to ~773 K using an internal graphite heater. The sample was kept at ~5 GPa and 773 K for 6 hours. Slowly the pressure was reduced and the sample was brought to atmospheric pressure. The retrieved sample was powdered well and the powdered sample was

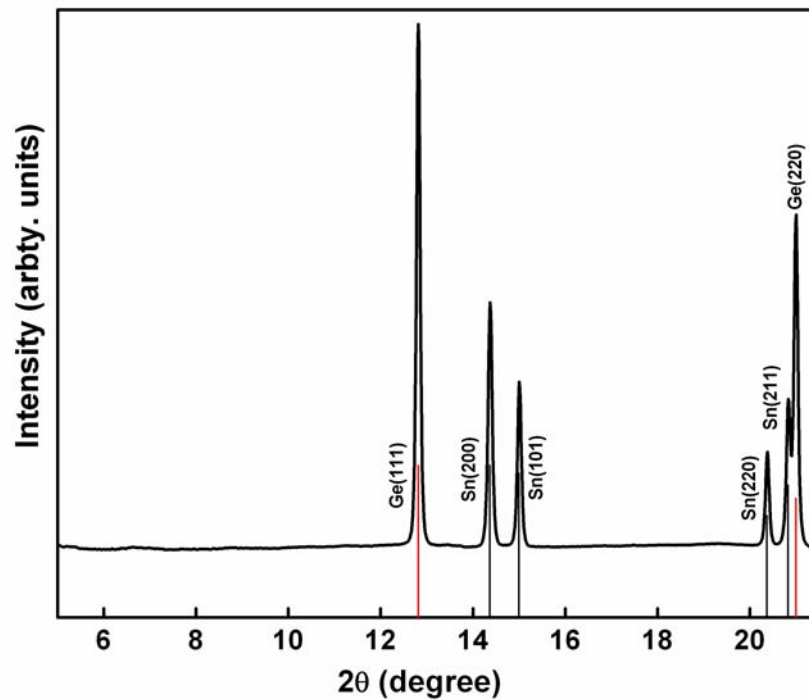


Fig.3.1. XRD study of Ge-Sn sample at ambient using synchrotron beam at INDUS-2.

characterized using the synchrotron beam at INDUS-2. XRD pattern of the powdered sample is shown in Fig.3.1. Analysis of the XRD pattern reveals that there is no phase formation. The aim of the work was to keep the sample at ~ 5 GPa and 773 K for a long period of time so that the elements Ge and β -Sn may react to form new Ge-Sn phase. Even though there is no new phase, the negative result shows that elevated pressure and temperature conditions are needed for the reaction of Ge and Sn elements. This preliminary experiment was done to explore the formation of Ge-Sn phase at P and T conditions below the β -Sn transition pressure of cubic germanium [24].

3.4 Formation of Ge-Sn Bonds at High P-T Conditions in a Laser Heated Diamond Anvil Cell

When experiments are conducted with LHDAC technique, the sample should be heated in a pristine environment. In several trial experiments involving laser heating of Ge+Sn mixture it was observed from Raman spectroscopy that there was undesirable chemical reaction with the ruby used for pressure estimation. To avoid this, control experiments up to 10 GPa at 300 K were performed to calibrate the variation of Ge TO(Γ) phonon mode against the well known ruby luminescence lines R_1 and R_2 [Table 3.1]. In this experiment, NaCl was used as pressure transmitting medium. The Ge equation of state thus obtained is shown in Table 3.1 and the experimental values are compared with other literature values. Further, Ge and β -Sn at 2:1 wt. ratio was pressurized up to 7.6 GPa and the sample was heated at ~ 2000 K using CO_2 laser. All portions of the sample were heated for about 30 minutes. Bright flashes were observed during heating. The laser heated sample was characterized by using in-situ Raman spectroscopy

Table 3.1. Comparison of the equation of state of Ge with that reported in Ref. 24 assuming a general second order polynomial equation: ω (cm^{-1}) = $a_0 + a_1 p + a_2 p^2$, a_0 , a_1 and a_2 in cm^{-1} , ($\text{cm}^{-1}/\text{GPa}$) and ($\text{cm}^{-1}/\text{GPa}^2$) respectively; P in GPa.

Parameters	other work [24]	This work
a_0 (cm^{-1})	300.6 ± 0.5	301.08
a_1 ($\text{cm}^{-1}/\text{GPa}$)	3.85 ± 0.05	4.74
a_2 ($\text{cm}^{-1}/\text{GPa}^2$)	-0.03 ± 0.006	-0.15

at high pressure and at 300 K (i.e., temperature quenched). The Raman spectra were taken from all the portions of the sample. The *in-situ* Raman spectra obtained at ~ 7.6

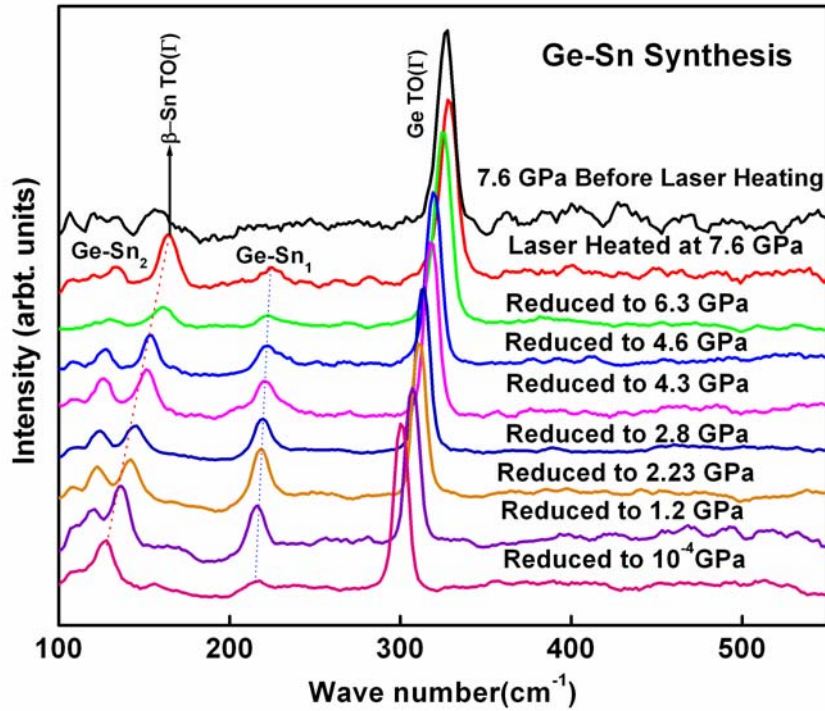


Fig.3.2. Raman Spectra of Ge-Sn before and after laser heating at 7.6 GPa and at other reduced pressures. The dotted line indicates the pressure dependence of Raman modes after laser heating.

GPa and ~ 300 K after laser heating the sample show, in addition to the characteristic first order TO (Γ) phonon modes of Ge and Sn, two additional modes at ~ 225 cm^{-1} and ~ 133 cm^{-1} . The pressure was reduced slowly and at each pressure, Raman spectra were taken. Fig.3.2 shows the Raman spectra of the laser heated sample at various pressures. At ambient P and T, Ge has a first order TO(Γ) phonon mode at ~ 300.7 cm^{-1} and Sn has a phonon mode, TO(Γ), at 126.6 cm^{-1} . With increasing pressure, this mode shifts to higher wave-number. At ~ 7.6 GPa, the Ge TO(Γ) mode is shifted to ~ 328.3 cm^{-1} . The β -Sn TO(Γ) mode is barely discernible before heating. This peak is commonly observed to be weak and is reported to pick up its intensity by cold working of the sample due to the changes in the orientation distribution of the crystallites [29]. After laser heating the sample at ~ 7.6 GPa and ~ 2000 K, two new modes in addition to the characteristic

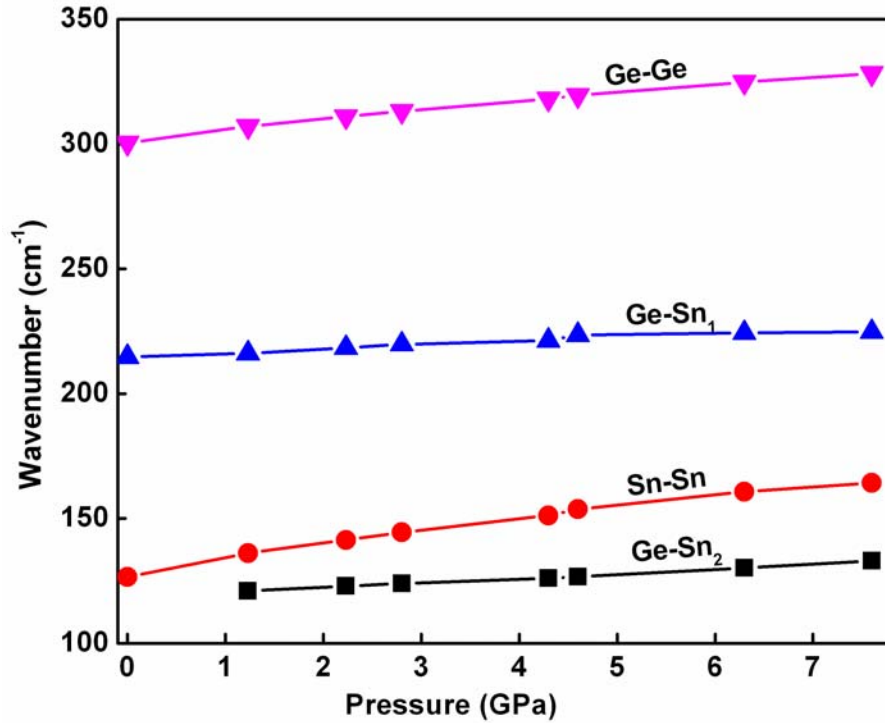


Figure 3.3. Pressure dependence of phonon modes of Ge, Sn, Ge-Sn₁ and Ge-Sn₂.

phonon modes were observed. The Raman mode observed between the characteristic modes of Ge and Sn are at $\sim 225 \text{ cm}^{-1}$, named as Ge-Sn₁. A phonon mode around this wave number range is well studied in thin film studies of Ge-Sn [8-9]. The Raman spectrum of metastable diamond cubic films of Sn-Ge alloy is reported. In this study, a downshift of Ge-Ge vibrational mode relative to the Raman peak of pure Ge was observed. For the Ge rich Sn-Ge alloy, a weak phonon mode around 240 cm^{-1} has been reported. This mode was assigned as Sn-Ge vibrational mode due to the formation of an extended random alloy having cubic diamond structure. Similarly, for Sn rich Sn-Ge alloy a Raman mode was observed at $\sim 220 \text{ cm}^{-1}$. A scaling law is also reported to relate the vibrational modes of Sn-Ge and Ge-Si alloys. By comparing the Ge-Sn phonon mode observed in thin film studies with this work, the Ge-Sn₁ mode observed at $\sim 225 \text{ cm}^{-1}$ may be due to Sn rich Ge-Sn system. But the presence of an additional mode at $\sim 133 \text{ cm}^{-1}$ can be due to a lower symmetry structure formed at high P-T conditions. The Ge-Sn₁ mode slowly increases in intensity on reducing the pressure further up to 4.3 GPa. Below 4.3 GPa, the intensity of the Ge-Sn₁ mode decreases upon decreasing the pressure. At ambient pressure, Ge-Sn₁ mode is seen at $\sim 215 \text{ cm}^{-1}$ whereas Ge-Sn₂ mode is too weak to observe. The β -Sn TO(Γ) phonon mode of Sn is not seen before heating the sample at $\sim 7.6 \text{ GPa}$. This peak picked up its intensity after laser heating and that may be due to the changes in the orientational distribution of the crystallites after heating [29]. The pressure dependence of phonon modes of Ge-Ge, Sn-Sn, Ge-Sn₁ and Ge-Sn₂ are shown in Fig.3.3. From this figure, it is clear that the pressure dependence of both Ge-Sn₁ and Ge-Sn₂ modes are almost similar. These phonon modes do not correspond to the high pressure phase of Ge and β -Sn [30]. Ge undergoes a pressure induced structural phase

transition at around 10 GPa from the ambient cubic diamond structure to tetragonal (β -Sn) structure [24]. High pressure study of Ge shows that the phonon mode at $\sim 213 \text{ cm}^{-1}$ corresponds to the high pressure β -Sn phase of Ge and the frequency of this mode increases with pressure [30]. By extrapolating Ge-Sn₁ mode up to 10 GPa, the frequency of the mode at ~ 10 GPa is about 234 cm^{-1} . This confirms that the new mode observed at ~ 7.6 GPa and ~ 2000 K is not from the β -Sn phase of Ge. Also, when the pressure is

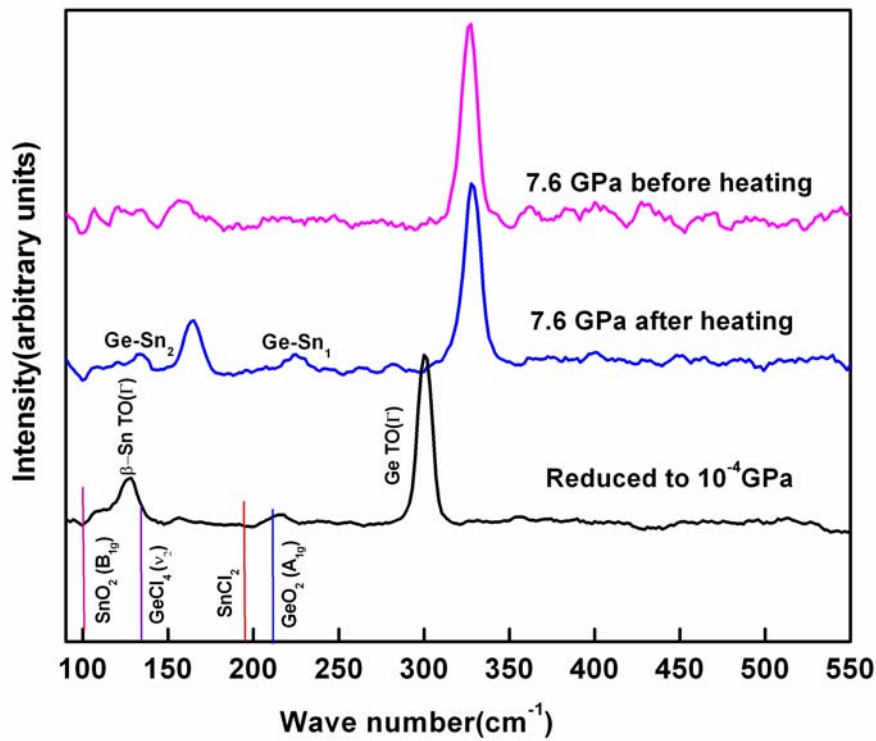


Fig.3.4. Raman spectra of Ge-Sn sample. The stick pattern shows the frequency (in cm^{-1}) of the phonon modes of SnO_2 , GeCl_4 , SnCl_2 and GeO_2 .

released, the β -Sn phase does not directly recover to the ambient cubic diamond phase. Depending on the decompression rate, they form several other high denser tetrahedral phases. The slow decompression of β -Sn phase of Ge leads to the tetragonal st12 phase and this phase persists as metastable phase at ambient pressure [31-34]. Similarly, the

rapid decompression of β -Sn phase of Ge leads to bc8 phase. The details of st12 and bc8 phases are explained in Chapter I. This experiment was conducted in NaCl medium. NaCl was used to achieve insulation of sample from the diamond anvils and also to provide the hydrostaticity. At high temperature, NaCl may react with Ge and β -Sn. The sample and the NaCl may react to form Germanium chloride or stannous chloride. Raman spectra of stannous chloride and Germanium tetrachloride are reported which show that none of their phonon modes match with that of Ge-Sn [35-36]. Since the laser heating experiment is carried out in dry NaCl atmosphere, there is least possibility of forming oxides such as GeO_2 , SnO and SnO_2 [37-39]. A comparison of phonon modes reported in these compounds do not match with that of Ge-Sn phase which is shown in Fig.3.4. The GeO_2 with trigonal structure have four A_{1g} symmetry modes and eight doubly degenerate polar modes of E symmetry. If GeO_2 contamination was present, a

Table 3.2. Mode Grüneisen parameters of various phonon modes at $(d\omega/dp)_{p=0}$.

Mode	Gruneisen parameter(γ)		
	Experiment	Theory	Present work
Ge TO(Γ)	1.14 \pm 0.01 ^a	1.1 \pm 0.1 ^b	1.17
Sn TO(Γ)	2.42 ^c	-----	3.08
GeSn ₁	-----	-----	0.67
GeSn ₂	-----	-----	0.72

^aReference 24,40; ^bReference 41 and ^cReference 29.

few modes belonging to GeO₂ is expected. Though the frequency of the expected A_{1g} mode lies in the proximity of Ge-Sn₁ mode, presence of GeO₂ can be ruled out based on the above consideration.

It will be quite interesting to compare the phonon modes observed in both Ge-Sn and Ge_{1-x}Si_x alloy in the context of Raman spectroscopy. In Ge-Sn system, four Raman modes are observed. But one of the phonon modes, Ge-Sn₂ is too weak to observe at ambient pressure. At ambient pressure, the phonon modes of Ge TO(Γ), β-Sn TO(Γ) and Ge-Sn are observed at ~300.7 cm⁻¹, ~126.6 cm⁻¹ and ~215 cm⁻¹ respectively. Similarly, in Ge_{1-x}Si_x alloy three modes at ~300 cm⁻¹, ~500 cm⁻¹ and ~400 cm⁻¹ corresponding to the vibrational modes of Ge-Ge, Si-Si and Ge-Si respectively are reported [42-43]. At ambient P and T, both Ge and Si crystallize in cubic diamond structure and the difference in size of Ge and Si atoms are below 13 % , obey Hume-Rothery conditions, hence these elements can easily react to form a cubic Ge_{1-x}Si_x alloy. In Ge_{1-x}Si_x system, only one phonon mode is observed at ~400 cm⁻¹ whereas in Ge-Sn system two modes are observed at ~133 cm⁻¹ and ~225 cm⁻¹ at ~7.6 GPa and 2000 K. Since the Ge_{1-x}Si_x phase is a high symmetric cubic phase, only one vibrational mode namely Ge-Si is expected from this system. In Ge-Sn system, both Ge and β-Sn are crystallized in different structures. Hence, we can interpret that after heating the sample at ~7.6 GPa, a lower symmetry structure may be formed from Ge and β-Sn. Hence, in addition to Ge-Sn₁ mode we observe one extra mode namely Ge-Sn₂.

The pressure dependence of the phonon frequencies are calculated with linear approximation as $\omega = \omega_0 + K^H P$. Here, ω_0 is the phonon frequency at zero pressure, P is

the hydrostatic pressure and $K^H = (\partial\omega/\partial p)_{p=0}$ is the hydrostatic linear pressure coefficient. The mode Grüneisen parameter is determined from the pressure coefficients using the relation

$$\gamma = - \partial \ln \omega / \partial \ln V = (B_0 / \omega_0) K^H$$

Here B_0 is the bulk modulus. The bulk modulus of Ge-Sn phase is obtained by linear interpolation of the bulk modulus of Ge ($B=74.37$ GPa) and Sn (55.55 GPa). The mode Grüneisen parameter of all the phonon modes at $P=0$ are shown in Table 3.2. The Grüneisen parameter of Ge TO(Γ) mode is matching well with the value obtained by Olego *et al* [24]. But the Grüneisen parameter of β -Sn TO(Γ) mode is slightly higher as compared to the value obtained by Olijnyk [29].

3.5. HPXRD Study of Ge-Sn Synthesized using LHDAC and Characterized at INDUS-2.

Ge and Sn samples were powdered well and mixed at 3:1 ratio. A pellet of size 100 μm was formed from Ge+Sn mixture. The pellet was pressurized up to 9 GPa by using diamond anvil cell. At ~ 9 GPa, the sample was laser heated using a CO_2 laser. Bright flashes were observed during heating. The fast laser quenched sample was characterized by using synchrotron radiation at INDUS-2. The laser heated sample was analyzed and found no significant change in the XRD pattern implying no new phase formation. The pressure was reduced slowly to the ambient. The XRD pattern the laser heated sample is as shown in Fig.3.5.

To summarize, Ge-Sn system was tried to be synthesized using Bridgman

opposed anvil apparatus. The heating of the sample was carried out at ~ 5 GPa and 773 K for 6 hrs. The characterization of the retrieved sample using synchrotron radiation showed no new phase formation. This shows that the above pressure and temperature

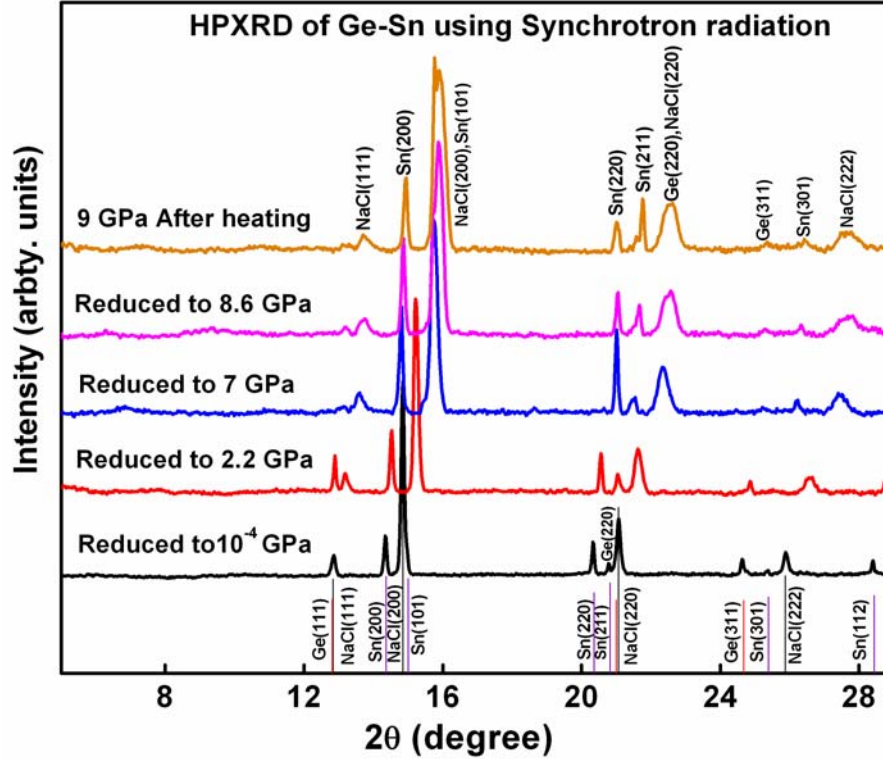


Fig.3.5. HPXRD patterns of Ge+Sn system heated at ~ 9 GPa and ~ 2000 K. The stick patterns from JCPDS are matched with the ambient pattern of Ge, Sn and the NaCl.

conditions may not be sufficient to form Ge-Sn phase. Hence the LHDAC experiments were carried out at higher pressures and temperature conditions. The laser heating of the Ge+Sn mixture in 2:1 wt. ratio was carried out at ~ 7.6 GPa and ~ 2000 K. After laser heating the sample, new phonon modes apart from the parent phonon modes were observed using *in-situ* Raman spectroscopy. The appearance of new phonon modes can

be interpreted as the formation of new Ge-Sn phase at the above P-T conditions. Also, the laser heating of Ge and Sn mixture was carried out at ~9 GPa and ~2000 K at 3:1 wt. ratio. The sample was heated about 30 minutes. The *in-situ* characterization of the sample using synchrotron radiation showed no new phase formation within the detection limits.

3.6 Evidence for Ge-C Bond Formation at High P-T Conditions using *in-situ* Raman Spectroscopy.

A pellet was formed from Ge and carbon foil with 1:1 wt. ratio and the sample was pressurized up to ~9.3 GPa. The sample at ~9.3 GPa was laser heated using a CO₂ laser for about 30 minutes at ~2000 K. The laser heated sample was characterized by using *in-situ* micro-Raman spectrometer. Raman spectra at various portions of the sample were recorded before and after laser heating. At ambient P and T, Ge has a first order TO(Γ) phonon mode at ~300.7 cm⁻¹ [44]. Carbon has a doubly degenerate E_{2g} mode at ~1580 cm⁻¹ and this line arises due to the in-plane vibrations of the adjacent carbon layers [45]. Another phonon mode, A_{1g} observed at ~1360 cm⁻¹, is associated with the in-plane vibrations formed due to structural imperfections [45]. At 9.3 GPa, TO(Γ) phonon mode of Ge is seen shifted to ~332 cm⁻¹ and the E_{2g} mode of carbon is shifted to 1641 cm⁻¹ [Fig.3.6 and Fig.3.7]. After laser heating, Ge TO(Γ) phonon mode is seen to shift to lower wave number at ~327 cm⁻¹. Also a new mode is seen to appear at ~203.3 cm⁻¹. Further the carbon mode shifts to ~1629 cm⁻¹ [Fig.3.7]. Occurrence of the new mode at ~203.3 cm⁻¹ in conjunction with significant softening of the Ge and C modes is indicative of formation of a new phase. Softening of the Ge and C

modes may also be partially due to a possible drop in the pressure (of ~1-2 GPa) post laser heating the sample. The drastic intensity reduction of the Ge TO(Γ) mode after laser heating [Fig.3.6] is indicative of consumption of Ge in a direct reaction with carbon.

A first principle calculation based on a generalized gradient approximation to the density functional theory is reported in Ge-C system by Pandey *et al* [23]. They explored the possibility of high pressure synthesis of Ge-C alloy with pressure. By studying the variation of Gibb's free energy with pressure they showed that the Ge-C system is stable only above ~25 GPa at 0 K. However, this prediction should be treated with caution since one of the elemental components Ge undergoes pressure induced structural phase transition at around 9 GPa [46]. Similarly, the calculations performed using a plane wave expansion within the local density approximation and the pseudo potential approximation showed that the alloy is stable around 15 GPa and at 0 K [22]. In this calculation also the energy released during the phase transition from cubic diamond to tetragonal phase is not taken in to account in the Hamiltonian [22]. In this experimental work, the Ge-C bond formation is observed at ~9.3 GPa and ~2000 K. But according to the above calculations, there is no possibility of bond formation at ~9.3 GPa. The above calculations, there is no possibility of bond formation at ~9.3 GPa. The pressure is not the only parameter to decide the reaction kinetics but the effect of temperature is also has to be taken into account. So by the simultaneous application of pressure and temperature there may be a possibility of reaction between Ge and C even at low pressure. Hence the formation of Ge-C bond can be possible at pressures less than ~9 GPa and high temperatures which is what is reported here.

The Ge-Sn and Ge-C compounds were synthesized in a Laser Heated Diamond

Anvil Cell (LHDAC) facility. In Ge-Sn system there was no pressure drop after laser heating the sample whereas a pressure drop of ~2 GPa was observed in Ge-C system [Fig.3.6 and Fig.3.7]. This considerable amount of pressure drop is usually observed in

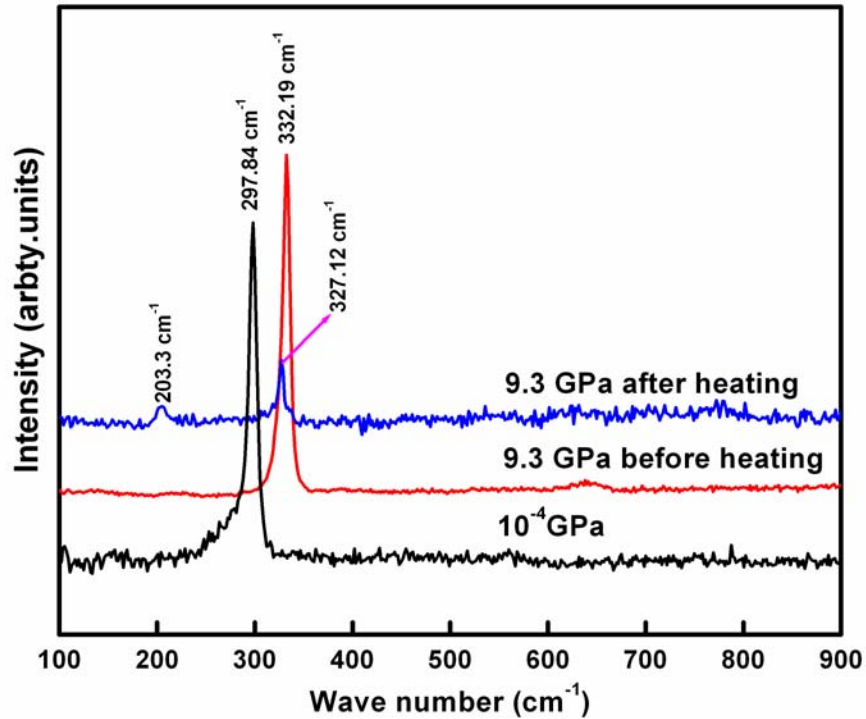


Fig.3.6. Raman spectra of Ge+C system at 300 K, depicting softening of the Ge vibrational mode post laser heating at 9.3 GPa.

laser heating experiments at high pressure. One possibility of the pressure drop may be due to the relaxation of gasket after laser heating. Additionally, a noticeable drop in intensity of Ge TO(Γ) phonon mode after laser heating can be due to the consumption of Ge during the direct reaction between Ge and carbon. The appearance of only one phonon mode at ~9.3 GPa and ~2000 K in Ge-C can be due to the formation of a higher symmetry Ge-C phase. In Ge-Sn system, two new modes namely Ge-Sn₁ and Ge-Sn₂ were observed. The appearance of the additional Ge Sn₂ mode can be interpreted

as the formation of a lower symmetry Ge-Sn phase at high P-T conditions.

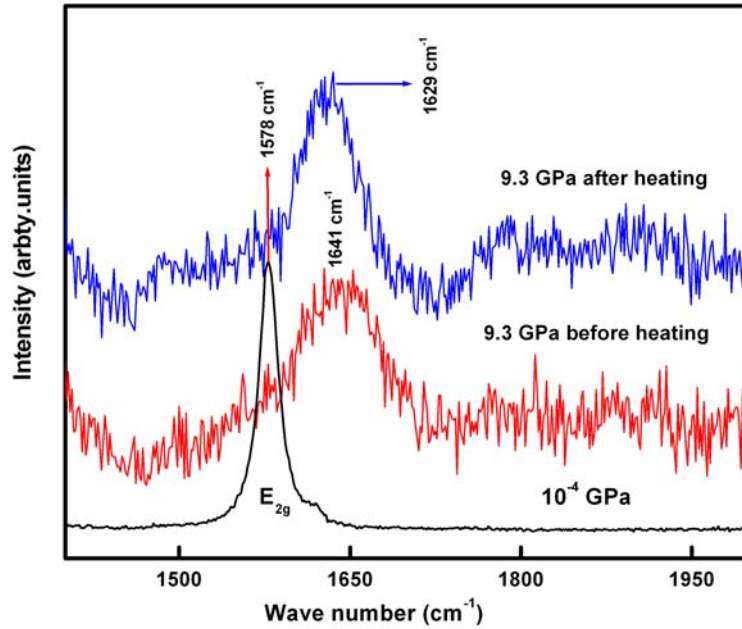


Fig.3.7. Raman spectra of Ge+C system at 300 K.

3.7 Investigation of Pb-C at HP-HT Conditions using LHDAC

Lead is a group IV element which crystallizes in face centered cubic structure at Room temperature. It transforms to the hexagonal-close packed structure at around 13 GPa [47-48]. Here we tried to synthesize and study the properties of Pb-C compound from the starting elements Pb and C. No phase diagram is reported for the Pb-C system. The PbC₂ compound was formed by increasing the solubility of carbon in lead at higher temperature using chemical reaction method was reported [49-50]. The solubility of carbon in liquid lead was reported to be 0.41, 0.79 and 1.60 at.% at the corresponding temperatures 1170, 1415 and 1555°C [49-50]. But the stability and crystal structure of PbC₂ compound are unknown. In this thesis work, the Pb+graphite mixture was pressuri-

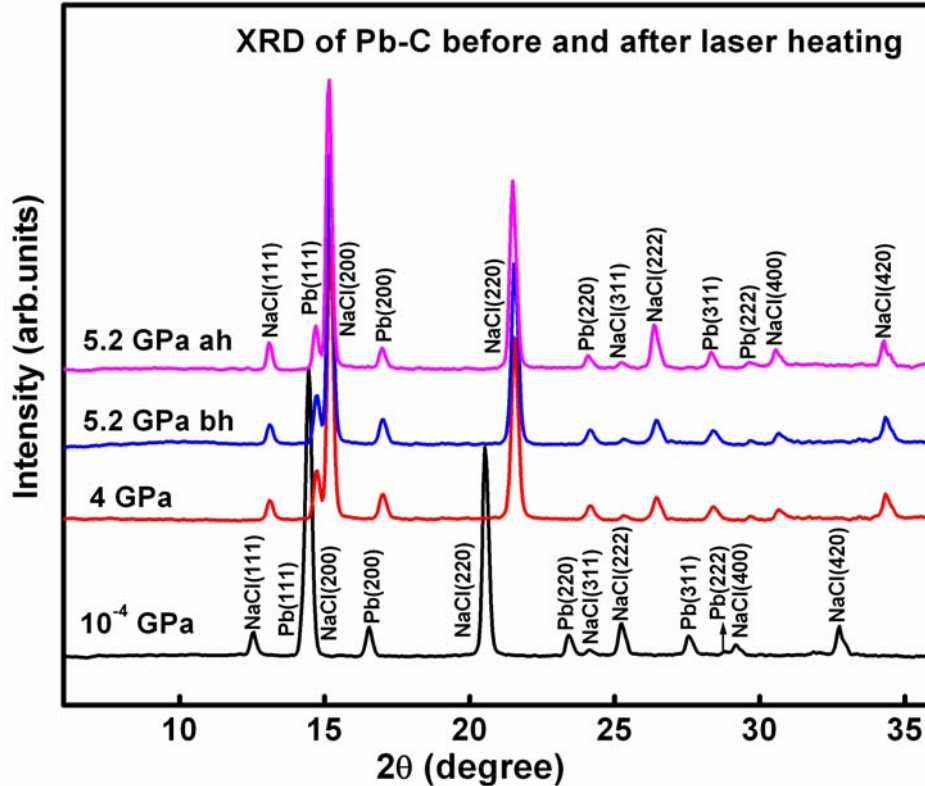


Fig.3.8. HPXRD pattern of Pb+C mixture pressurized up to 5.2 GPa and then laser heated using CO₂ laser.

Zed up to ~5.2 GPa and the sample was laser heated with CO₂ laser for about 30 minutes. The HPXRD pattern of the sample after laser heating does not show any indication of any new phase formation. Fig.3.8 shows the HPXRD pattern of Pb-C before and after laser heating at ~5.2 GPa and also at intermediate pressure. Also, *in-situ* Raman spectroscopy was carried out to investigate any new bond formation. Lead crystallizes as an fcc structure and its crystal lattice is Raman inactive. Graphite has a Raman active mode at around 1580 cm⁻¹ as shown in Fig.3.9. At ~ 5.2 GPa, the graphite Mode is shifted to new ~1603 cm⁻¹. The laser heating of the sample at ~5.2 GPa does not show any indication of bond formation.

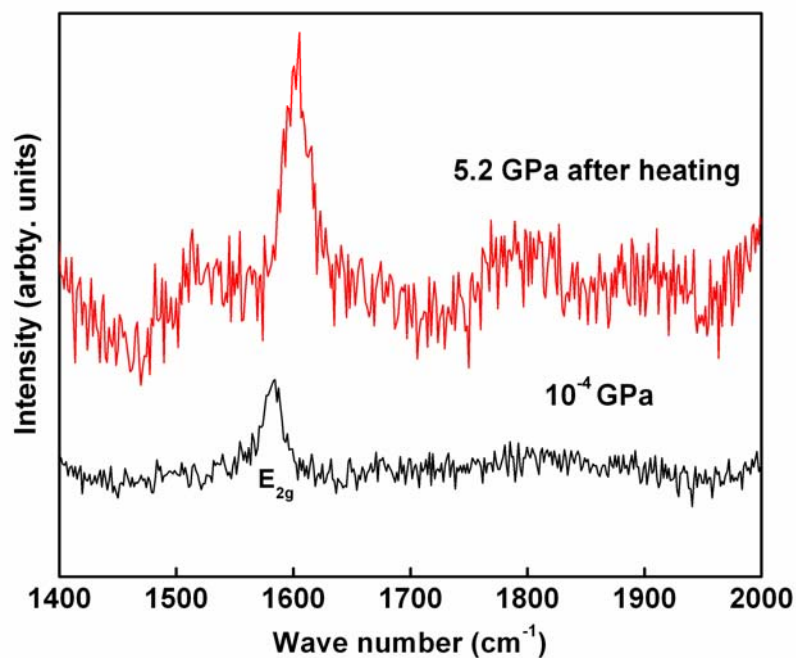


Fig.3.9. Raman spectra of Pb-C at ambient and 5.2 GPa in the graphite range.

3.8 Conclusion

Ge-Sn compound was synthesized using *in-situ* Raman spectroscopy in a laser heated diamond anvil cell. At ~ 7.6 GPa and ~ 2000 K apart from characteristic optical phonon modes of Ge and Sn, two new modes were observed. One mode was observed at ~ 225 cm^{-1} labeled as Ge-Sn₁ and the other one at ~ 133 cm^{-1} labeled Ge-Sn₂ mode. When the pressure is reduced to the ambient, the Ge-Sn₁ mode remains stable at ~ 215 cm^{-1} whereas the Ge-Sn₂ mode is very weak to observe at ambient. The mode Grüneisen parameters of the modes are also calculated and compared with other literature values. The characterization of Ge-Sn sample using synchrotron radiation at INDUS-2 was performed at ~ 9 GPa and ~ 2000 K. But no appreciable results could be obtained. The synthesis of Ge-C system was also explored using LHDAC and Raman spectroscopy. Raman spectra at various regions of the laser heated sample at ~ 9.3 GPa and 300 K

shows in addition to the characteristic Ge TO(Γ) and E_{2g} phonon modes of C, both of which are considerably softened, a new mode appearing at $\sim 203.3 \text{ cm}^{-1}$. These are ascribed to Ge-C bond formation. The LHDAC synthesis of Pb-C system was attempted at $\sim 5.2 \text{ GPa}$ and $\sim 2000 \text{ K}$. HPXRD and the Raman study of Pb-C at 5 GPa and 2000 K show no indication of compound formation.

References

- [1] Xiaobo Hu, and Xiangang Xu, "Thermal conductivity of 4H-SiC single crystals" *Journal of Applied Physics* **113** 053503(1-4) (2013)
- [2] T. P. Pearsall, "Silicon-germanium alloys and heterostructures: Optical and electronic properties" *Crit. Review. Solid State Mater. Sci.* **15** 551-2168 (1989)
- [3] Y. Chibane and M. Ferhat, "Electronic structure of $\text{Sn}_x\text{Ge}_{1-x}$ alloys for small Sn compositions: Unusual structural and electronic properties" *Journal of Applied Physics* **107** 053512(1-8) (2010)
- [4] Gang He and Harry A. Atwater, "Interband Transitions in $\text{Sn}_x\text{Ge}_{1-x}$ Alloys" *Physical Review Letters* **79** 1937-1940 (1997)
- [5] R. W. Olesinski and G. J. Abbaschian, *J. Phase Equilibria* **5** 2659(1984)
- [6] X. Deng, B.-K. Yang, S. A. Hackney, M. Krishnamurthy and D. R. M. Williams, "Formation of self-assembled quantum wires during epitaxial growth of strained Ge-Sn alloys on Ge (100): trench excavation by migrating Sn islands" *Physical Review Letters* **80** 1022-1025 (1998)
- [7] S. Stefanov, J. C. Conde, A. Benedetti, C. Serra, J. Werner, M. Oehme, J.

- Schulze, D. Buca, B. Holländer, S. Mantl and S. Chiusi, “Laser synthesis of germanium tin alloys on virtual germanium” *Appl. Phys. Lett.* **100** 104101(1-3) (2012)
- [8] J. Taraci, S. Zollner, M. R. McCartney, J. Menendez, M. A. Santana-Aranada, D. J. Smith, A. Haaland, A. V. Tutukin, G. Gunderson, G. Wolf and J. Kouvetakis, “Synthesis of Silicon-Based Infrared Semiconductors in the Ge-Sn System Using Molecular Chemistry Methods” *J. Am. Chem. Soc.* **123** 10980-10987 (2001)
- [9] M. Bauer, J. Taraci, J. Tolle, A. V. G. Chizmeshya, S. Zollner, D. J. Smith, J. Smith, J. Menendez, C. Hu and J. Kouvetakis, “Ge-Sn semiconductors for band-gap and lattice engineering” *Appl. Phys. Lett.* **81** 2992-2994 (2002)
- [10] S. Oguz, W. Paul, T. F. Deutsch, B-Y. Tsaur and D. V. Murphy, “Synthesis of metastable, semiconducting Ge-Sn alloys by pulsed UV laser crystallization” *Appl. Phys. Lett.* **43** 848-850 (1983)
- [11] T. Soma, K-I. Kamada and H-M. Kagaya, “Prediction of α -phase Ge-Sn solid solution under pressure” *Solid State Communications* **67** 155-158 (1988)
- [12] T. Soma, N. Mori and H-M. Kagaya, “Equation of state for α -phase Ge-Sn solid solution” *Solid State Communications* **75** 831-833 (1990)
- [13] R. Pandey, M. Rerat, M. Causa, “First-principles study of stability, band structure, and optical properties of the ordered $\text{Ge}_{0.50}\text{Sn}_{0.50}$ alloy” *Appl. Phys. Lett.* **75** 4127-4129 (1999)
- [14] G. A. Voronina, C. Pantea, T. W. Zerda, J. Zhang, L. Wang, Y. Zhao, “In situ X-ray diffraction study of germanium at pressures up to 11 GPa and temperatures up

- to 950 K” *Journal of Physics and Chemistry of Solids* **64** 2113-2119 (2003)
- [15] M. Liu, L. -G. Liu, *High Temp.-High Press.*, **18** 79 (1986)
- [16] Andrea Di Cicco, Anna Chiara Frasini, Marco Minicucci, Emiliano Principi, Jean-Paul Itie` and Pascal Munsch, “High-pressure and high-temperature study of phase transitions in solid germanium” *phys. stat. sol. (b)* **240** 19-28 (2003)
- [17] K. J. Chang and Marvin L. Cohen, “First-principles study of the structural properties of Ge” *Physical Review B* **34** 8581-8590 (1986)
- [18] C. Guillaume, G. Serghiou, A. Thomson, J-P. Morniroli, D. J. Frost, N. Odling and M. Mezouar, “Tuning between mixing and reactivity in the Ge-Sn system using pressure and temperature” *J. Am. Chem. Soc.* **131** 7550-7552 (2009)
- [19] G. Serghiou, C. L. Guillaume, C. E. Jeffree, A. Thomson, D. J. Frost, J-P. Morniroli and N. Odling, “Imaging of mixing and reaction in group IV systems recovered from high pressures and temperatures” *High Pressure Research.* **30** 44-50 (2010)
- [20] Z. T. Liu, J. Z. Zhu, N. K. Xu and X. L. Xheng, “Structure and Properties of Germanium Carbide films prepared by RF sputtering in Ar/CH₄” *Jpn. J. Appl. Phys.* **36** 3625-3628 (1997)
- [21] N. Saito, I. Nakaaki, H. Iwata and T. Yamaguchi, “Optical and electrical properties of undoped and oxygen-doped a-GeC:H prepared by magnetron sputtering” *Thin Solid Films* **515** 3766- 3771 (2007)
- [22] O. F. Sankey, A. A. Demkov, W. T PetusKey and P. F. McMillan, “Energetics

- Modelling. electronic structure of the hypothetical cubic zincblende form of GeC*
Modelling. Mater. Sci. Eng. **1** 741-754 (1993).
- [23] R. Pandey, M. Rerat, C. Darrigan and M. Causa, “A theoretical study of stability, electronic, and optical properties of GeC and SnC” *J. Appl. Phys.*, **88** 6462-6466 (2000)
- [24] Diego Olego and Manuel Cardona, “Pressure dependence of Raman phonons of Ge and 3C-SiC” *Physical Review B* **25** 1151-1160 (1982)
- [25] K. Wattal (2007) Nuclear Fuel cycle. BARC highlights, Bhabha Atomic Research Centre, Chapter 4: Basic studies.
- [26] William A Frad (1968), Metal Carbides. In Harry Julius Emeléus, Advances in inorganic chemistry and radiochemistry. volume 12, page 213.
- [27] N. Subramanian, N. V. Chandra Shekar, N. R. Sanjay Kumar and P. Ch. Sahu, “Development of laser-heated diamond anvil cell facility for synthesis of novel materials” *Current Science* **91** 175-182 (2006)
- [28] A. K. Sinha, G. M. Bhalerao, A. Jaiswal, R. K. Gupta, M. N. Singh, Adu Verma and R. V. Nandedkar, “Commissioning experiences of hard x-ray beam line (B-12) on Indus-2 for high resolution powder diffraction” *Proceedings of DAE Solid State Physics Symposium* P-365 (2006).
- [29] Helmut. Olijnyk, “Pressure dependence of Raman phonons of metallic β -Sn” *Physical Review B* **46** 6589-6591(1992)
- [30] H. Olijnyk, “Raman Scattering in metals up to 50 GPa” *High Pressure Research* **10** 461-464 (1992)

- [31] F. P. Bundy and J. S. kasper, "A new dense form of solid germanium" *Science* **139** 340-341 (1963)
- [32] R. J. Nelmes, M. I. McMahon, N. G. Wright, D. R. Allan and J. S. Loveday, "Stability and crystal structure of BCS germanium" *Physical Review B* **48** R9883-R9886 (1993)
- [33] S. B. Gadri, E. F. Skelton and A. W. Webb, "High pressure studies of Ge using synchrotron radiation" *J. Appl. Phys.* **54** 3609 (1983)
- [34] Carmen S. Menoni, Jing Zhu Hu and Ian L. Spain, "Germanium at high pressures" *Physical Review B* **34** 362-368 (1986)
- [35] Laurence S. Foster, J. W. Drenan, A. F. Williston, "Preparation of Germanium Tetrachloride, GeCl₄" *J. Am. Chem. Soc.* **64** 3042-3042 (1942)
- [36] J. H. R. Clarke and C. Solomons, "Raman spectra and the structure of molten stannous chloride and molten mixtures of stannous chloride and potassium chloride" *J. Chem. Physics* **47** 1823-1826 (1967)
- [37] J. F. Scott, "Raman spectra of GeO₂" *Phys. Rev. B* **1** 3488-3493 (1970)
- [38] Matthias Batzill, Ulrike Diebold, "The surface and materials science of tin oxide" *Progress in Surface Science* **79** 47-154 (2005)
- [39] A. Die'guez, A. Romano-Rodri'guez, A. Vila' and J. R. Morante, "The complete Raman spectrum of nanometric SnO₂ particles" *J. Appl. Phys.* **90** 1550-1557 (2001)
- [40] J. B. Renucci, M. A. Renucci and M. Cardona, "Volume dependence of the Raman frequencies of Ge-Si alloys" *Solid State Communications* **9** 1651-1654

- (1971)
- [41] T. Soma, H. Matsuo and Y. Saitoh, "Mode Grüneisen parameters for long-wave phonons under pressure of Si and Ge" *Solid State Communications* **39** 913-916 (1981)
- [42] W. J. Byra, "Raman scattering in Ge-Si alloys" *Solid State Communications* **12** 253-257 (1973)
- [43] D. W. Feldman, M. Ashkin and James H. Parker, "Raman scattering by local modes in germanium rich Silicon-Germanium alloys" *Physical Review Letters* **17** 1209-1212 (1966)
- [44] J. H. Parker, D. W. Feldman and M. Ashkin, "Raman Scattering by Silicon and Germanium" *Phys. Rev.* **155** 712-714 (1967)
- [45] R. Vidano and D. B. Fischbach, "New Lines in the Raman Spectra of Carbons and Graphite" *Journal of The American Ceramic* **61** 11-17 (1978)
- [46] M. Baublitz and A. L. Ruoff, "X-ray diffraction from high pressure Ge using synchrotron radiation" *J. Appl. Phys.* **53** 5669-5671 (1982)
- [47] T. Takahashi, H. K. Mao and W. A. Bassett, "Lead: X-ray Diffraction Study of a High-Pressure Polymorph" *Science* **165** 1352-1353 (1969)
- [48] H. K. Mao, Y. Wu, J. F. Shu, J. Z. Hu, R. J. Hemley and D. E. Cox, "High - pressure phase transition and equation of state of lead to 238 GPa" *Solid State Communications* **74** 1027-1029 (1990)
- [49] O. Ruff and B. Bergdahl, *Z. Anorg. Chem.* **106** 91 (1919)

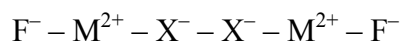
[50] J. F. Durand, *Compt. Rend* **177** 693 (1923)

Chapter IV

Pressure Induced Structural Phase Transition Studies of PbFX (X=Cl, Br) Systems

4.1 Introduction

Ionic layered compounds of the form MFX, where M is a divalent metallic cation (Ca^{2+} , Sr^{2+} , Ba^{2+} , Pb^{2+} or Eu^{2+}) and $\text{X} = \text{Cl}^-$, Br^- or I^- , crystallize in tetragonal structure with space group P4/nmm [1]. A typical unit cell of MFX has two formula units in which the arrangement of atomic layers perpendicular to the c-axis is in the following sequence



The unit cell of PbFCl compound (matlockite) is shown in Fig.4.1. These materials have interesting properties such as photoconductivity [2], photoluminescence [3-4] and anisotropic ionic conductivity [5-6] and find application in various fields. For example, BaFBr doped with Eu^{2+} ($\text{BaFBr}:\text{Eu}^{2+}$) has been successfully applied for detecting X-rays as Imaging phosphors due to the photo stimulated luminescence property [7]. Similarly, $\text{BaFCl}:\text{Sm}^{2+}$ is used as a pressure sensor in the high pressure experiments [8]. Based on detailed luminescence study, pure PbFCl has been demonstrated to be an excellent scintillation detector material for neutrino detection [9]. High pressure structural behavior of the matlockite structure compounds such as BaFCl, BaFBr and BaFI have been extensively studied [10-18]. These systems undergo a series of symmetry lowering structural transitions: tetragonal \rightarrow orthorhombic \rightarrow monoclinic and have been attributed to a gradual anisotropic distortion of the charge distribution in the planes perpendicular to

the stacking direction [11-13]. Detailed high pressure structural behavior studies on PbFCl and PbFBr have not been reported yet. Replacement of Ba^{2+} with Pb^{2+} can be expected to result in stronger attraction between the two adjacent Cl^- layers on account of

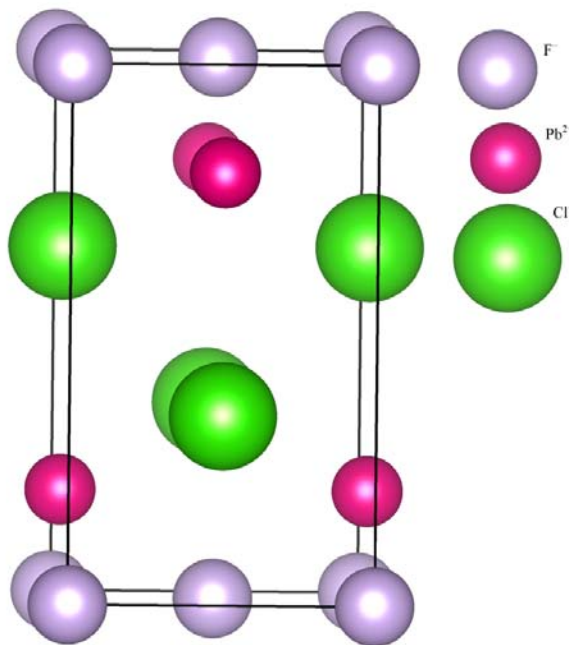


Fig.4.1. Unit cell of PbFCl compound. The spheres with the labels F^- , Pb^{2+} and Cl^- represent the type of ions. Ionic positions of PbFCl are Pb (0 0.5 0.2); F (0 0 0) and Cl (0 0.5 0.65).

the larger electronegativity of Pb^{2+} (Fig.4.1). It will be interesting therefore to see if PbFCl and PbFBr exhibit a similar structural sequence induced by pressure and study the stability range.

4.2 Experimental Details

Stoichiometric mixtures of PbF_2 and $\text{PbX}_2 \cdot n\text{H}_2\text{O}$ ($n \sim 2$) in nitrogen atmosphere using solid state reaction method. Powder X-ray diffraction pattern of PbFCl showed that

the compound was in single phase with tetragonal matlockite structure ($P4/nmm$). The lattice parameters obtained from the powder pattern were: $a = 4.097(3) \text{ \AA}$ and $c = 7.224(2) \text{ \AA}$ and these values matched well with the Joint Committee for Powder Diffraction Standard (JCPDS) values of $a = 4.1104(2) \text{ \AA}$ and $c = 7.2325(5) \text{ \AA}$ [19]. Similarly the lattice parameters obtained for PbFBr were: $a = 4.189(4) \text{ \AA}$ and $c = 7.597(1) \text{ \AA}$ and these values matched well with the Joint Committee for Powder Diffraction Standard (JCPDS) values of $a = 4.191 \text{ \AA}$ and $c = 7.591 \text{ \AA}$ [20]. A Mao-Bell type diamond anvil cell (DAC) with culet size of $\sim 500 \text{ \mu m}$ in diameter was used for the high pressure experiments. A stainless steel gasket was preindented to a thickness of 50 \mu m ; a hole of diameter 200 \mu m was drilled at its centre. The finely powdered sample was loaded into the gasket hole. A 4:1 mixture of methanol and ethanol was used as the pressure transmitting medium. Pressure was determined using the equation of state of gold which was loaded along with the sample. HPXRD experiments were performed on the sample in angle dispersive geometry using $\text{Mo K}_{\alpha 1}$ X-ray radiation obtained from an 18 kW rotating anode X-ray generator and monochromatized by a graphite monochromator. An image plate based mar345dtb diffractometer with overall resolution of $\delta d/d \sim 0.001$ was used for detecting the diffracted X-rays. The sample to detector distance was calibrated using LaB_6 . Each XRD pattern was recorded with an exposure time of ~ 2 hours. The XRD image was reduced from 2-dimension (2D) XRD to 1-dimension (1D) by Fit2d software for further analysis [21]. *In-situ* Raman study was also carried out on PbFCl. In this study the pressure was estimated by standard ruby fluorescence technique [22]. Raman spectra of the sample was recorded for both increasing and decreasing pressure cycle using a Renishaw *in-via* Raman spectrometer (1 \mu m spatial resolution; 514.5 nm excitation from

argon laser).

4.3 High Pressure Structural Stability Studies of PbFCl using X-ray Diffraction

Representative XRD patterns of PbFCl at several pressures are shown in Fig.4.2. These were analyzed using powd [23] and NBS-Aids*83 programmes [24] to obtain the

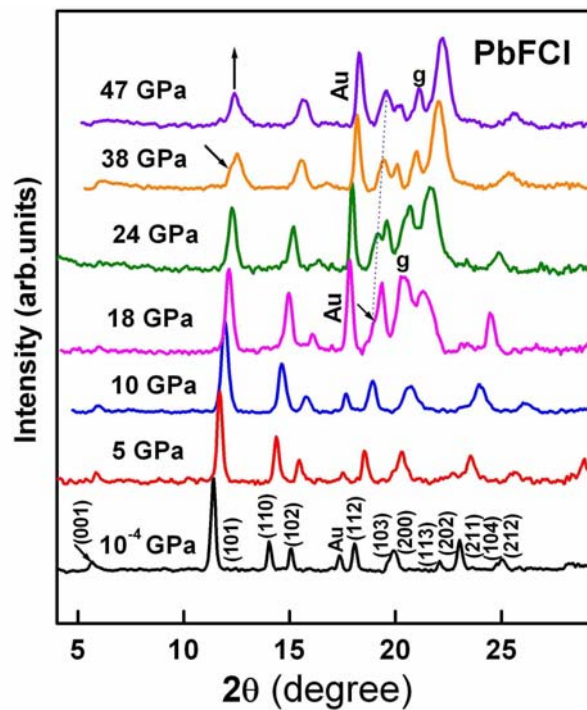


Fig.4.2. The angle dispersive X-ray diffraction spectra of PbFCl at various pressures. The slanted arrow indicates the emergence of new peaks. ‘Au’ is the pressure marker. The intensity of (301)_o peak for the high pressure orthorhombic phase also increases upward arrow indicates the intensity enhancement of the new peaks. ‘g’ is the gasket peak. The dotted line indicates the intensity enhancement of the new peak at around 18 GPa.

lattice parameters. The XRD pattern at ~ 18 GPa shows a new peak emerging at $2\theta \approx 19^\circ$. On further pressurizing the sample, the intensity of the new peak is seen to increase. In addition to the new peak, other significant changes are also observed in the XRD patterns. For instance, the intensity of the (102) peak decreases, whereas that of the (200) peak increases drastically as shown in Fig.4.3. The analysis of the HPXRD pattern at ~ 21 GPa showed that the new structure is orthorhombic with lattice parameters $a = 7.751(1)$ Å, $b = 3.346(5)$ Å and $c = 3.838(3)$ Å with possible space group *Pbam*. The

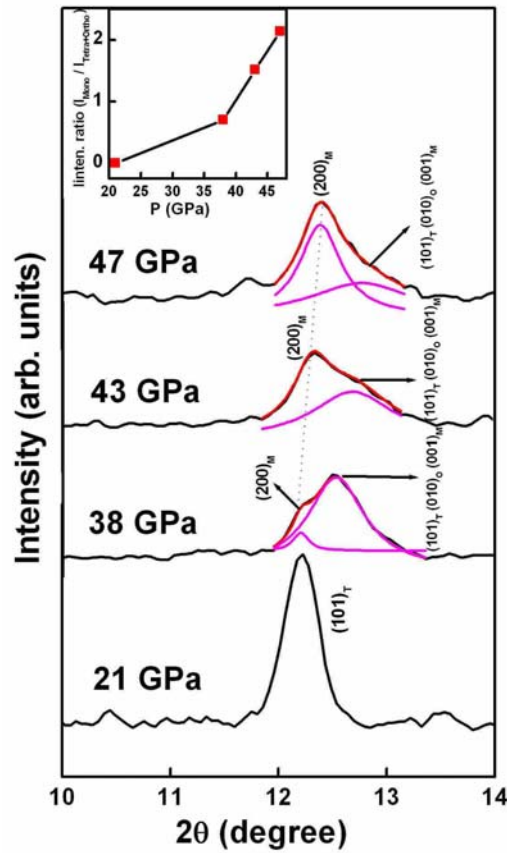


Figure 4.3. Splitting of $(101)_T$ peak of the tetragonal phase at around 38 GPa. The dotted line indicates the intensity enhancement of the new peak. Inset is the intensity ratio of the new peak $(200)_M$ for the monoclinic phase to the $(101)_T$ peak of the tetragonal phase.

starting tetragonal phase was seen to coexist with the high pressure orthorhombic phase up to ~ 38 GPa. When pressure is applied on the tetragonal lattice of PbFCl compound, there can be a large compression of the electron charge density of Cl⁻ ions along c-axis as compared to the a-b plane. This causes the anisotropic redistribution of the charge

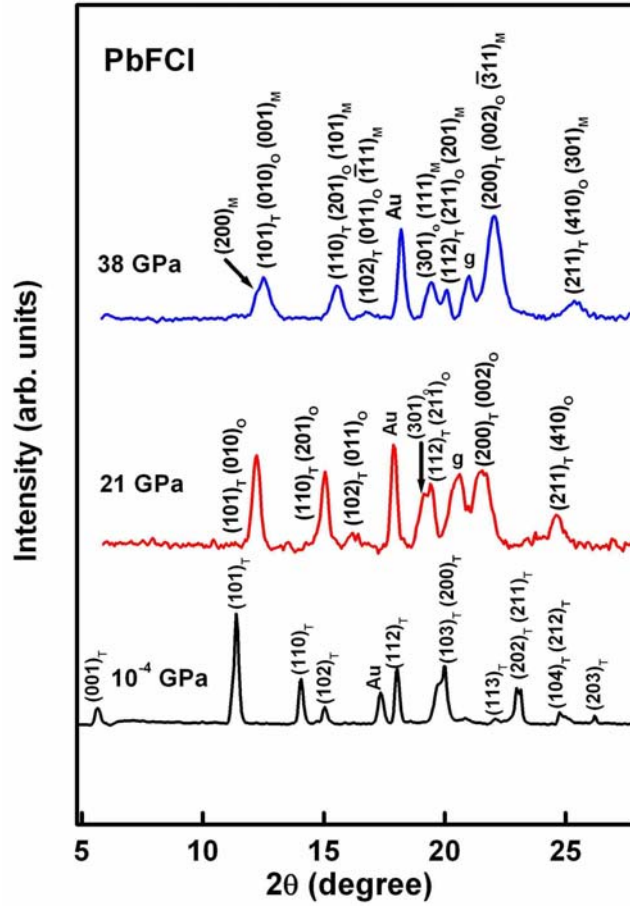


Fig.4.4. The X-ray diffraction pattern of PbFCl at ambient, 21 GPa and at 38 GPa. The suffixes ‘T’, ‘O’, and ‘M’ to the (h k l) indices represent the

cloud along the a-b plane which leads to a gradual distortion (stretching of a-axis) of the tetragonal lattice [11-13].

On further increasing the pressure, around 38 GPa, a second new peak emerges at

$2\theta = 12.2^\circ$ as shown in Fig.4.2. The intensity of this new peak enhances on further increasing pressure (Fig.4.3). The (102) peak belonging to the starting tetragonal phase is seen to reduce in intensity drastically and almost vanishes at ~ 47 GPa as shown in Fig.4.3. The splitting of $(101)_T$ peak of the ambient tetragonal phase to a doublet at

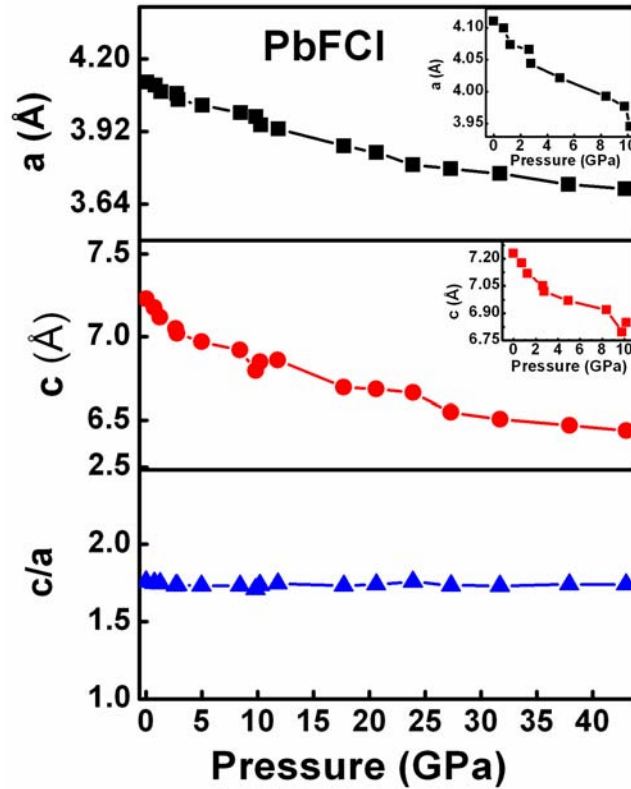


Fig.4.5. Pressure dependence of lattice lattice parameters and c/a ratio of tetragonal phase of PbFCl. The pressure dependence of a and c up to 10 GPa is shown as inset.

around 38 GPa is shown in Fig.4.3. The intensity of this peak is seen to increase on further increasing pressure and is represented as a dotted line. The drastic increase in intensity of the new peak $(200)_M$ for the monoclinic phase to that of the parent peak is shown as inset (Fig.4.3). At around 47 GPa the lattice is almost transformed to

monoclinic phase. The intensity of (301)_O peak for high pressure orthorhombic phase also increases with pressure (Fig.4.3 and Fig.4.4). The XRD pattern at ~38 GPa was taken up for detailed analysis. The pattern could be indexed to a mixture of the tetragonal, orthorhombic and monoclinic phases. The monoclinic phase was seen to be similar to that in BaFCl, namely having space group $P2_1/m$. The lattice parameters for the three co-existing phases at ~38GPa: $a_{\text{Tetra}}=3.720(3)$ Å and $c_{\text{Tetra}}=6.509(1)$ Å; $a_{\text{Ortho}}=7.599(1)$ Å, $b_{\text{Ortho}}=3.281(3)$ Å and $c_{\text{Ortho}}=3.562(1)$ Å and $a_{\text{Mono}}=7.340(3)$ Å, $b_{\text{Mono}}=3.546(4)$ Å, $c_{\text{Mono}}=3.428(5)$ Å and $\beta_{\text{Mono}}=107.86$; with two formula units in the unit cell. This co-existence of phases over a wide pressure range is typical of systems that undergo gradual symmetry lowering transition sequence, for example, like in BaFX systems [13, 15, 25]. It will be interesting to study the mechanism of structural phase transition of PbFCl in comparison with similar matlockite compounds. In PbFCl crystal lattice, the adjacent Cl⁻ ion layers are bonded by weak ionic bonding. There exists an attraction of the Pb²⁺ ions with both Cl⁻ and F⁻ ions. Similarly there exists repulsion between the adjacent layers containing chloride ions and also between fluoride ions (Fig.4.1). The pressure dependence of a, c and c/a ratio of tetragonal lattice is shown in Fig.4.5. From the Fig.4.6, it is clear that for pressures below 10 GPa, the variation of lattice parameter ‘c’ with pressure is slightly faster as compared to ‘a’. At higher pressure (beyond 15 GPa), the lattice parameter ‘c’ increases much faster than that of ‘a’ [Fig.4.6]. This anisotropic compression of lattice parameters ‘a’ and ‘c’ of the tetragonal lattice of PbFCl arise from the weak bonding of adjacent chloride ion layers. This anisotropic compression leads to the redistribution of the charge cloud of the Cl⁻ ions in the a-b plane. This in turn causes the gradual distortion of tetragonal lattice into a lower

symmetry orthorhombic lattice. The phase transition thus observed is sluggish in nature due to the small Gibb's free energy difference between the tetragonal and orthorhombic phases [15]. On further pressurizing the lattice, the orthorhombic lattice gets tilted in the a-b plane which leads to the phase transformation from orthorhombic to monoclinic

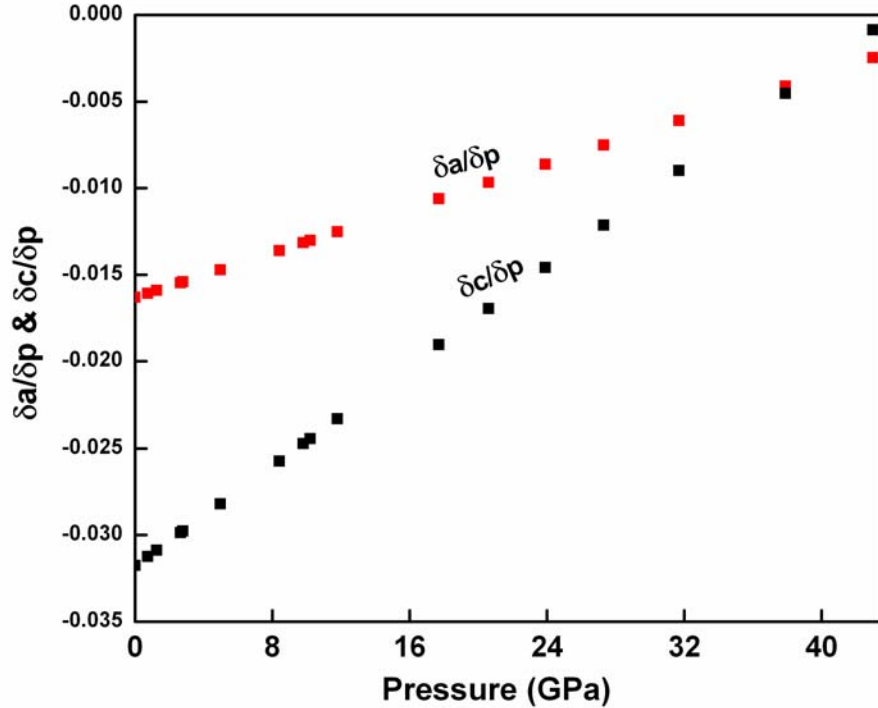


Fig.4.6. Pressure dependence derivative of lattice lattice parameters a and c of tetragonal phase of PbFCl.

phase at ~38 GPa [26]. Another possibility is that at ~18 GPa the tetragonal phase gradually starts to tilt with pressure in the a-b plane. Above 18 GPa, the continuous tilting of the tetragonal lattice with respect to the c-axis leads to the phase transition at around 38 GPa. The phase transitions observed are also not sharp, but continuous. This is due to the small Gibb's free energy difference between these phases [15]. Fig.4.7 shows the variation of lattice spacings $d_{(hkl)}$ of PbFCl as a function of pressure before and after

the transition. The dotted lines at ~18 GPa and ~38 GPa indicate the emergence of new phases. The capital bold letters T, O and M at the top of the graph represent the tetragonal, orthorhombic and monoclinic phases respectively. The indices with subscripts T, 'O' indicate the mixture of tetragonal and the orthorhombic phases. Similarly the indices with subscripts 'T', 'O' and 'M' indicate the mixture of

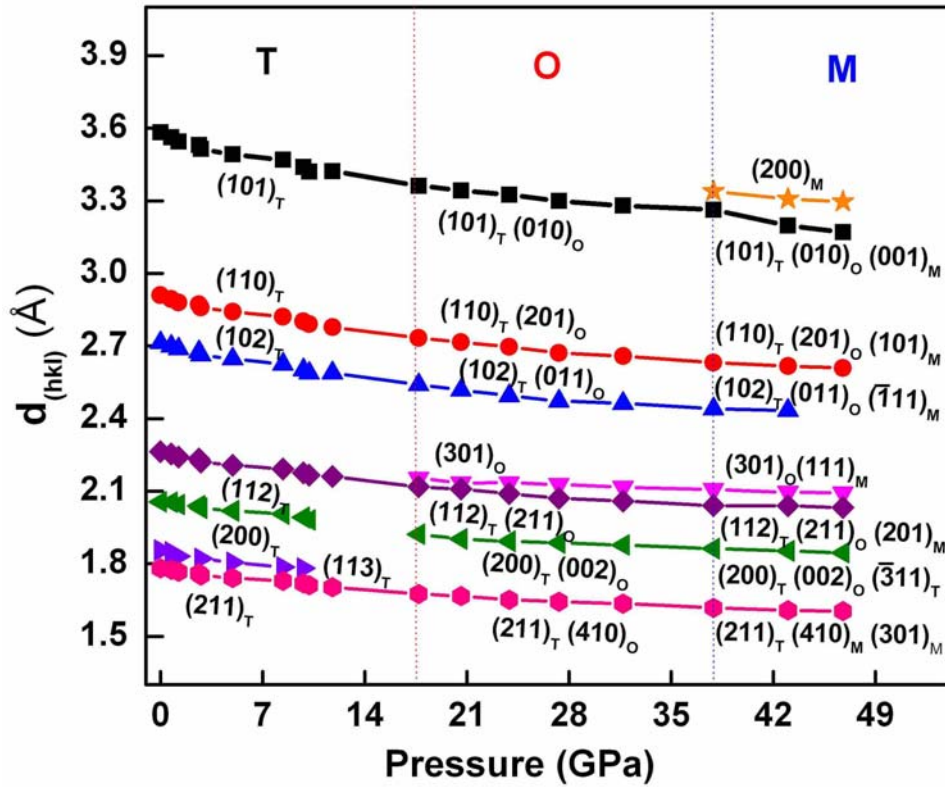


Fig.4.7. P Vs $d_{(hkl)}$ spacings of PbFCl before and after the phase transitions.

tetragonal, orthorhombic and monoclinic phases respectively. The indices with the subscript 'M' indicate the monoclinic phase. The P-V curve for the tetragonal phase is shown in Fig. 4.8. The data has been fitted to the Murnaghan equation of state [27]. The solid line is the best fit to the Murnaghan equation of state and is given by

$$P(V) = \left(\frac{B_0}{B_0'} \right) \left[\left(\frac{V}{V_0} \right)^{-B_0'} - 1 \right]$$

where B_0 and B_0' are the bulk modulus and the first derivative of bulk modulus at zero pressure. V_0 and V are the volumes at zero pressure and at pressure P . The bulk

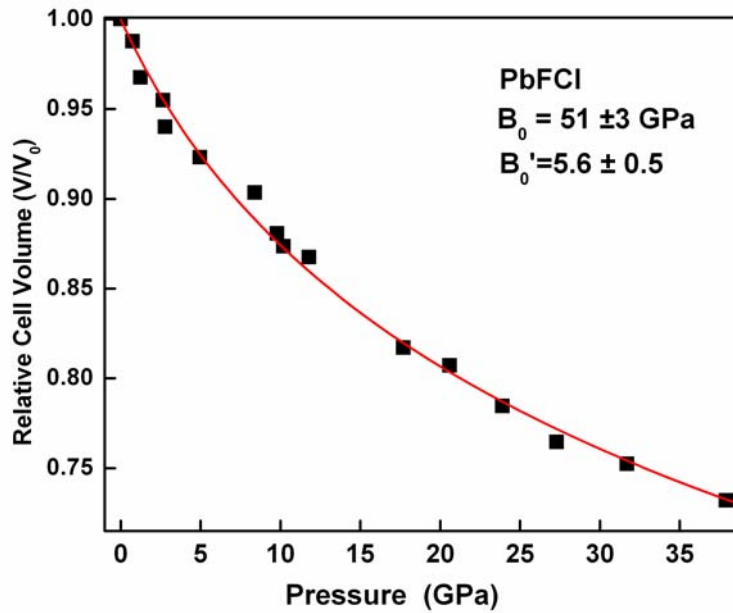


Figure 4.8. P-V data of the tetragonal phase of PbFCl. The solid line is the best fit to the Murnaghan equation of state.

modulus and its first derivative obtained for the tetragonal phase are $B_T = 51 \pm 3$ GPa and $B_T' = 5.6$. These values are comparable to the calculated bulk modulus of $B_T = 47$ GPa and $B_T' = 4.1$ GPa using a shell model [28]. Lattice dynamical calculations were carried out by Mittel *et al* on matlockite compounds MFX using shell model [28]. Using this model, the elastic constants, equation of state, phonon dispersion relations, density of states etc of the matlockite compounds were studied and compared with the experimental

values. The bulk modulus of PbFCl is compared with the similar matlockite compounds as shown in Table 4.1. The bulk modulus of PbFCl is marginally more than that of BaFCl. This variation can be attributed to the large electro negativity of Pb (2.33 in Pauling units) in comparison to Ba (0.89 in Pauling units) which leads to strong interlayer attraction and in turn leading to the lower compressibility of PbFCl [29]. This is also reflected in the transition pressures to lower symmetry phases in both of the compounds. For instance, the tetragonal \rightarrow orthorhombic \rightarrow monoclinic transition

Table 4.1. Experimental and computed bulk moduli of different matlockite compounds.

Compounds	BaFCl (Ref. 14)	BaFBr (Ref. 13)	PbFCl (This work)	PbFBr (Ref. 29)
Bulk Moduli	$B_0 = 45 \pm 3$ $B_0' = 5.2 \pm 0.5$	$B_0 = 38 \pm 11$ $B_0' = 7.6 \pm 2$	$B_0 = 51 \pm 3$ $B_0' = 5.6$	$B_0 = 43(15)$ $B_0' = 6(3)$

Table 4.2. Phase transition pressures of BaFCl and PbFCl compounds.

Compounds	Transition pressures (GPa)		Ref.
	Ortho.	Mono	
BaFCl	10.8	21	[12]
PbFCl	18	38	This work

pressures are 10.8 and 21 GPa for BaFCl whereas it is 18 and 38 GPa respectively for PbFCl (Table 4.2).

4.4 Pressure Induced Tetragonal to Orthorhombic Structural Transition in PbFBr

The XRD patterns of PbFBr at various pressures are shown in Fig.4.9. Since the XRD patterns of Pt do not merge with the PbFBr XRD patterns, 'Pt' has been used as a

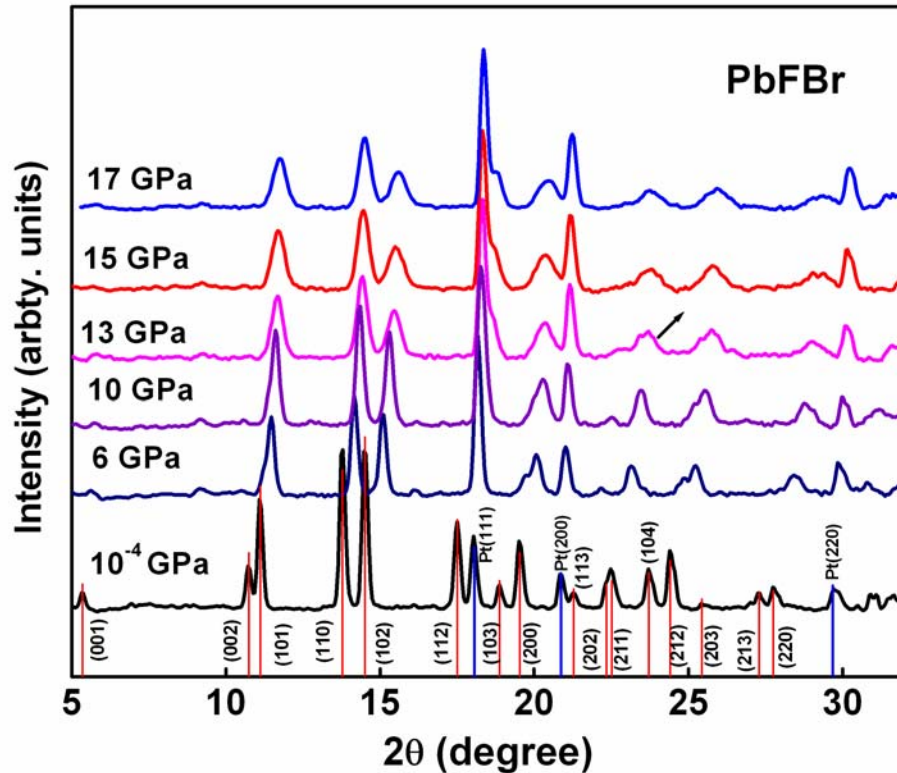


Fig.4.9. X-ray diffraction pattern of PbFBr at various pressures. The stick patterns from JCPDS are matched with the ambient pattern of PbFBr. Pt (111), Pt (200) and Pt (220) are the peaks obtained from “Pt” which is used as pressure calibrant. The stick patterns of “Pt” from JCPDS are also matching well with the ambient pattern of “Pt”.

pressure calibrant for this experiment. The peaks marked as Pt (111), Pt (200) and Pt (220) are the three prominent peaks from Pt. The XRD patterns were analyzed using powd [22] and NBS-Aids*83 programmes [23] to obtain the lattice parameters. At ~13 GPa, notable changes in the intensities of XRD pattern are observed and shown in Fig.4.9. The intensity of peak (001) is seen to reduce slowly and above ~13 GPa it vanishes completely. The peak (002) is prominent at ambient pressure and its intensity reduces slowly upon pressurizing further and finally merges with (101) peak. The peak (112) is completely merged with Pt (111) peak at intermediate pressures and is gradually

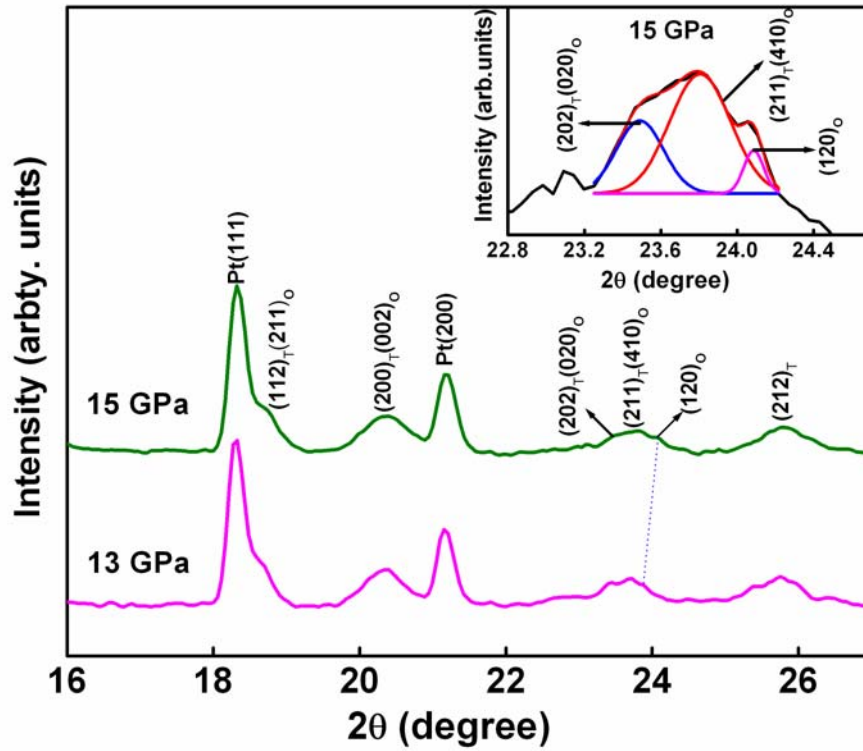


Fig.4.10. The HPXRD patterns of PbFBr at ~13 GPa and ~15 GPa. The dotted line indicates the increase in intensity of the new peak. The slanted arrow with the index (120)_O is the new peak. The new peak along with the (202)_T and (210)_T peaks are fitted to Gaussian fitting to resolve the peaks.

resolving above ~ 13 GPa. Until 10 GPa, the (202) and (211) peaks are merged and at around 13 GPa these peaks well resolved and an additional peak also appeared at $\sim 24^\circ$. The evolution of the new peak is shown in Fig.4.10. The dotted line indicates the increase in intensity of the peak with pressure. Above ~ 15 GPa, the peak is completely merged with the (202) and the (211) peaks. The analysis of the HPXRD pattern at ~ 21 GPa showed that the new structure is orthorhombic with lattice parameters $a = 7.927(1)$ Å, $b = 3.4928(5)$ Å and $c = 4.0202(3)$ Å. The lattice parameters corresponding to the tetragonal phase is $a = 3.9905$ Å and $c = 6.9895$ Å. Fig.4.11 shows the indexing of starting

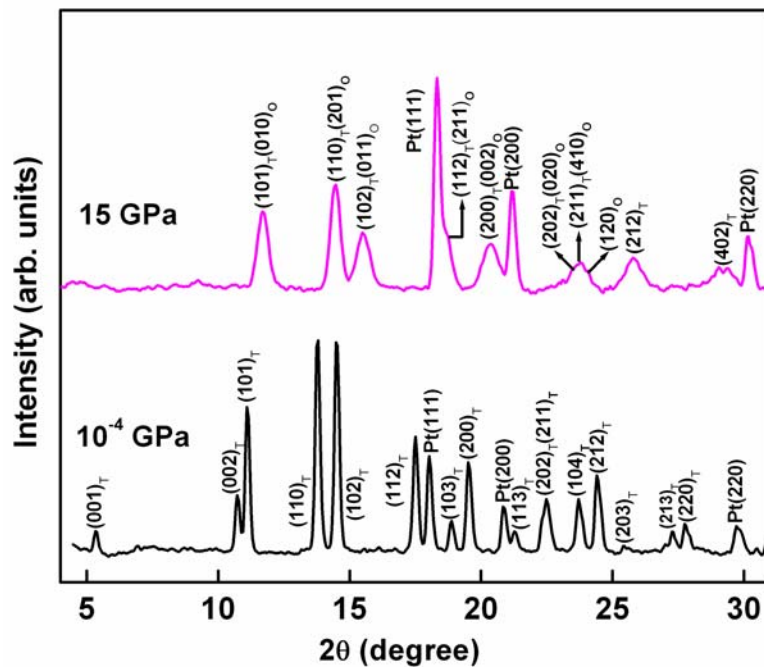


Fig.4.11. The indexing of XRD pattern at ambient and at around 15 GPa. The indices with subscripts “T” indicate the starting tetragonal phase and the indices with subscripts “T” and “O” indicate the mixture of tetragonal and orthorhombic phase. The Pt (111), Pt (200) and Pt (220) indicate the Pt peaks which are used as pressure calibrant.

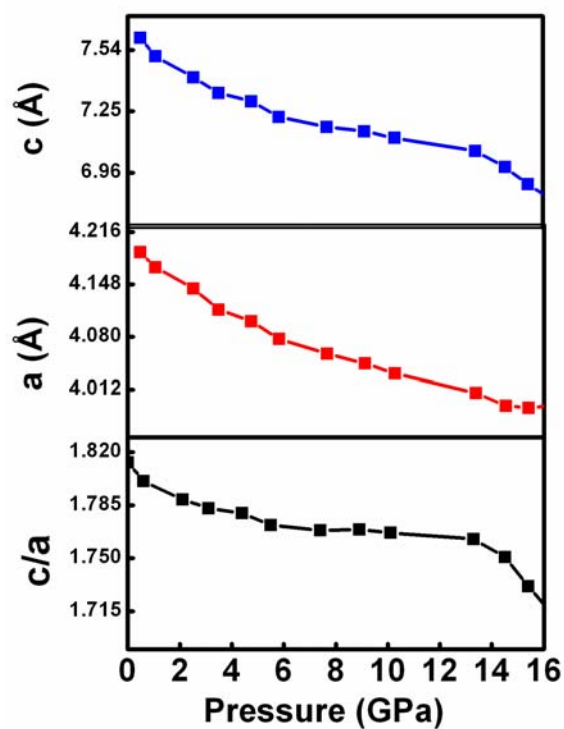


Fig.4.12. The pressure dependence of lattice parameters and c/a ratio of PbFBr.

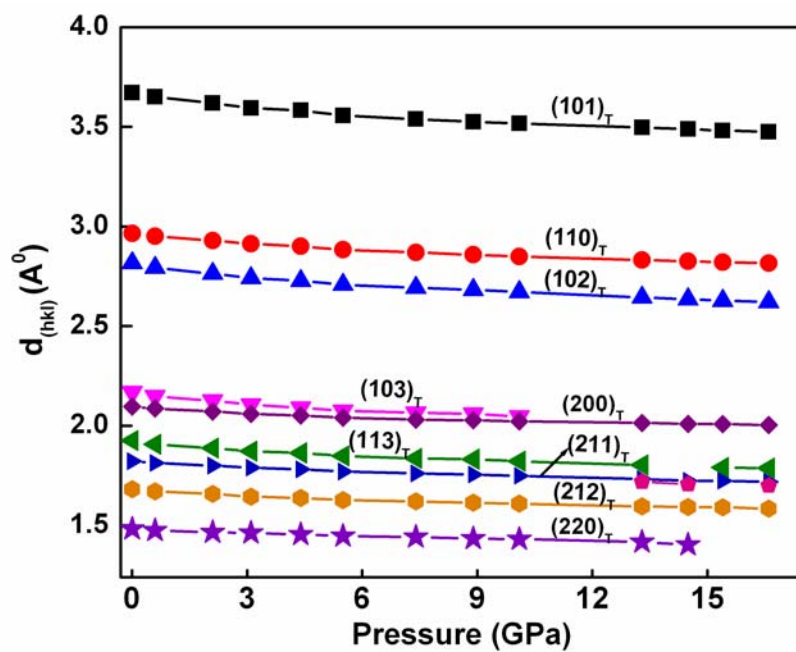


Fig.4.13. The pressure dependence of lattice spacings $d_{(hkl)}$ of PbFBr at different pressures.

tetragonal and the high pressure orthorhombic phases. The indices with “T” indicate the tetragonal phase and the indices with “T” and “O” indicate the mixture of tetragonal and orthorhombic phases. The HPXRD analysis at around 15 GPa shows the observed phase transition is not sharp but continuous in nature similar to other matlockite systems. The transition pressure for the starting tetragonal to orthorhombic phase for PbFBr system is lower than that of PbFCl system. Unlike PbFCl compound, the c/a ratio of PbFBr system shows interesting behavior with pressure [Fig.4.12]. Up to ~ 12 GPa, it decreases slowly with pressure, beyond which the rate of decrease enhances. When pressure is applied on PbFBr, the redistribution of charges in Br^- ions and the Pb^{2+} ions along the a - b plane leads to the phase transition of tetragonal lattice to orthorhombic lattice around 13 GPa. Fig.4.13 shows pressure dependence of d spacings of PbFBr. The lattice spacings vary monotonically with pressure.

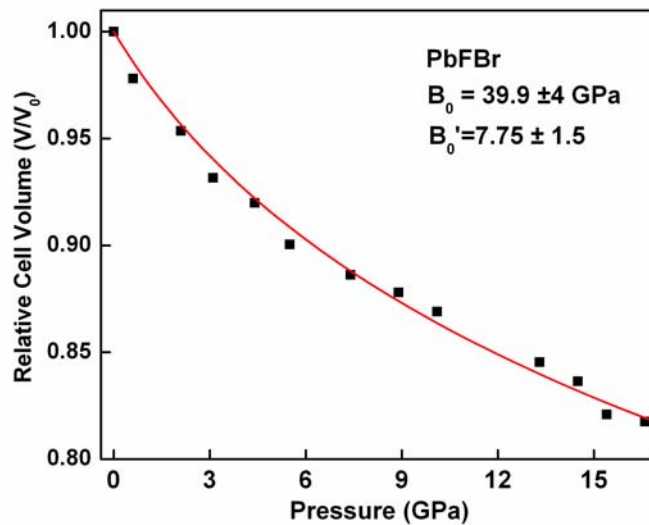


Fig.4.14. P-V data of the tetragonal phase of PbFCl. The solid line is the best fit to the Murnaghan equation of state.

The P-V curve corresponding to the parent tetragonal phase is fitted to the

Murnaghan equation of state. The bulk moduli obtained from this experiment is $B_0 = 39.9 \pm 4$ GPa and $B_0' = 7.7 \pm 1.5$. This value is comparable with the values $B_0 = 43(15)$ and $B_T' = 6(3)$ obtained by by Decremps *et al* [30].

4.5 Summary

PbFCl exhibits interesting structural phase transitions at high pressures. Like BaFCl, BaFBr and BaFI compounds, PbFCl also undergoes a pressure induced structural phase transition from the tetragonal phase to monoclinic phase ($P2_1/m$) via an intermediate orthorhombic phase. All the three phases are coexisting up to 38 GPa and around 47 GPa the orthorhombic lattice almost transforms to monoclinic lattice. The structural stability of PbFCl compound can be understood in terms of anisotropic coordination and polarizability of Pb^{2+} and Cl^- ions. High pressure X-ray diffraction studies have been carried out on PbFBr compound up to ~ 17 GPa. The starting tetragonal phase undergoes a structural phase transition at ~ 13 GPa to orthorhombic phase. The bulk modulus values obtained by us are compared with similar matlockite compounds.

References

- [1] W. Nieuwenkamp and J. M. Bijvoet, *Z. Kristallogr.* **81** 469 (1932)
- [2] A. F. Halff and J. Schoonman, "The Ionic Conductivity of PbFCl" *J. Solid State Chem.* **27** 397-405 (1979)
- [3] J. H. Eijkelenkamp, "Some Observations on the Photoluminescence of PbFCl and PbFBr Single Crystals" *J. Solid State Chem.* **19** 313-323 (1976)

- [4] A. J. H. Eijkelenkamp, "Photoluminescence of PbFCl and PbFBr single crystals" *Solid State Commun.* **18** 295-296 (1976)
- [5] J. Schoonman, A. F. Halff and G. Blasse, "Mixed anionic conduction in PbFCl" *Solid State Commun.* **13** 677-679 (1973)
- [6] A. F. Halff and J. Schoonman, "The Ionic Conductivity of PbFCl" *J. Solid State Chem.* **27** 397-405 (1979)
- [7] K. Takahashi, K. Kohda, J. Miyahara, Y. Kanemitsu, K. Amitani and S. Shionoya, "Mechanism of Photostimulated Luminescence in BaFX:Eu²⁺ (X=Cl, Br) phosphors" *J. Lumin.* **31/32** 266-268 (1984)
- [8] P. Comodi, P. F. Zanazzi, "Improved calibration curve for the Sm²⁺:BaFCl pressure sensor" *J. Appl. Crystall.* **26** 843-845 (1993)
- [9] J. Chen, D. Shen, G. Ren, R. Mao and Z. Yin, "A high-density inorganic scintillator: lead fluoride chloride" *J. Phys. D: Appl. Phys* **37** 938-941 (2004)
- [10] Y. R. Shen, U. Englisch, L. Chudinovskikh, F. Porsch, R. Haberkorn, H. P. Beck and W. B. Holzapfel, "A structural study on the PbFCl-type compounds MFCl (M =Ba, Sr and Ca) and BaFBr under high pressure" *J. Phys.: Condens. Matter* **6** 3197-3206 (1994)
- [11] N. Subramanian, N. V. Chandra Shekar, P. Ch. Sahu, M. Yousuf and K. Govinda Rajan, "Crystal structure of the high-pressure phase of BaFCl" *Physical Review B* **58** R555-R558 (1998)
- [12] N. Subramanian *PhD Dissertation Indian Institute of Science* (2000)

- [13] N. Subramanian, N. V. Chandra Shekar, P. Ch. Sahu, K. Govinda Rajan and A. L. Ruoff, "Evidence of an intermediate high-pressure phase in BaFBr and BaFI" *Physica B* **351** 5-10 (2004)
- [14] F. Decremps, M. Fischer, A. Polian and J. P. Itie, "Ionic layered PbFCl-type compounds under high pressure" *Physical Review B* **59** 4011-4022 (1999)
- [15] Sundarakannan, T. R. Ravindran, R. Kesavamoorthy, S. V. M. Satyanarayana, "High pressure Raman spectroscopic study of BaFCl" *Solid State Communications* **124** 385-389 (2002)
- [16] M. Sieskind and J. Morel, "Structural Considerations and Polarization Energy of Some PbFCl-Type Compounds" *J. Solid State Chemistry* **144** 339-348 (1999)
- [17] F. Decremps, M. Gauthier, J-C. Chervin, M. Fischer and A. Polian, "Unexpected value of transition pressure in the ionic layered BaFI compound observed by Raman scattering" *Physical Review B* **66** 024115(1-5) (2002)
- [18] A. H. Reshak, Z. Charifi and H. Baaziz, "First-principles study of the optical properties of PbFX (X = Cl, Br, I) compounds in its matlockite-type structure" *Eur. Phys. J. B* **60** 463-468 (2007)
- [19] Joint Committee on Powder Diffraction Standards, file No. 26-0311
- [20] Joint Committee on Powder Diffraction Standards, file No. 23-0325 (2003)
- [21] Andy Hammersley, *Fit2D1987-2004 version: V12.077*
- [22] J. D Barnett, S. Block, and G. J. Piermarini, "An Optical Fluorescence System for Quantitative Pressure Measurement in the Diamond-Anvil Cell", *Rev. Sci.instrum.*

44 1-8 (1973).

- [23] E. Wu, Interactive Powder Diffraction Data Interpretation and Indexing Version 2.2
- [24] A. D. Mighell, C. R. Hubbard, J. K. Stalick, U. S. Technical note: NBS 1141 (1981)NBS*AIDS83 is a development of NBS*AIDS80)
- [25] N. Yedukondalu and G. Vaitheeswaran, “Vibrational properties of BaClF, BaBrF and BaIF under high pressure” *Journal of Physics: Conference Series* **377** 012070(1-5) (2012)
- [26] T. Kurobori, M. Liu, H. Tsunekawa, Y. Hirose and M. Takeuchi, “Molecular dynamics simulation of the pressure-induced phase transition in BaFCl” *Radiation Effects & Defects in Solids* **157** 799-495 (2002)
- [27] F. D Murnaghan, “The compressibility of media under extreme pressures”, *Proc. Nat Acad. Sci.*, **30** 244-247 (1944)
- [28] R. Mittal, S. L. Chaplot, A. Shen, S. N. Achary and A. K. Tyagi, “Lattice dynamics and inelastic neutron scattering studies of MF_X (M=Ba, Sr, Pb; X=Cl, Br,I)” *Physical Review B* **67** 134303(1-12) (2003)
- [29] R. L. Dekock, H. B. Gray *Chemical Structure and Bonding* (1980) (The Benjamin / Cummings Publishing Company, Inc)
- [30] F. Decremps, M. Fischer, A. Polian, J.P. Itie, and M. Sieskind, “Prediction of cell variations with pressure of ionic layered crystal application to the matlockite family” *Eur. Phys. J. B* **9** 49-57 (1999)

Chapter V

High Pressure Raman Spectroscopy of PbFCl

5.1 Introduction

Lattice dynamical calculations have been carried out on MFX (M = Sr, Ba, Pb and X = Cl, Br, I) compounds using shell model which provide the understanding of elastic constants, equation of state, phonons and thermo dynamic properties of these layered compounds [1]. The frequencies and symmetries of even parity lattice vibrations of BaFCl, BaFBr and SrFCl compounds using polarized Raman spectroscopy is reported by Scott [2]. High pressure Raman study of BaFCl single crystals was studied up to ~25.6 GPa by Sundarakannan *et al* [3]. In this study, they observed that the starting tetragonal phase of BaFCl transformed into a mixture of tetragonal and orthorhombic phases at ~10.8 GPa. High pressure behavior of optical phonons of layered BaFI was studied up to 61 GPa by Decremps *et al* [4]. In this study, the pressure dependence of the phonon modes B_{1g} , E_g and A_{1g} is reported up to 55 GPa and they observed a phase transition from tetragonal to monoclinic structure at 55 GPa [4]. Further a large variation in the Grüneisen parameter of A_{1g} mode between 0 and 10 GPa is also reported. The pressure dependence of phonon modes of PbFCl compound up to 3.9 GPa was studied by Adams *et al* [5].

In a typical layered compound like β -GaSe [6] and hexagonal BN [7], two kinds of Raman active modes are observed. One is the high frequency intra-layer vibration

mode and the other is the low frequency shear-type-rigid-layer vibration mode. In these materials, within the layers the crystal bonding is primarily of covalent in nature where as the inter-layer interaction is of ionic or Coulomb in nature. Similarly, in $\text{Mg}(\text{OH})_2$ and $\text{Ca}(\text{OH})_2$ compounds two types of bonds are observed. One of the bonds is a highly ionic M-O bond and the other one is a strongly covalent O-H bond. The interlayer interaction is mainly dispersive with small electrostatic contribution [8]. These compounds are model systems for matlockite compounds. In matlockite compounds, the adjacent halide ion layers are weakly bonded which makes these materials soft and more compressible. But in matlockite compounds the bonding is ionic in nature. Also, in these compounds the adjacent layers are weakly bonded by halide ion layers. So it will be to study high pressure behavior of phonon modes of these compounds and get an handle on the inter and interlayer bondings that stabilize the anisotropic layered arrangement.

In PbFX compounds, the layered behavior is attributed to the asymmetric coordination of high polarizability Pb^{2+} and X^- ions. PbFCl is the prototype matlockite structure compound with space group $P4/nmm$ (D_{4h}^7 , no.129) and crystallizes in tetragonal structure [9]. In this work, we report our results of PbFCl using *in-situ* Raman spectroscopy under high pressure.

5.2 Experimental Details

A Mao-Bell type diamond anvil cell (DAC) with culet size of ~ 500 μm in diameter was used for the high pressure Raman spectroscopy experiments. A stainless steel gasket was preindented to a thickness of 50 μm ; a hole of diameter 200 μm was drilled at its centre. Finely powdered PbFCl sample was loaded into the gasket hole. A

4:1 mixture of methanol and ethanol was used as the pressure transmitting medium. Pressure was estimated by standard ruby fluorescence technique [10]. The sample was excited by Ar⁺ ion laser with 514.5 nm wavelength. Raman spectra of the sample was recorded for both increasing and decreasing pressure cycle using Renishaw *in-via* Raman spectrometer having 1 μm spatial resolution. The Rayleigh line rejection filter used in the spectrometer allows ripple free measurement of the Raman spectra up to 50 cm^{-1} . The maximum pressure attained in this experiment was ~ 41 GPa. The Rayleigh line rejection filter used in the spectrometer allows ripple free measurement of the Raman spectra up to 50 cm^{-1} .

5.3 Results and Discussion

PbFCl crystallizes in tetragonal structure with space group $P4/nmm$, D_{4h}^7 , and has two formula units in its unit cell. Two formula units in PbFCl results in a division of $3N = 18$ degrees of freedom into modes of the following symmetries [11].

$$\Gamma_{18} = 2A_{1g} + B_{1g} + 3E_g + 3A_{2u} + 3E_u$$

where $2A_{1g}$, B_{1g} and $3E_g$ are six Raman active modes, $2A_{2u}$ and $2E_u$, four IR active modes and A_{2u} and E_u are acoustical modes. The atomic displacements of phonon modes $A_{1g}(1)$, $A_{1g}(2)$, $E_g(1)$, $E_g(2)$ and $E_g(3)$ is shown in Fig.5.1. The low frequency $A_{1g}(1)$ mode shows the atomic displacements Pb^{2+} ions and the chloride ion layers are moving against each moving against each other. The B_{1g} mode shows the alternative F^- ions are moving in opposed directions. All the E_g modes correspond to atomic displacements confined in the

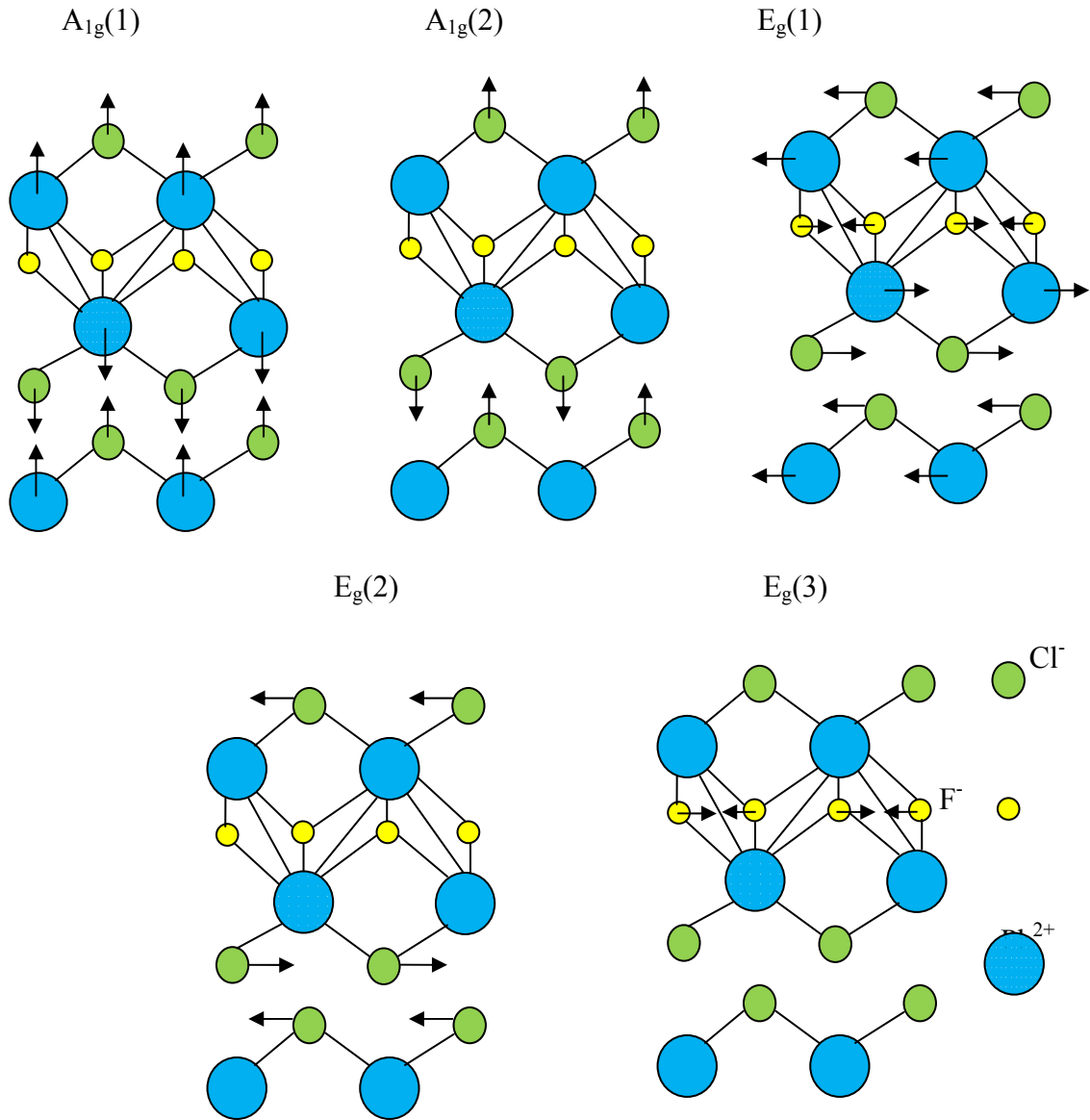


Fig.5.1. The atomic displacements of phonon modes $A_{1g}(1)$, $A_{1g}(2)$, $E_g(1)$, $E_g(2)$ and $E_g(3)$ of PbFCl compound. This figure is drawn based on the theoretical calculations carried out by Mohammadou M'erawa *et al* to study the atomic displacements of BaFCl compound [12].

a-b plane. The $E_g(1)$ mode shows that both Pb^{2+} ions and Cl^- ions are moving in the same

direction. But in the adjacent layers both Pb^{2+} and Cl^- ions moving in the same direction but opposite direction with respect to the first layer. In addition the F^- ions are moving against each other. In $E_g(2)$ adjacent chloride ions are moving against each other. In $E_g(3)$, the F^- ions are moving against each other [12].

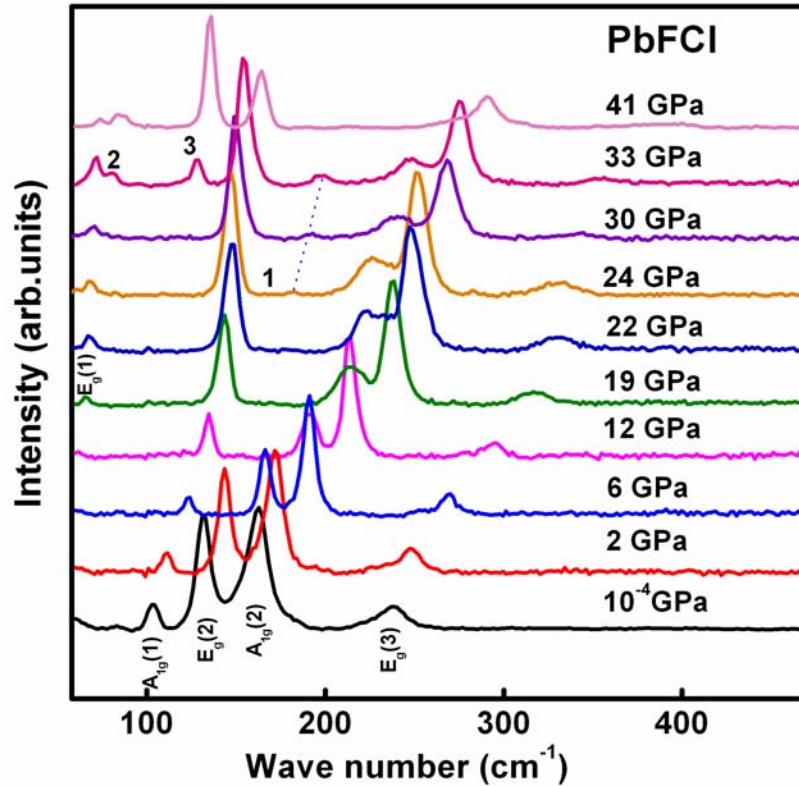


Fig.5.2. Raman spectra of PbFCI at various pressures. The modes are designated below the ambient pattern (10^{-4} GPa). The mode labelled 1 belongs to the orthorhombic phase and 2 and 3 modes belonging to the monoclinic phase.

At ambient pressure, four Raman active modes viz. $A_{1g}(1)$, $E_g(2)$, $A_{1g}(2)$ and $E_g(3)$ are seen at 103.5 cm^{-1} , 132 cm^{-1} , 162 cm^{-1} and 237 cm^{-1} respectively. The $E_g(1)$ mode is reported at $\sim 43 \text{ cm}^{-1}$ at ambient pressure. This mode is blue shifted with

pressure and we observe this mode at ~16 GPa and the corresponding wave number is ~66 GPa. The wave number of Raman modes were determined from a fit of the peaks with a Lorentzian profile. It is evident from Fig.5.2 that all the modes are continuously blue shifted upon raising the pressure.

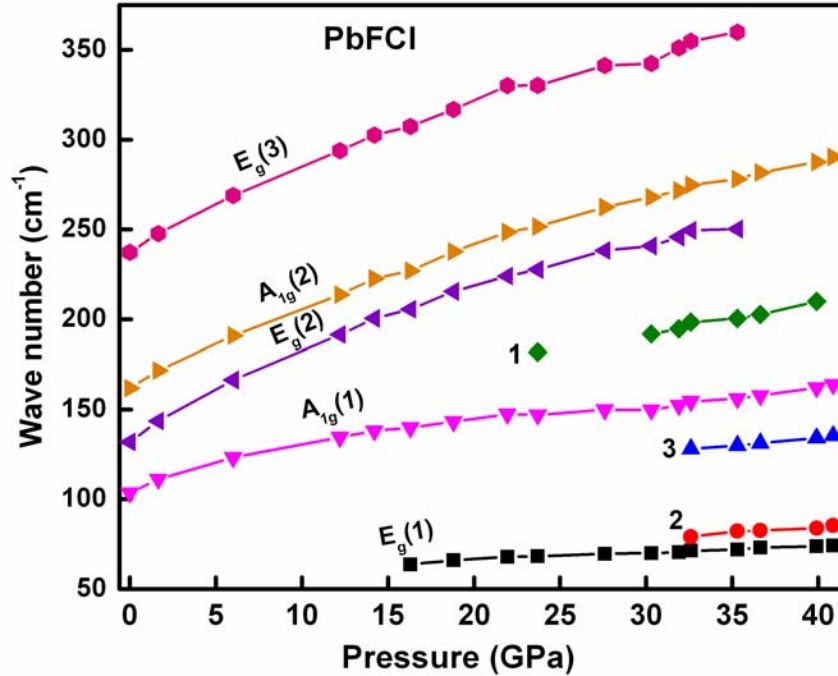


Fig.5.3. Pressure dependence of Raman modes of PbFCl. The numbers 1, 2 and 3 indicate the pressure dependence of new modes corresponding to the orthorhombic (mode1) and monoclinic phases (modes 2 and 3).

A large change in the intensity of $A_{1g}(1)$ mode is observed. The intensity of the mode $E_g(2)$ is gradually decreasing and it finally merges with $A_{1g}(2)$ mode. The large broadening and the intensity reduction of this mode with pressure indicate a signature of distortion of the tetragonal lattice. Almost similar trend is observed in the intensity of $E_g(3)$ mode. The intensity of the mode $A_{1g}(2)$ is almost constant up to ~ 24 GPa and

thereafter its intensity seen to reduce. In addition, a new mode appears at 182 cm^{-1} and the intensity of this mode is seen to increase upon pressurizing the sample further. The pressure dependence of the phonon modes are shown in Fig.5.3. The drastic change in the intensity of the $A_{1g}(1)$ mode and also the drastic reduction of intensities in $E_g(2)$ and

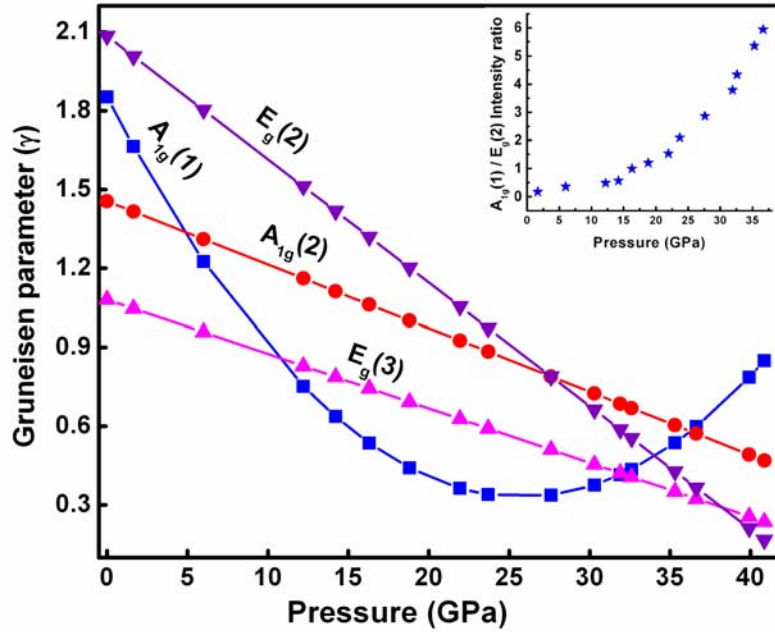


Fig.5.4. Pressure dependence of Grüneisen parameters of PbFCl. Inset is the pressure Vs intensity ratio between $A_{1g}(1)$ and $E_g(2)$ modes. Pressure dependence of Grüneisen parameters of PbFCl. Inset is the pressure Vs intensity ratio between $A_{1g}(1)$ and $E_g(2)$ Raman modes.

$E_g(3)$ modes hint the formation of new phase. XRD analysis (Chapter IV) shows that the appearance of new mode is due to the symmetry lowering of the starting tetragonal structure to orthorhombic structure. The existence of all the modes along with the new mode above ~ 24 GPa suggests that the coexistence of parent tetragonal and the high pressure orthorhombic phases.

On further pressurizing the sample, at around 33 GPa two additional modes are observed. The intensities of the modes $A_{1g}(1)$ and $A_{1g}(2)$ are reduced drastically. Appearance of new modes is due to the phase transition of tetragonal/orthorhombic phase. This new phase is identified as monoclinic with space group $P2_1/m$ from our high pressure XRD experiments [13]. The factor group analysis carried out on BaFCl by Sundarakannan *et al* showed that for the space group $P2_1/m$, there are nine Raman active modes, six IR active modes and three acoustic modes [3]. So nine Raman active modes are expected for the monoclinic phase of PbFCl. In accordance with our HPXRD studies of PbFCl, all the three phases viz. tetragonal, orthorhombic and monoclinic are coexisting up to ~ 38 GPa [Chapter IV]. The phase transition thus obtained is not sharp but sluggish in nature and can be due to a small Gibb's free energy difference between ambient and the high pressure phases [3, 14]. The vanishing of $E_g(2)$ mode above ~ 33 GPa shows the nucleation of monoclinic phase at the expense of tetragonal/orthorhombic phases. The pressure dependence of Raman modes $E_g(2)$, $E_g(3)$ and $A_{1g}(2)$ are fitted to second order polynomials and the mode $A_{1g}(1)$ to a third order polynomial. As is evident from Fig.5.2, the pressure dependence of the Raman modes $A_{1g}(2)$, $E_g(2)$ and $E_g(3)$ are almost similar. It is very interesting to study the pressure dependence of $A_{1g}(1)$ mode. Initially this mode increases with pressure up to ~ 24 GPa and after that the mode varies very slowly up to ~ 33 GPa. Thereafter, its frequency increases with pressure. The pressure dependence of phonon dispersion related to the mode Grüneisen parameters is given by

$$\gamma_i = -(\partial \ln \omega_i / \partial \ln V) = (1/\beta \omega_i)(d\omega_i/dp)$$

where ω_i is the phonon frequency of the i^{th} mode, β is the isothermal compressibility, V is

the volume of the crystal and P is the pressure [15].

$$\gamma_i = (B_0/\omega_0)(d\omega_i/dp)_{p=0}$$

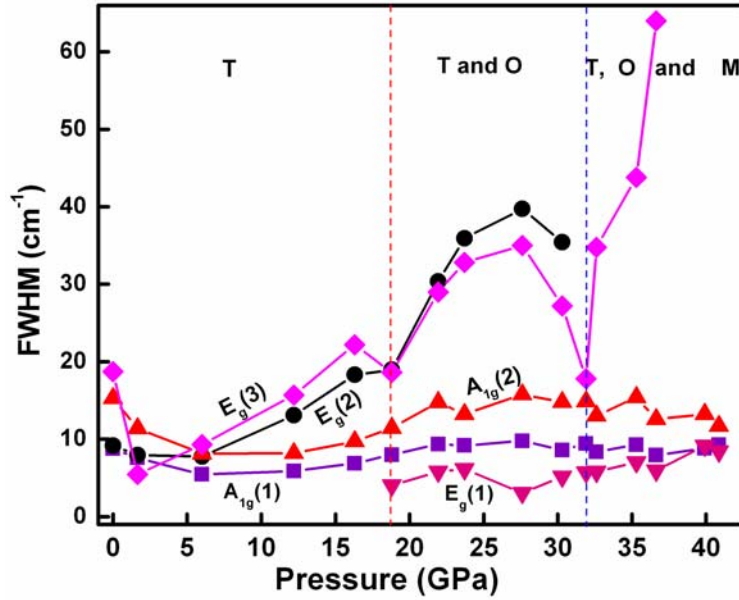


Fig.5.5. Pressure dependence of FWHM of Raman modes of PbFCl. The dotted vertical lines represent the transition pressures at ~ 18 GPa and ~ 32 GPa respectively. T represents the tetragonal phase. T and O represent the mixture of tetragonal and the orthorhombic phases respectively. T, O and M represent the Tetragonal, orthorhombic and the monoclinic phases respectively.

The mode Grüneisen parameters are calculated for the tetragonal and the orthogonal phases with the bulk moduli 51 ± 3 and 149 ± 10 respectively. The pressure dependence of Grüneisen parameters are shown in Fig.5.3.

The atomic motions related to the optical phonon modes can be understood from the following mechanism. Since the adjacent chloride ions are moving in opposite

directions, a large strain will be generated which leads to the broadening of the modes with pressure. In $E_g(3)$ mode, the compression of lattice leads to the repulsion between nearby F^- ions try to push the F^- ions far apart in order to minimize the energy of the system. Fig.5.4 shows the pressure dependence of Grüneisen parameters of Raman

Table 5.1. Grüneisen parameters (γ) of phonon modes $A_{1g}(1)$, $A_{1g}(2)$, $E_{1g}(1)$, $E_{1g}(2)$, $E_{1g}(3)$ and mode 3 at $P=0$.

Raman modes	Grüneisen parameters (γ)
$E_{1g}(1)$	2.02
$E_{1g}(2)$	2.08
$E_{1g}(3)$	1.08
$A_{1g}(1)$	1.85
$A_{1g}(2)$	1.46
mode 3	1.81

modes of $PbFCl$. The pressure dependence of Grüneisen parameter γ of $A_{1g}(1)$ mode is very interesting as it shows a non-monotonic behavior with a single minimum at $P \sim 26$ GPa. This unusual behavior of the $A_{1g}(1)$ mode is due to the destabilizing effect of pressure along the weakly bonded adjacent chloride ion layers along the c-axis inducing a structural transition to probably an isotropically bonded non-layer phase [4, 16]. As is evident from the Fig.5.4, the slope of $E_g(2)$ mode is steeper as compared to the $A_{1g}(2)$ and $E_g(3)$ modes. The reason for this is as follows; the Cl^- ions situated at the adjacent layers

of $E_g(2)$ moves in opposite directions which will generate repulsion between Cl^- ions. On increasing the pressure, the compression is more along the c-axis due to the weak bonding between the adjacent layers containing the Cl^- ions. Initially the Grüneisen parameter of the mode $A_{1g}(1)$ decreases much faster than that of $E_g(2)$. This is due to the attraction between the oppositely charged Pb^{2+} and the Cl^- ions. This variation is drastic up to ~ 18 GPa and after that it decreases slowly with pressure up to ~ 24 GPa. Thereafter it increases with pressure. Since at ~ 18 GPa, the tetragonal lattice is transformed to orthorhombic lattice, hence on pressurizing further the lattice resist to deform further. But above 26 GPa, the lattice is again distorted slowly with pressure.

The pressure dependence of width of the modes $A_{1g}(1)$, $A_{1g}(2)$ and $E_g(1)$ are almost similar as shown in Fig.5.5. There is a sharp increase in the width of $E_g(2)$ and $E_g(3)$ modes with pressure up to ~ 24 GPa and after that the width reduces gradually with pressure. This sudden change of width signals a phase transition to orthorhombic phase. Beyond ~ 24 GPa the width of these two modes decrease slowly at first and then decrease drastically with pressure. Above ~ 32 GPa, the width of $E_g(3)$ mode drastically increases with pressure.

In $PbFCl$ the asymmetric coordination of the chloride ions produces a large electric field at the anion and hence the dipole moment. Therefore pressure generates large compression along the c-axis. We know that the pressure increases the electron density between the non-bonded atoms and reduces that of the bonded atoms. This leads to the breaking (or weakening) and forming of new bonds. This causes the increase in coordination numbers and lowering of symmetry of the system. Based on these

arguments and the Raman results we can say that the compression along the *c*-axis and the repulsion between the Fluoride ions cause redistribution of charge density over *a*-*b* plane. Hence there is a distortion in the tetragonal lattice. The shortening of *c* parameter and the elongation of *a* parameter leads to orthorhombic phase.

Above 30 GPa, the repulsions between the chloride ions between the adjacent layers along the *c*-axis slowly increases with pressure and surpasses the attraction between the Pb^{2+} and Cl^- ions. This may cause slight elongation of the *c* parameter in orthorhombic lattice and also in the tetragonal lattice which is observed in our XRD studies. The reason for the anomalous behavior of *c/a* value above ~ 30 GPa from the HPXRD studies is similar to the anomaly in the $A_{1g}(1)$ Raman mode behavior. This repulsion between the adjacent Cl^- layers will once again redistribute charge cloud in *a*-*b* plane leads to the monoclinic lattice. The increase in the *c*-value shows the increase of nonlayer-layer behavior. The coexistence of parent tetragonal and the daughter phases are due to the small differences in free energies. The increase in the intensity of mode 3 shows the gradual distortions of either tetragonal or orthorhombic lattices to monoclinic lattice.

5.4 Conclusion

High pressure *in-situ* Raman spectroscopy of PbFCl compound is studied up to 41 GPa. The pressure dependence of optical phonon modes and the new modes for the high pressure phases are described. The pressure dependence of mode Grüneisen parameters of different modes are explained. The broadening of the spectral lines and the

causes for the broadening at high pressure is also discussed. The $A_{1g}(1)$ phonon mode shows unusual behavior with pressure. This unusual behavior can be attributed to the layer-non layer transition at high pressure [16].

References

1. R. Mittal, S. L. Chaplot, A. Sen, S. N. Achary and A. K. Tyagi, "Lattice dynamics and inelastic neutron scattering studies of MFX (M=Ba, Sr, Pb; X=Cl, Br,I)" *Physical Review B* **67** 134303 (1-12) (2003)
2. J. M. Scott, "Raman spectra of BaFCl, BaFBr and SrFCl" *J. of Chem. Phys.* **49** 2766-2769 (1967)
3. B. Sundarakannan, T. R. Ravindran, R. Kesavamoorthy, S. V. M. Satyanarayana, "High pressure Raman spectroscopic study of BaFCl" *Solid State Communications* **124** 385-389 (2002)
4. F. Decremps, M. Gauthier, J.-C. Chervin, M. Fischer and A. Polian, "Unexpected value of transition pressure in the ionic layered BaFI compound observed by Raman scattering" *Physical Review B* **66** 02415(1-5) 2002
5. D. M. Adams and T-K Tan, "Vibrational spectroscopy at high pressures: Pressure dependence of the Raman active modes of CdX₂ and PbFX type layer materials" *J. Phys. Chem. Solids* **42** 559-562 (1981)
6. T. J. Wieting and J. L. Verble, "Interlayer bonding and the lattice vibrations of β -GaSe" *Physical Review B* **5** 1473-1479 (1971)
7. Takashi Kuzuba, Yoichiro Sato, Shinobu Yamaoka and Koh Era, "Raman-scattering study of high-pressure effects on the anisotropy of force constants of

- Hexagonal boron nitride” *Physical Review B* **18** 4440-4443 (1978)
8. Ph. Baranek, A. Lichanot, R. Orlando and R. Dovesi, “Structural and vibrational properties of solid $\text{Mg}(\text{OH})_2$ and $\text{Ca}(\text{OH})_2$ -performances of various Hamiltonians” *Chemical Physics Letters* **340** 362-369 (2001)
 9. W. Nieuwenkamp and J. M. Bijvoet, *Z. Kristallogr.* **81** 469 (1932)
 10. G. J. Piermarini, S. Block, J. D. Barnett and R. A. Forman, “Calibration of the pressure dependence of the R_1 ruby fluorescence line to 195 kbar” *J. Appl. Phys.* **46** 2774-2780 (1975)
 11. Rulmont, “Spectres infrarouges et Raman des fluorhalogénures de plomb PbFX ($X = \text{Cl}, \text{Br}, \text{I}$)” *Spectrochimica Acta* **30A** 161 (1974)
 12. M. Merawa, Y. Noë, B. Civalleri, R. Brown and R. Dovesi, “Raman and infrared vibrational frequencies and elastic properties of solid BaFCl calculated with various Hamiltonians: an *ab initio* study”, *J. Phys.: Condens. Matter* **17** 535-548 (2005)
 13. Y. A. Sorb, D. Sornadurai, N. Subramanian and P. Ch. Sahu, “Structural stability of PbFCl under high pressure” (To be published)
 14. N. Yedukondalu and G. Vaitheeswaran, “Vibrational properties of BaClF , BaBrF and BaIF under high pressure” *Journal of Physics: Conference Series* **377** 012070(1-5) (2012)
 15. A. Jayaraman, “Diamond anvil cell and high-pressure physical investigations” *Reviews of Modern Physics* **55** 65-108 (1983)

16. Y. A. Sorb, N. Subramanian and T. R. Ravindran, “High pressure Raman spectroscopy of layered matlockite PbFCl” *J. Phys. Condens.Matter*, (In print, 2013)

Chapter VI

Summary

This thesis work addressed two themes. The first one was “Exploration of Formation of Novel Intra-Group Phases involving Group IV Elements using LHDAC Technique”. The other one was “Pressure induced structural phase transition studies of PbFX (X=Cl, Br) systems”. Preliminary experiments for the synthesis of Ge-Sn system was carried out using Bridgman HP-HT cell in an opposed anvil configuration. This preliminary experiment was carried out to explore the formation of Ge-Sn phase at P and T conditions below the high pressure β -Sn phase of germanium. Since this device had a pressure limitation of ~ 5 GPa, laser heated diamond anvil cell technique and Raman spectroscopy has been used for exploring bond formation in Ge-Sn, Ge-C and Pb-C at HP-HT conditions. Pressure induced structural behavior studies have been carried out on matlockite compounds using HPXRD technique on PbFCl and PbFBr in angle dispersive geometry using a laboratory X-ray diffractometer employing 18 kW rotating anode X-ray generator and imaging plate system. Raman spectroscopy has also been carried out to understand the behavior of phonon modes of PbFCl compound and its high pressure phases.

Preliminary experiments on Ge-Sn using Bridgman HP-HT cell has been done at 5 GPa and 550°C, and the characterization of the retrieved sample at high pressure (HP) using synchrotron radiation does not indicate formation of any new phase. The maximum pressure that could be attained using the Bridgman HP-HT cell at our

laboratory without damaging the anvils was 5 GPa at a maximum temperature of $\sim 550^{\circ}\text{C}$. Also, in-situ characterization of the sample cannot be done with this device. Since diamond is transparent to almost entire electromagnetic radiation, the pressure induced phenomena of materials squeezed under high pressure in a diamond anvil cell can be studied by using X-ray diffraction technique, Raman spectroscopy etc. As diamond is transparent to IR radiation, the sample can be heated to very high temperatures at megabar pressures. Ge-Sn sample could be synthesized at ~ 7.6 GPa and ~ 2000 K using the LHDAC technique and the laser quenched sample were characterized by using *in-situ* Raman spectroscopy. At ambient P and T, Ge and Sn have their characteristic first order TO (Γ) Raman phonon modes at $\sim 300\text{ cm}^{-1}$ and 132 cm^{-1} respectively. At ~ 9 GPa, these modes shift to $\sim 328\text{ cm}^{-1}$ and $\sim 164\text{ cm}^{-1}$ respectively. After laser heating the Ge+Sn elemental mixture at ~ 9 GPa, in addition to the parent modes, we observed new Raman modes at $\sim 225\text{ cm}^{-1}$ and $\sim 133\text{ cm}^{-1}$. The former mode softens upon pressure reduction to $\sim 215\text{ cm}^{-1}$ at 10^{-4} GPa (~ 1 atm.) and is ascribed to a Ge-Sn vibrational mode. Raman spectroscopy of Ge-Sn thin films does show a Ge-Sn band intermediate between the Ge-Ge and Sn-Sn bands at around this wave number. Pressure variation of the 133 cm^{-1} mode is almost akin to that of the 225 cm^{-1} mode, and quite different from those of the Ge-Ge and Sn-Sn modes. This hinted that this mode may also correspond to another Ge-Sn mode and be associated with a lower symmetry structure formation at high P-T conditions. The characterization of the sample by synchrotron based X-ray diffraction technique showed no indication of reaction between the Ge and Sn.

The synthesis of Ge-C system was also carried out using LHDAC technique.

Laser heating of Ge+C sample at ~ 9.3 GPa and ~ 2000 K for prolonged heating of about ~ 30 minutes followed by Raman spectroscopy of the laser quenched sample showed, in addition to the characteristic Ge TO (Γ) and C phonon modes (both of which are considerably softened under pressure), a new mode appearing at 203.3 cm^{-1} . These could be ascribed to Ge-C bond formation. However, the investigation of Pb-C system at ~ 5.2 GPa and ~ 2000 K in a laser heated diamond anvil cell and HPXRD pattern of the laser heated sample do not indicate any new phase formation.

These LHDAC experiments offer scope for stimulating further studies involving other group-IV elements such as carbon and phosphorous [1]. Phosphorous carbide in thin film form has been synthesized using Pulsed Laser Ablation (PLA) technique [2]. The thermodynamic stability and properties of different possible phases of phosphorus carbide as a function of composition has been reported using density functional theory [1]. In this study, calculation is performed on P_4C_3 , PC and P_3C_4 and possible structures of these phases having minimum free energy. The favored structure for P_4C_3 is defect zinc-blende structure, for PC the favoured structure is GaSe-like and β -InS-like and for P_3C_4 the lowest energy structure is β - C_3N_4 -like [1]. The difficulty with the P-C compound formation using LHDAC technique stems from the handling of phosphorous. The only stable form of phosphorus at ambient conditions is the black phosphorus. Preliminary attempts have been made in our laboratory to synthesize phosphorus carbide at HP-HT conditions in a laser heated diamond anvil cell. But the experiment was not successful in the sense that Raman spectra recorded before and after laser heating did not show any differences. However, synthesis can be possible by varying the pressure and temperature conditions.

$\text{Si}_{1-x}\text{Ge}_x$ alloy has been used to make heterojunction bipolar transistors having cut off frequency of about 100 GHz which is higher than that of Si [3]. However the difficulty with this Si-Ge technology is that 4 % lattice mismatch between the elements Ge and Si. This creates compressive strain on $\text{Si}_{1-x}\text{Ge}_x$ layers grown on Si. The problem can be solved by incorporating carbon in Si-Ge material. This intra group-IV ternary semiconductor material stimulates intense interest in the development of new inorganic alloys and compounds based on Group IV elements. After synthesizing these compounds, the mechanical and optical properties of compounds can be studied. For instance the mechanical property of the sample can be studied by nanoindentation technique. The difficulties with the laser heated sample for hardness measurement are, holding the sample on a substrate, surface roughness of the sample and the thickness of the reacted product. The indentation into any sample should be one tenth of the thickness to avoid the influence of the substrate on the mechanical property measurements [4]. But the hardness measurement of the pressure quenched C_{70} and graphite sample has been reported using designer diamond anvils [5]. In this study, the tip of the nanoindenter is moved onto the sample sitting inside the gasket over the diamond. Band gap measurement will give idea about the nature of semiconductor. However, band gap measurement of the laser quenched sample is very difficult due to the small size of the sample and difficulties in retrieving the sample from the gasket. Optical measurement of the sample in the UV range can be used to study the band gap of the material. High pressure phase transition studies can be done on these systems using XRD and Raman spectroscopy.

High pressure structural stability studies have been carried out on PbFCl and

PbFBr compounds. PbFCl undergoes pressure induced structural phase transitions at ~ 18 GPa and ~ 38 GPa to orthorhombic and monoclinic ($P2_1/m$) phases respectively. The zero pressure bulk modulus obtained for the tetragonal phase is $\sim 51 \pm 3$ GPa and compares well with theoretically predicted values. The ambient tetragonal phase is seen to coexist with the high pressure orthorhombic phase up to ~ 38 GPa and at around 47 GPa, the orthorhombic lattice almost transforms to the monoclinic lattice completely. This symmetry lowering structural behavior under pressure is similar to other matlockite structure compounds such as BaFCl, BaFBr and BaFI. The pressure dependence of Raman modes $A_{1g}(1)$, $E_g(2)$, $A_{1g}(2)$ and $E_g(3)$ are studied. Grüneisen parameters of all the modes with pressure are also discussed where the mode $A_{1g}(1)$ shows an anomalous behavior. The results show that PbFCl has a larger structural stability range compared to BaFCl and this is attributed to the larger anisotropic coordination of the Pb^{2+} cation and the Cl^- anions and the large polarization energy in comparison to BaFCl. High pressure study of PbFBr has been carried out up to ~ 17 GPa. The tetragonal to orthorhombic phase transition is observed at ~ 15 GPa. The bulk moduli obtained from this experiment is $B_0 = 39.9 \pm 4$ GPa and $B_0' = 7.7 \pm 1.5$.

High pressure study of PbFCl and PbFBr compounds reveal that the behavior of these compounds are similar to other matlockite compounds such as BaFCl, BaFBr, BaFI etc. All these compounds undergo a phase transition in the sequence: tetragonal to orthorhombic and orthorhombic to monoclinic. The difference in transition pressures of these compounds depend on the type of M^{2+} ions and X^- ions substituted in MF X compounds. For example, the substitution of Pb^{2+} in the place of Ba^{2+} in PbFCl gives more structural stability to PbFCl as compared to BaFCl. High pressure Raman study of

these compounds is useful to probe the unusual behavior of Raman modes in the layered compounds.

References

- [1] Frederik Claeysens, Judy N. Hart, Neil L. Allan and Josep M. Oliva, “Solid phases of phosphorus carbide: An *ab initio* study” *Phys. Review B* **79**, 134115(1-14) (2009)
- [2] F. Claeysens , G. M. Fuge, N. L. Allan, P. W. May and M. N. R. Ashfold, “Phosphorus carbides: theory and experiment” *Dalton Transactions* 3085-3092 [(2004) 10.1039/B402740J]
- [3] J. Kouvetakis, D. Nesting and David J. Smith, “Synthesis and Atomic and Electronic Structure of New Si-Ge-C Alloys and Compounds” *Chem. Mater.* **10** 2935-2949 (1998)
- [4] J. Reed Patterson, Anatoliy Kudryavtsev and Yogesh K. Vohra, “X-ray diffraction and nanoindentation studies of nanocrystalline graphite at high pressures” *Applied Physics Letters* **81** 2073-2075 (2002)
- [5] Jeremy R. Patterson, Shane A. Catledge, Yogesh K. Vohra, Jagannadham Akella and Samuel T. Weir “Electrical and mechanical properties of C₇₀ fullerene and graphite under high pressures studied using designer diamond anvils”, *Physical Review Letters* **85** 5364-5367 (2000)

List of Publications:

Peer reviewed Journal papers:

1. Y. A. Sorb, N. Subramanian and T. R. Ravindran, "High pressure Raman spectroscopy of layered matlockite PbFCl" *J. Phys. Condens. Matter*, 2013 [In print, 2013]
2. Y. A. Sorb, N. Subramanian, T. R. Ravindran and P. Ch. Sahu, Synthesis of Ge-Sn at HP-HT in a Laser Heated Diamond Anvil Cell (To be published)
3. Y. A. Sorb, D. Sornadurai, N. Subramanian and P. Ch. Sahu, Structural stability of PbFCl under high pressure (To be published)

Peer reviewed Conference papers:

1. Y. A. Sorb, N. Subramanian, T. R. Ravindran and P. Ch. Sahu, Solid State Physics: Proc. of the 55th DAE Solid State Physics Symposium, Volume 55, Manipal, 2010, AIP Conf. Proc. No. 1349 (AIP, New York, 2011)
2. Y. A. Sorb, N. Subramanian, T. R. Ravindran and P. Ch. Sahu, Solid State Physics: Proc. of the 56th DAE Solid State Physics Symposium, SRM university 2011, AIP Conf. Proc. 1447, 145 (2012); doi: 10.1063/1.4709923

Papers in National/International conferences

1. Y. A. Sorb, N. R Sanjay Kumar, N. V. Chandra Shekar, M. Sekar, T. R. Ravindran, N. Subramanian and P. Ch. Sahu , 21st AGM-MRSI theme symposium on Advanced Ceramics Materials-Monolithics to Composites, P.41
2. Y. A. Sorb, N. Subramanian, T. R. Ravindran and P. Ch. Sahu, International confere-

nce on High Pressure Science and Technology AIRAPT-231, BARC

3. N. Subramanian and Y. A. Sorb, "Pressure induced structural changes in BaFCl and PbFCl: A comparison" *24th Annual General Meeting of Materials Research Society of India (MRSI) Kalpakkam, India P.41 (2013)*
4. Y. A. Sorb, N. Subramanian and T. R. Ravindran, "Unusual behavior of interlayer vibrational modes of PbFCl at high pressure" *24th Annual General Meeting of Materials Research Society of India (MRSI) Kalpakkam, India P.42 (2013)*

Publications not related to Thesis work

1. K. Kamali, T. R. Ravindran, C. Ravi, Y. Sorb, N. Subramanian, and A. K. Arora, *Physical Review B* 86 144301 (2012)

Awards

1. The poster titled "Exploration of Possible Novel Phases in Ge-Sn System Using LHDAC" got poster award in MRSI conference conducted 21st AGM-MRSI theme symposium on Advanced Ceramics Materials-Monolithics to Composites.